INFORMATION TO USERS

This manuscript has been reproduced from the microfilm master. UMI films the text directly from the original or copy submitted. Thus, some thesis and dissertation copies are in typewriter face, while others may be from any type of computer printer.

The quality of this reproduction is dependent upon the quality of the copy submitted. Broken or indistinct print, colored or poor quality illustrations and photographs, print bleedthrough, substandard margins, and improper alignment can adversely affect reproduction.

In the unlikely event that the author did not send UMI a complete manuscript and there are missing pages, these will be noted. Also, if unauthorized copyright material had to be removed, a note will indicate the deletion.

Oversize materials (e.g., maps, drawings, charts) are reproduced by sectioning the original, beginning at the upper left-hand corner and continuing from left to right in equal sections with small overlaps.

Photographs included in the original manuscript have been reproduced xerographically in this copy. Higher quality 6" x 9" black and white photographic prints are available for any photographs or illustrations appearing in this copy for an additional charge. Contact UMI directly to order.

Bell & Howell Information and Learning
300 North Zeeb Road, Ann Arbor, MI 48106-1346 USA

UMI®
800-521-0600

Cytochrome c Peroxidase: Its role in nitrosative stress and purification as a GST-fusion protein

Iolie C. Bakas

A Thesis

in

The Department

of

Chemistry and Biochemistry

Presented in Partial Fulfillment of the Requirements

for the Degree of Masters of Science at

Concordia University

Montreal, Quebec, Canada

July 1999

Abstract

Cytochrome c peroxidase: Its role in nitrosative stress and purification as a GST-fusion protein

Iolie C. Bakas, M.Sc.
Concordia University, 1999.

Cytochrome c Peroxidase (CCP) is a hemoprotein found in the intermembrane space of yeast mitochondria. One of its roles is to protect the cell against oxidative stress by reducing mitochondrial H_2O_2 to H_2O. Titration of CCP with peroxynitrite [ONOO(H)] formed a species with an absorption spectrum identical to compound I/II at a ONOO(H)/CCP ratio of 1.65 ± 0.10. Titration of the CCP species formed with ferrocytochrome c, gives a ratio of ferrocytochrome c/CCP = 1.87, indicating that the species formed is compound I. An estimate of the second-order rate constant for the reaction of peroxynitrite with CCP at pH 7.0 is $6.9 \pm 2.2 \times 10^5\ M^{-1}s^{-1}$. We propose that the end product of the reaction of CCP with peroxynitrite is nitrite and not the $NO_2^{\cdot}$ radical, since excess nitrite does not induce reduction of compound I. We conclude that CCP is a protective enzyme against nitrosative as well as peroxidative stress.

A silent *BamH* I mutation was introduced into the mature sequence of CCP gene as well as *BamH* I and *EcoR* I restriction sites at its 5'- and 3'-ends, respectively. Cloning of this DNA into the pGEX 2T vector yields the GST-CCP construct, and expression of this construct in *E. coli* produces ~ 530 mg GST-CCP fusion protein per 12 L of culture. Purification of the fusion protein involves a single affinity chromatography

step and free CCP is obtained by cleavage of the fusion protein with thrombin. After recrystallization 60 mg of highly pure enzyme was produced with 61.5% of the expected activity based on heme content. Further investigations are necessary to improve the yield and activity of CCP as obtained using this procedure.

To my father, mother and Christo for believing in me

Acknowledgements

I would like to thank my supervisor, Ann English for her insightful ideas, valuable guidance and discussions which made completion of this study possible. Also, I would like to thank her for reading and editing this manuscript.

Thanks to Drs J. M. Kornblat and P. Joyce for letting me use their instruments, and all the graduate students in Dr. English's lab for being great labmates and friends.

Thanks to Angelo Filosa for performing the mass spectrometry run on CCP(GS), and to David Michels and Marcy Wright for their help with the molecular biology part of my thesis.

Finally, thanks to my parents, brother and my friend Ismini for all the support and encouragement they gave me, and for always being there for me.

Table of contents

List of Figures

List of Tables

List of Schemes

LIST OF ABBREVIATIONS

$ABTS^+$	2,2'-azino-bis-(3-ethyl-1,2-dihydrobenzothiazoline 6-sulfonate) radical cation
Apo-CCP	CCP which does not possess the heme
B.M. U	cleavage unit of Boehringer Manheim Thrombin
CCP	cytochrome c peroxidase
compound I	CCP + 1 equivalent of H_2O_2
cyt c	cytochrome c
DEAE	diethylaminoethyl cellulose
DTPA	diethylenetriamine pentaacetic acid
EDTA	ethylenediamine tetraacetic acid
EDRF	endothelium derived relaxing factor
ESI	electrospray ionization
GPx	glutathione peroxidase
GS 4B	glutathione Sepharose 4B resin
GST	glutathione S transferase
holo-CCP	CCP with the heme added
HRP	horseradish peroxidase
IPTG	isopropyl β-$_D$-thiogalactopyranoside
KPi	potassium phosphate buffer
MCD	magnetic circular dichroism
MPO	myeloperoxidase
NAD(P)H	nicotinamide adenine dinucleotide (phosphate), reduced form
NOS	nitric oxide synthase
eNOS	endothelial NOS
mNOS	macrophage NOS
nNOS	neuronal NOS
PCR	polymerase chain reaction
PLGPx	phospholipid hydroperoxide GPx
RNS	reactive nitrogen species
ROS	reactive oxygen species
SBW	signal band width
SOD	superoxide dismutase
TFA	trifluroacetic acid
Xgal	5-bromo-4-chloroindolyl-β-D-galactosidase

1.0 GENERAL INTRODUCTION

1.1 THE CATALYTIC CYCLE OF CYTOCHROME C PEROXIDASE

Cytochrome c peroxidase (CCP) was first discovered by Altschul et al. in 1940 (1) as a result of a study on the mechanism of the oxidation of ferrocytochrome c. It is a 33.8 kDa heme-containing protein with 294 amino acid residues, located in the intermembrane space of mitochondria of baker's yeast. It is also found in the periplasmic space of bacteria (2) and lately, it was observed that mitochondria of the parasite *Schistosoma mansoni* exhibit CCP activity (3). The x-ray structure of yeast CCP, which has been refined to 1.7 Å (4), reveals that it is mainly α–helical in structure (46%), and folds into two distinctly defined domains, with the heme active site situated at the domain interface (Figure 1.1).

The prosthetic group is a protoporphyrin IX heme, which is noncovalently bound to the polypeptide. It is buried ~ 10 Å away from the molecular surface presumably due to the high reactivity of the catalytic intermediates, compound I and compound II. His 175 coordinates to the heme iron giving rise to a high-spin pentacoordinate ferric enzyme. The distal pocket of CCP is lined by Arg 48, Trp 51 and His 52 (Figure 1.2). A large channel, formed at the interface between the two domains, connects the distal side of the heme crevice with the molecular surface. This channel is the only obvious route to and from the active site for peroxides and alcohol by-products (3, 5) (Figure 1.2).

The turnover of CCP follows the classical heme peroxidase mechanism (eqns 1-3).

$$P(Fe^{III}) + ROOH \longrightarrow P^{\bullet}(Fe^{IV}=O) + ROH \qquad (1)$$

$$P^{\bullet}(Fe^{IV}=O) + 1e^{-} \longrightarrow P(Fe^{IV}=O) \qquad (2)$$

Figure 1.1 Yeast cytochrome c peroxidase backbone generated from the x-ray coordinates (4) using RasMol (7). The heme is shown in bold.

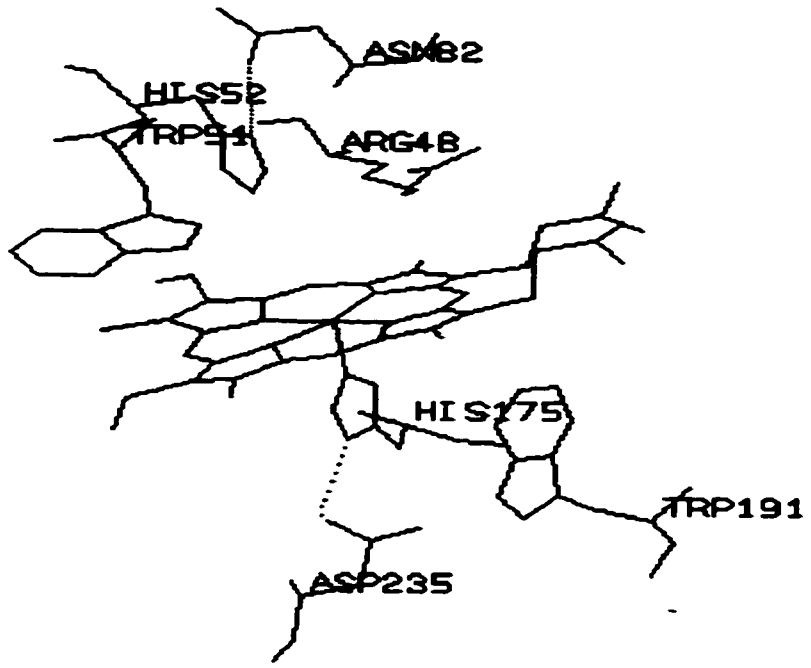

Figure 1.2 The active site of yeast cytochrome c peroxidase.

The distal pocket contains the key catalytic residues Trp 51, His 52, Arg 48. His 175 is the axial ligand of the heme iron. Asn 82 and Asp 235, which H-bond to His 52 and His 175, respectively, are also important for catalysis. Additionally, Trp 191, which is the protein radical site, is shown on the proximal side of the heme.

$$P(Fe^{IV}=O) + 1e^- + 2H^+ \longrightarrow P(Fe^{III}) + H_2O \qquad (3)$$

Compound I, [$P^{\cdot}(Fe^{IV}=O)$], which is formed in the first step, is two oxidizing equivalents above the resting ferric state. One of the oxidizing equivalents remains at the heme as $Fe^{IV}=O$ and the second is stored as a protein radical on Trp 191 (6). The proposed mechanism of compound I formation (Figure 1.3) is that first O_α of H_2O_2 coordinates to the iron heme. His 52 plays a role as an acid - base catalyst by removing a proton from O_α and transferring it to O_β. A H_2O molecule is formed as a leaving group and is expelled from the active site. Arg 48 moves towards the iron to H-bond with the oxene atom, and displaces H_2O 645, which was originally situated at the active site. The $Fe^{V}=O$ species formed upon heterolytic cleavage of H_2O_2 is rapidly converted to $Fe^{IV}=O$ by abstracting an electron from Trp 191 forming an organic radical cation on the polypeptide.

Compound I is reduced back to the resting, ferric form in two steps. One molecule of ferrocytochrome c binds to compound I and reduces the Trp radical to form compound II ($Fe^{IV}=O$). A second molecule of ferrocytochrome c binds and reduces compound II to the resting state. The catalytic cycle of CCP can be summarized by eqns 4 – 6:

$$CCP(Fe^{III}) + H_2O_2 \longrightarrow \underset{\textit{Compound I}}{CCP(Fe^{IV}=O,\ Trp191^{\cdot}) + H_2O} \qquad (4)$$

$$CCP(Fe^{IV}=O, Trp191^{\cdot}) + \text{cyt c}(Fe^{II}) \longrightarrow \underset{\textit{Compound II}}{CCP(Fe^{IV}=O) + \text{cyt c}(Fe^{III})} \qquad (5)$$

$$CCP(Fe^{IV}=O) + \text{cyt c}(Fe^{II}) + 2H^+ \longrightarrow CCP(Fe^{III}) + \text{cyt c}(Fe^{III}) + H_2O \qquad (6)$$

Figure 1.3 Proposed mechanism of compound I formation.

(a) The putative ES complex of CCP is shown where O_α of H-O-O-H is bound to the Fe^{III} ring. In this state, Trp 51 H-bonds with O_α and His 52 with O_β. The asterisk represents the active-site water molecule, H_2O 645. **(b)** His 52 donates a proton to O_β. After heterolytic cleavage of the O-O bond, Arg 48 moves forward by displacing the active site H_2O 645 and H-bonds with the oxene ligand. (C) Fe^{IV}=O center of compound I is shown, with H-bonds between the oxene ligand and both Trp 51 and Arg 48. This diagram was taken from (6).

A

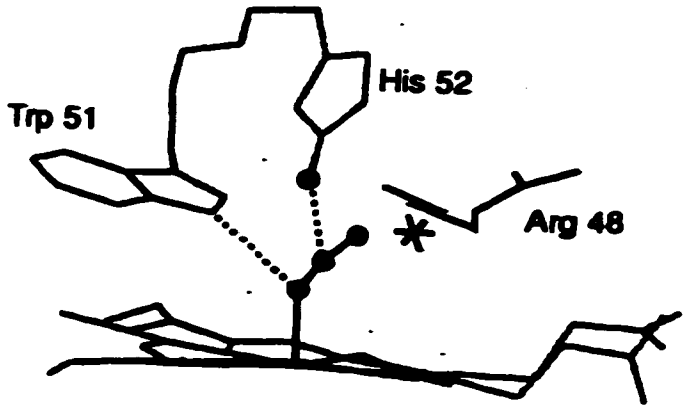

B

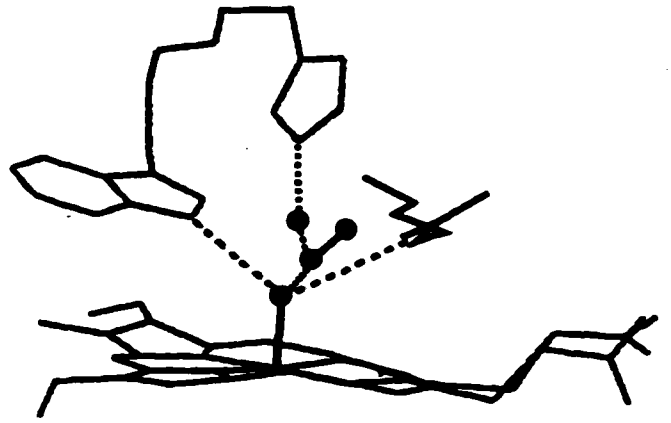

C

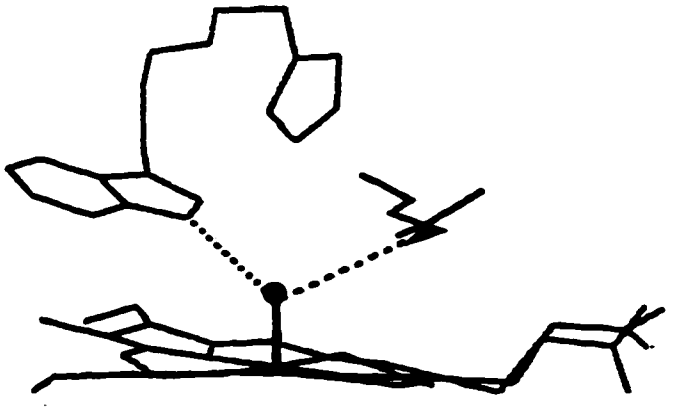

1.2 OUTLINE OF THESIS

Peroxynitrite is a reactive nitrogen species (8) that possesses the reactivity of a radical even though is not a radical itself (9, 10). Peroxynitrite has been correlated to a number of disease states because of its ability to nitrate tyrosines (9). With increasing information on the toxic powers of peroxynitrite to the cell (9), it is likely that a system is present to detoxify peroxynitrite. Considering the role of CCP as a protective enzyme in the cell (11, 12), it is of interest to establish the behavior of CCP towards peroxynitrite.

The purification method of recombinant CCP from *E. coli* available to date is time consuming (13, 14, 15). Since a future goal of our group is the preparation of many CCP mutants for intramolecular electron-transfer studies, an easier CCP purification method is desirable. Herein, we report the construction of a system which expresses and purifies CCP as a GST-CCP fusion protein, utilizing a single affinity-chromatography step.

2.0 ROLE OF CCP IN NITROSATIVE STRESS

2.1 INTRODUCTION

2.1.1 Reactive oxygen species (ROS) and antioxidants

A lot of studies have focused recently on the toxicity of oxygen to organisms. It is known that for aerobes, oxygen is essential for life but, at the same time, it can be harmful under certain conditions to the cell. Many theories existed as to the cause of oxygen toxicity but it was not until the work of McCord and Fridovich (16) that the superoxide radical ($O_2^{\cdot -}$) was actually implicated in different pathologies, a fact strongly supported by the concurrent finding of the role of superoxide dismutase (SOD) in the cell (16,17). Cu-Zn SOD was discovered and isolated in 1938 by Mann and Keilin (18). It was crystallized (19) and extensively studied (20) but its biological function remained unkown. A study on aerobic oxidation of sulfite (SO_3^{-2}) and the implication of xanthine oxidase in this, led to the discovery of superoxide radical ($O_2^{\cdot -}$) as the oxidizing species (eqns 7,8) (16, 21):

$$\text{Xanthine} + 2O_2 \xrightarrow{\text{xanthine oxidase}} \text{Uric acid} + 2O_2^{\cdot -} \quad (7)$$

$$\text{Sulfite } (SO_3^{-2}) + O_2^{\cdot -} \longrightarrow \text{Sulfate } (SO_3^{-3}) \quad (8)$$

Reduction of ferricytochrome c by xanthine oxidase under aerobic conditions and its inhibition when impurities of "other enzymes" were present, led McCord and Fridovich (16, 17) to the conclusion that SOD was the "enzyme impurity" responsible for the scavenging of the superoxide radical, the reducing agent of ferricytochrome c (eqns 9,10):

$$\text{Cyt c}(Fe^{III}) + O_2^{\cdot -} + 2H^+ \longrightarrow \text{Cyt c}\ (Fe^{II}) + H_2O \quad (9)$$

$$O_2^{\cdot -} + O_2^{\cdot -} + 2H^+ \xrightarrow{\text{SOD}} O_2 + H_2O_2 \quad (10)$$

The finding that $O_2^{\cdot -}$ is produced by some enzymes (eg, xanthine oxidase) and is efficiently scavenged by others (eg, SOD), led to the view that the superoxide radical is an agent of oxygen toxicity (16, 17, 21, 22). Support for this statement is the fact that SOD is ubiquitous in aerobes and absent in obligate anaerobes (17, 22). The superoxide radical belongs to the ROS (reactive oxygen species) family (see Table 2.1) but not all species in this family are radicals (eg, H_2O_2). Radicals are chemical species that contain one or more unpaired electrons. Due to this, radicals are generally extremely reactive, with short half lives and low steady-state concentrations (23, 24).

Molecular oxygen, is a biradical since it has two unpaired electrons in its $2\pi^*$ antibonding orbitals. Nevertheless, it is not highly reactive since these two unpaired electrons are of parallel spin. Based on the Pauli's exclusion principle, an orbital can hold two electrons and they must have opposite spins. To favor an oxidation reaction with molecular oxygen, the pair of electrons to be accepted must have spins parallel to one another but antiparallel to those of O_2. It is a very restricted situation for a pair of electrons of parallel spins to be accepted at once; thus, one electron at a time is donated to molecular oxygen which produces ROS (eqns 11-13) that are capable of becoming toxic to the cell (23, 25):

$$O_2 + e^- \longrightarrow O_2^{\cdot -} \quad (11)$$

Table 2.1 Reactive oxygen species (ROS) (8).

Radicals	Non-radicals
$O_2^{\cdot -}$, Superoxide	H_2O_2, Hydrogen peroxide
$HO_2^{\cdot}$, Hydroperoxyl[a]	HOCl, Hypochlorous acid
$OH^{\cdot}$, Hydroxyl	O_3, Ozone
$LO_2^{\cdot}$, Peroxyl	$^1\Delta_g$, Singlet oxygen
$LO^{\cdot}$, Alkoxyl	

[a] The pK_a for this species is 4.75, therefore < 1% of the total $O_2^{\cdot -}/HO_2^{\cdot}$ is present as $HO_2^{\cdot}$, at pH 7 (26).

$$O_2^{\cdot -} + e^- + 2H^+ \rightarrow H_2O_2 \qquad (12)$$

$$H_2O_2 + e^- \rightarrow HO^{\cdot} + OH^- \qquad (13)$$

$$HO^{\cdot} + e^- \rightarrow OH^- \qquad (14)$$

There are various processes that generate ROS in biological systems. In a healthy organism, radicals are necessary to carry out important biological reactions, but when the accumulation of radicals exceeds the required levels, either due to weakened antioxidant defense mechanisms or from exogenous sources, then damage is likely to occur. Exogenous sources such as tobacco smoke, ionizing radiation, air pollutants such as

nitrogen oxides (27) and metabolism of xenobiotics such as carbon tetrachloride lead to oxygen radical production.

One of the major reasons for oxygen radical production in the body is in the defense against foreign substances. Neutrophils, or polymorphonuclear leukocytes, phagocytose and destroy small organisms, especially bacteria, with the assistance of the superoxide radical. When neutrophils become activated by invading microorganisms or other stimuli, they increase their consumption of oxygen, which is commonly called a respiratory burst. Much of this oxygen is converted to the superoxide radical by an enzyme, called NAD(P)H oxidase, localized within or on the outer surface of the membrane of neutrophils. NAD(P)H serves as the reducing agent to convert molecular oxygen to superoxide radical, which is then converted to hydrogen peroxide, both spontaneously and with the help of SOD. Activated neutrophils also release myeloperoxidase (MPO) which activates H_2O_2. The product of this activation, compound I of MPO, oxidizes a variety of substrates, including Cl^- to HOCl. It seems that most of H_2O_2 produced is used to make HOCl (28) which is a very potent antimicrobial agent. HOCl can also oxidize drugs, and the oxidation of certain drugs by activated neutrophils produces chemically reactive metabolites. This process can either mediate some of the antiinflammatory effects of a drug (eg, inhibition of myeloperoxidase if inflammation is due to neutrophils) (29) or it can be responsible for some idiosyncratic drug reactions and prove lethal to the cell (24, 26).

Oxygen radicals are also produced by the oxidation of endogenous small molecules such as cathecholamines, thiols, flavins, or by the activity of some membrane bound enzymes such as lipooxygenase and cyclooxygenase. The synthesis pathway of

thromboxanes and prostaglandins, which is catalyzed by these enzymes, also involves oxygen radical production. The radicals produced provide important feedback control of prostaglandin synthesis since they have inhibitory effect on cyclooxygenase (23). Cytoplasmic proteins such as xanthine oxidase (eqn 7) and aldehyde dehydrogenase can be also considered endogenous sources of oxygen radicals (18, 26).

During normal oxidative respiration, radicals are formed in the successive reduction of molecular oxygen to water (eqns 11 – 14). If for some reason, one of the highly controlled and tightly bound radicals escapes, radical reactions are initiated and toxicity to the cell is inevitable (24). The hydroxyl radical is the most reactive oxygen radical which reacts with biological molecules with second-order rate constants in the range of $10^9 - 10^{10}$ $M^{-1}s^{-1}$ (24). The main source of $OH^{\cdot}$ production *in vivo* is the metal-catalyzed Fenton reaction (eqns 15,16) (23, 30). Reaction 17, which was first studied by Haber and Weiss (31) and is called the Haber-Weiss reaction, can also produce $OH^{\cdot}$. However, in aqueous solution the bimolecular rate constant is virtually zero, especially *in vivo* where the steady-state concentrations of $O_2^{\cdot -}$ and H_2O_2 are low. Because equation 17 is the sum of equations 15 and 16, it is often called the metal ion-catalyzed Haber-Weiss reaction (30).

$$O_2^{\cdot -} + Fe^{III} \rightarrow O_2 + Fe^{II} \qquad (15)$$

$$Fe^{II} + H_2O_2 \rightarrow Fe^{III} + OH^- + OH^{\cdot} \qquad (16)$$

$$O_2^{\cdot -} + H_2O_2 \rightarrow O_2 + OH^- + OH^{\cdot} \qquad (17)$$

Even though radicals have such a short half life and thus a short radius of action,

they are toxic because their action is propagating. When a radical oxidizes a compound, another radical is produced and a chain reaction is generated. If important biological molecules such as lipids, nucleic acids and proteins are oxidized, much damage can be caused. Lipid peroxidation for example, disrupts the function of the cell membrane by altering its shape and fluidity (30 ,32). The mechanism of lipid peroxidation is shown in Scheme 1. A peroxy radical ($x^{\cdot}$) removes a hydrogen from a methylene carbon in polyunsaturated fatty acids, which leads to carbon radical formation. Rearrangement produces a conjugated diene radical which reacts with O_2 to form a lipid peroxy radical. This species can either react with another polyunsaturated lipid (LH) and propagate the reaction or it can form an endoperoxide radical which will give rise to toxic end products such as organic oxygen radicals and short-chain products (23 ,30). Organic oxygen radicals formed from lipid peroxidation, alcoxyl ($LO^{\cdot}$) and peroxyl ($LO_2^{\cdot}$) radicals are able to damage molecules other than polyunsaturated fatty acids, and thus enhance and propagate the initial reaction shown in Scheme 1 (25). Additionally, hydroperoxides, alcohols and aldehydes, all possible byproducts of lipid peroxidation, can inhibit protein synthesis as shown in studies on rat liver microsomes. How protein inhibition is related to the presence of lipid peroxidation byproducts can be explained by the action of 4-hydroxyalkenals on the cell. 4-Hydroxyalkenals (products of lipid peroxidation) are electrophilic reagents which react with nucleophiles in a similar way to alkylating agents. Since the strongest tissue nucleophile is the sulfhydryl anion RS^{-} of low molecular weight thiols such as glutathione or protein-bound cysteines, it can be concluded that the deleterious effects of 4-hydroxyalkenals are due to electrophilic attack on essential SH groups (23, 33).

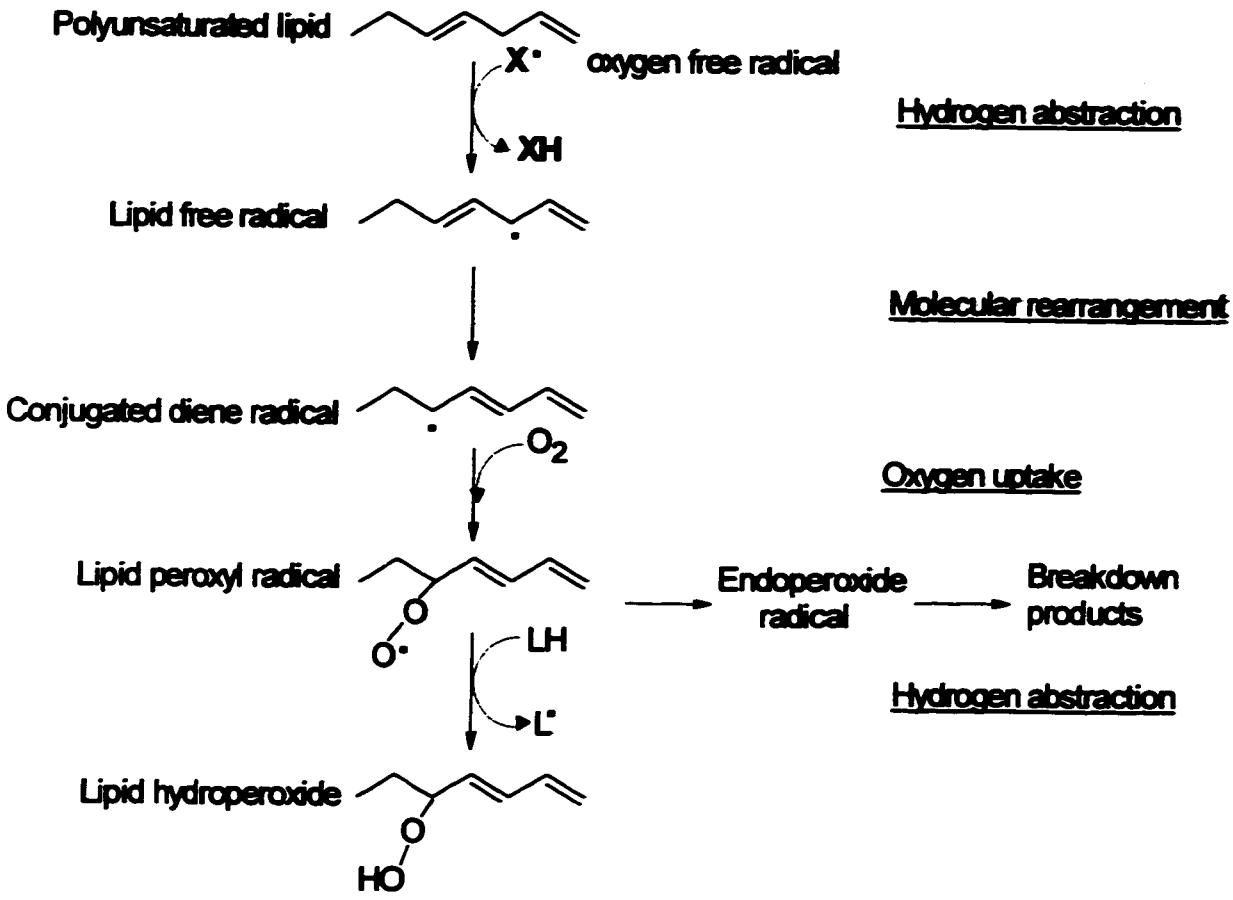

Scheme 1 Mechanism of lipid peroxidation reactions. Scheme was adapted from (23). X˙ = peroxyl radical, LH = polyunsaturated lipid.

Oxidized proteins become more sensitive to proteolysis. Radicals prefer amino acids with sulfur groups, cysteine and methionine, or unsaturated side chains such as tyrosine, phenylalanine, histidine and tryptophan (34, 35). Reactions of oxygen radicals with the specified amino acids cause structural disturbances, crosslinking and eventual aggregation of proteins (23, 24, 25). Nucleic acid damage by radicals *in vivo* involves alteration of thymine and cytosine bases mostly. The deoxyribose sugar and adenine base are attacked to a lesser extent.

Destruction of the basic molecular units in an organism leads to pathological conditions. Some of the diseases that involve radical damage are rheumatoid arthritis, atherosclerosis, cancer, Parkinson's disease, aging, and Alzheimer's disease. Organisms have developed a number of antioxidant defense mechanisms. These are different depending on whether they are involved in protection inside or outside the cell. Intracellular protection seems to be the most important since oxygen utilization occurs within the cell. Defense mechanisms within cells include enzymes that can bind and scavenge reduced oxygen species such as superoxide radical or hydrogen peroxide. Even though iron could facilitate the Fenton reaction (eqn 16), a low iron pool is maintained by the cell because iron is necessary for the activity of protective enzymes such as catalase and superoxide dismutase, as well as for all the heme proteins and enzymes vital to the normal function of the cell such as the cytochromes located in mitochondria (25, 30). Any internal iron not required by the cells is stored in ferritin which has a capacity of up to 4500 mol of iron/mol of protein (30).

The hydrophobic interior of membranes generates different radicals from those found in the aqueous environment of the cytosol. Therefore, different antioxidants are

required, but mostly it is the "structural organization" of membranes that seems to be important for their protection since the higher the degree of unsaturation of the polyene, the greater the susceptibility to oxidation (26). Therefore, correct ratios of phospholipid to cholesterol, as well as the type of phospholipid, can prove essential for the survival of the membrane (25).

The source of oxygen radicals in the extracellular space arises mainly from activated neutrophils and substrate oxidations. Thus, in the extracellular space, protection is achieved by completely depleting the area from reactive transition metals such as iron. This is done again with the help of ferritin. Lactoferrin is also important since it serves the same role as ferritin. While the area is depleted from iron and thus the Fenton reaction (eqn 16) is inhibited, we would expect that no $O_2^{\cdot -}$ will be present. Nevertheless, levels of $O_2^{\cdot -}$ and H_2O_2 are necessary and have to remain constant since $O_2^{\cdot -}$ is important as signaling molecule between cells, and H_2O_2 induces platelet aggregation (25).

Defense mechanisms can be categorized as primary defense and secondary defense mechanisms (23). Primary defense mechanisms scavenge radicals at the site of production, thus, reducing their concentration, which in turn decreases the initiation rate of radical reactions. On the other hand, secondary defense mechanisms trap the propagator radicals and stop the progress of their harmful effects at an early stage. Enzymes such as SOD, catalase and glutathione peroxidase (GPx) are part of the primary defense mechanisms. SOD is found both in mitochondria and the cytosol at sites where oxidative metabolism is taking place. Its function is to protect the cell against oxidative

injury by converting superoxide radicals into lower-energy forms of oxygen (i.e. H_2O_2) (eqn 10) (25).

Catalase is a special kind of peroxidase in the sense that it uses H_2O_2 both as an oxidizing and reducing substrate (5):

$$2H_2O_2 \longrightarrow 2H_2O + O_2 \qquad (18)$$

Its major biological function appears to be the prevention of H_2O_2 build up. As outlined in Section 1.1, peroxidases usually catalyze heterolysis of the RO-OH bond (where R = H or an alkyl group) and are capable of storing both oxidizing equivalents at their active center for utilization in the oxidation of a variety of substrates ranging from halogens to small proteins, depending on the function of each specific peroxidase (5). Compound I is the catalytic intermediate in which the two oxidizing equivalents of peroxide are stored. One is stored as oxyferryl ($Fe^{IV} = O$) heme iron and the other in the form of a radical, either on the porphyrin ring or the polypeptide (eqns 1 - 3). Upon binding of a reducing substrate to the active site of the peroxidase, the radical site is reduced and thus, compound II is formed. Another molecule of reducing substrate is needed to convert compound II to the resting form of the peroxidase (eqns 1 – 3) (5, 6). The role of a peroxidase depends on the nature of the donor molecules in eqns 2 and 3.

MPO is considered an enzyme important for defense since it uses Cl^- as a reducing substrate to produce HOCl, which is a potent antimicrobial agent. This is due to its strong oxidizing and chlorinating properties; it reacts with a variety of biological compounds including sulfhydryls, aromatic and aliphatic amino acids and nitrogen containing compounds. Glutathione peroxidase (GPx), a selenium containing enzyme, offers important protection to the cell against oxidative stress by scavenging

reactive oxygen species at the expense of reduced glutathione. Two forms of glutathione peroxidase have been identified; the cytosolic GPx utilizes H_2O_2 whereas PLGPx (phospholipid hydroperoxide glutathione peroxidase) is specific for organic hydroperoxides and thus, protects biological membranes against lipid peroxidation (36). Animals and humans in natural settings consuming Se-deficient diets have a significant reduction of GPx activity. In a wide variety of tissues, GPx decline is accompanied by an increase in tissue peroxide levels and disease states, a fact that underlines the importance of glutathione peroxidase as an antioxidant enzyme (36).

Enzymes such as horseradish peroxidase (HRP) and CCP, do not have a clearly defined function. HRP is a plant peroxidase which oxidizes aromatic molecules including indole plant growth hormones. Depending on the substrate, it can go through the classical peroxidase cycle (eqns 1 – 3), but it can also carry out a two-electron substrate oxidation (eqns 19 - 20) when, for example, the reducing substrate is iodide (37).

$$HRP + H_2O_2 \longrightarrow HRP\text{-}I + H_2O \qquad (19)$$

$$HRP\text{-}I + I^- \xrightarrow{H^+} HRP + HOI \qquad (20)$$

It is very difficult to establish a single role for HRP in the plant cell since it uses a variety of substrates, and its catalytic turnover is dependent on the choice of substrate. On the other hand, CCP, a yeast mitochondrial protein, exhibits high specificity for ferrocytochrome c as the reducing substrate (1) and it has been shown that it is important for defense against oxidative stress (38).

2.1.2 Reactive Nitrogen Species (RNS) and antioxidants

In addition to oxygen, nitrogen is also abundant and important in life. It is incorporated into all of the major classes of biomolecules, the basic building units of our system (8). However, it is only recently that a physiological role has been recognized for RNS (reactive nitrogen species) (Table 2.2) (8). One of the best known RNS and most widely discussed, due to its importance and broad range of action, is $NO^{\cdot}$. It is used by the cell mainly as a messenger (41). Its hydrophobic nature enables it to readily diffuse out of the cell where it is produced, to neighboring cells. It has a short half-life of 5-6 seconds and for this reason, it reacts locally. $NO^{\cdot}$ is converted to nitrites and nitrates by H_2O and oxygen in aqueous solution (eqns 21 – 22) (42 ,43):

$$2\,NO^{\cdot} + O_2 \longrightarrow 2\,NO_2^{\cdot} \qquad (21)$$

$$2\,NO_2^{\cdot} + H_2O \longrightarrow NO_2^{-} + NO_3^{-} + 2\,H^{+} \qquad (22)$$

Acetylcholine, histamine and bradykinin are vasolidators that activate endothelial cells to release a hormone called EDRF (endothelium-derived relaxing factor). EDRF causes muscle relaxation by binding to the iron heme of soluble guanylate cyclase and increasing cGMP production (44). Furchgott, suggested that the EDRF was actually $NO^{\cdot}$ (45). Based on this suggestion, researchers were able to prove that $NO^{\cdot}$ is identical to EDRF in biological activity, stability and susceptibility to inhibitors and potentiators (43). It was a shock to many scientists that a toxic gaseous molecule in the atmosphere is actually used as a messenger in nature (41). $NO^{\cdot}$ as a messenger molecule regulates immune function, causes blood vessel dilation and also inhibits platelet aggregation (42,

Table 2.2 Reactive nitrogen species (RNS) (8).

Radicals	Non-radicals
$NO^{\cdot}$, Nitric oxide	HNO_2 , Nitrous acid[a]
$NO_2^{\cdot}$, Nitrogen dioxide	N_2O_3 , Dinitrogen trioxide
	N_2O_4 , Dinitrogen tetroxide
	$ONOO^-$, Peroxynitrite[b]
	LOONO , Alkyl peroxynitrites

[a] $pK_a = 3.15$ (39).
[b] $pK_a = 6.9$ (40).

46, 47). $NO^{\cdot}$ is synthesized *in vivo,* by NO synthase (NOS) by the deamination of one of the two chemically equivalent amino groups of L-arginine (42, 46). There are at least three different forms of NO synthase including macrophage or inducible (iNOS), endothelial (eNOS) and neuronal NOS (nNOS). The location of NOS clearly identifies its function; thus, iNOS is responsible for defense, eNOS regulates muscle relaxation and vassal dilation and nNOS occurs in nerve fibers and functions as a neurotransmitter (47). The constitutive enzymes, found in blood vessels and neurons (eNOS and nNOS), are Ca^{+2}/calmodulin dependent and produce low levels of NO whereas, iNOS, found mainly in macrophages and neutrophils, is calmodulin independent. Both the constitutive and

inducible type of NOS are dependent on NADPH levels (46, 47).

Even though $NO^{\cdot}$ is highly important, excess can cause problems, such as glycolysis inhibition, mitochondrial respiratory-chain blockage or DNA replication abortion (8). The toxic effects can be, for example, the result of direct binding of $NO^{\cdot}$ to mitochondrial cytochrome c oxidase, or can be caused indirectly from a toxic product formed between $NO^{\cdot}$ and $O_2^{\cdot -}$, peroxynitrite ($ONOO^-$) (15):

$$NO^{\cdot} + O_2^{\cdot -} \longrightarrow ONOO^- \qquad (23)$$

Indirect evidence that this radical – radical coupling reaction occurs *in vivo* comes from the fact that in activated neutrophils, where superoxide production is enhanced, platelet aggregation is increased (indicating that $NO^{\cdot}$, which would normally inhibit platelet aggregation, has been depleted). But when SOD is present (which scavenges $O_2^{\cdot -}$), normal inhibition of platelet aggregation is evident, proving that $NO^{\cdot}$ levels have been restored. This indicates that $O_2^{\cdot -}$ inactivates $NO^{\cdot}$ (46). Reaction (23) is first-order in both $NO^{\cdot}$ and $O_2^{\cdot -}$ concentration, with a rate constant of $6.7 \times 10^9\ M^{-1}s^{-1}$, which is near the diffusion-controlled limit (48). Thus, $ONOO^-$ formation competes with the rate of $O_2^{\cdot -}$ dismutation by SOD which has a rate constant of $2 \times 10^9\ M^{-1}s^{-1}$ (22, 49). The relative concentrations of $O_2^{\cdot -}$ and $NO^{\cdot}$ radicals appear to be critical in sites where both coexist, such as sites of tissue injury. The balance between them seems to be the key determinant of whether an injury will be repaired or result in chronic inflammation (8).

Even though $ONOO^-$ is not a radical, its presence has been correlated with

pathological conditions such as Parkinson's disease, rheumatoid arthritis and Alzheimer's disease (9). $ONOO^-$ is highly reactive and its targets consist of a broad range of functional groups. Some of its main reactions identified so far are the oxidation of sulfhydryls (50), enzymes with iron/sulfur centers, peroxidases (46), and zinc-thiolate centers (51). It can also react with lipids, and nucleotides causing DNA strand breaks or mutations. However, nitration of phenols, especially tyrosines, appears to be one of the most damaging reactions carried out by $ONOO^-$ since it can affect the phosphorylation levels of key enzymes in signaling pathways or block the polymerization of structural proteins like actin in assembling vital filaments of the cytoskeleton (9). The latter arises because nitration of tyrosine decreases the pK_a of tyrosine from 10 to about 7.5, creating a negatively charged hydrophilic residue that disrupts subunit interactions.

Peroxynitrite is an isomer of nitrate but is 36 kcal/mol higher in energy. $ONOO^-$ is unusually stable in alkaline buffer due to the fact that at high pH, it is found in the cis conformation (9, 52). In this conformation, the negative charge is distributed over all 4 atoms (see Scheme 2). Because of the charge delocalization over the entire molecule, a weak partial bond is formed between the terminal oxygens which has the strength of a H-bond. This is revealed by *ab initio* quantum mechanical calculations based upon the cis isomer in the gas phase (10) (Scheme 2). Also, the terminal oxygen is restricted from approaching nitrogen, which is necessary if nitrate is to be formed. When peroxynitrite becomes protonated, it isomerizes to the trans conformation. Protonation destroys the negative charge and lowers the energy barrier for the interconversion from the cis to trans conformer from 30 to 13 kcal/mol (9, 52). The terminal peroxide oxygen

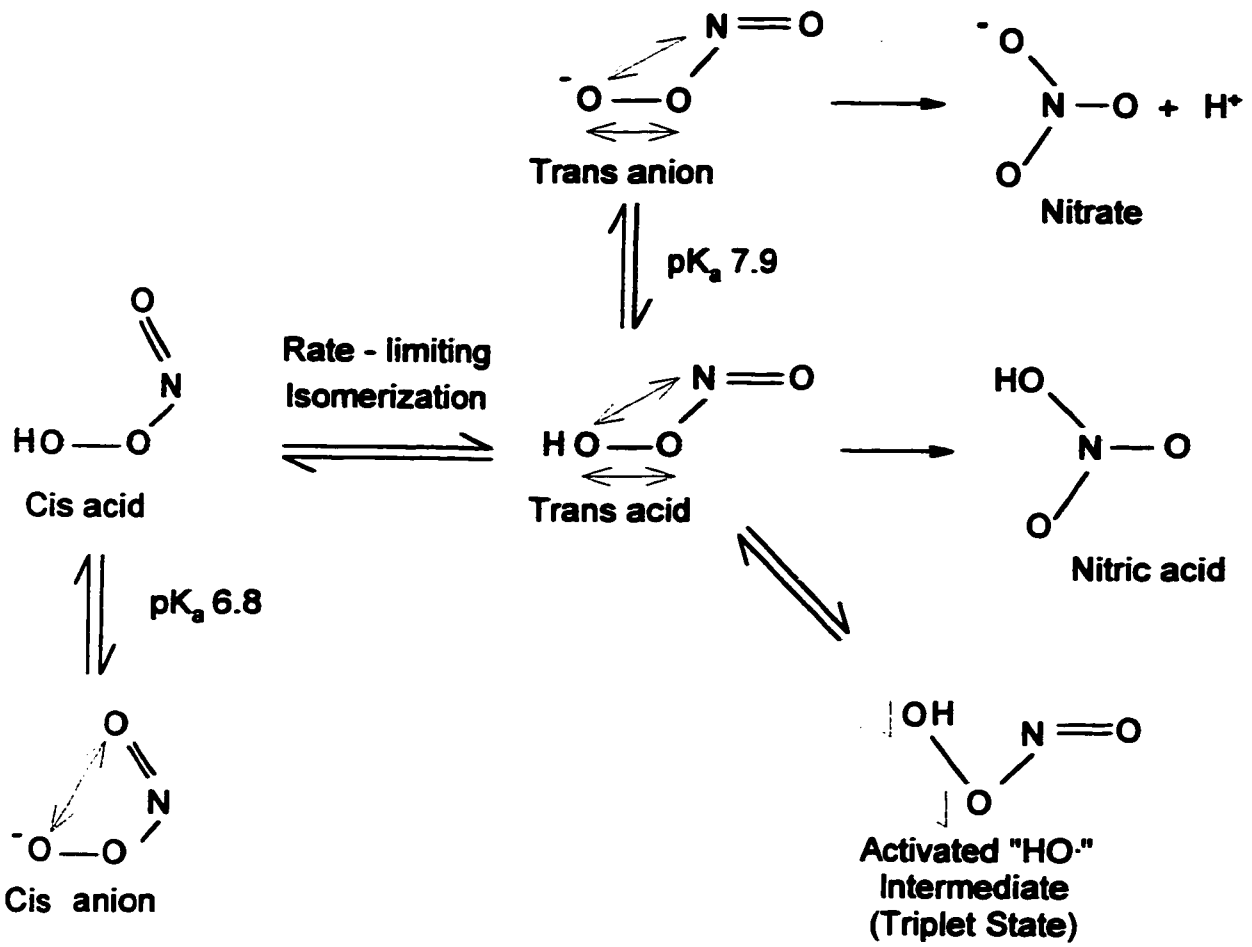

Scheme 2 Decomposition and reactivity of peroxynitrite as a function of pH (9, 52, 53). Idendification of cis and trans forms of the anion is based on gas-phase calculations (10).

can approach the nitrogen by O-O bond stretching and N-O-O bond bending in both trans peroxynitrite anion and trans peroxynitrous acid, to form nitrate and nitric acid, respectively, via internal rearrangement (Scheme 2) (53). Trans peroxynitrous acid reportedly can become vibrationally activated to form a triplet state which possesses a reactivity similar to the $HO^{\bullet}$ radical (9, 10). This suggests that peroxynitrite may effectively form a biradical which contributes to its ability to initiate radical reactions even though it is not a radical itself (9, 10). The hydroxyl radical-like reactivity of peroxynitrite decreases at alkaline pH with an apparent pK_a of 8.0, as was revealed by the decrease in the concentration of the oxidation products derived from the reaction of peroxynitrite with $ABTS^{+}$ at alkaline pH (10, 53). Thus, the toxicity and reactivity of $ONOO^{-}$, as well as its decomposition, are functions of its conformation and, the pH of the solution.

A more recent analysis of the mechanism of action of peroxynitrite at physiological conditions exists (54). Implicit in the newer treatment is that the solvated cis and trans anions have similar energies. This analysis takes into consideration three possible forms of peroxynitrite, the anion ($ONOO^{-}$), the acid (ONOOH) and the activated acid (ONOOH*) (Scheme 3 and Table 2.3). The reactions of the activated acid resemble those of the $HO^{\bullet}$ radical since both are zero-order in biotarget and are also one-electron oxidation reactions. Nevertheless, this can not be the most important reaction of peroxynitrite *in vivo* because the rate of formation of the activated acid is slow (Table 2.3). The rate-determining step for the conversion of the ground-state acid to the activated form, has a rate constant of 0.9 s^{-1} at 37°C (pH 7.4), which is close to the rate of

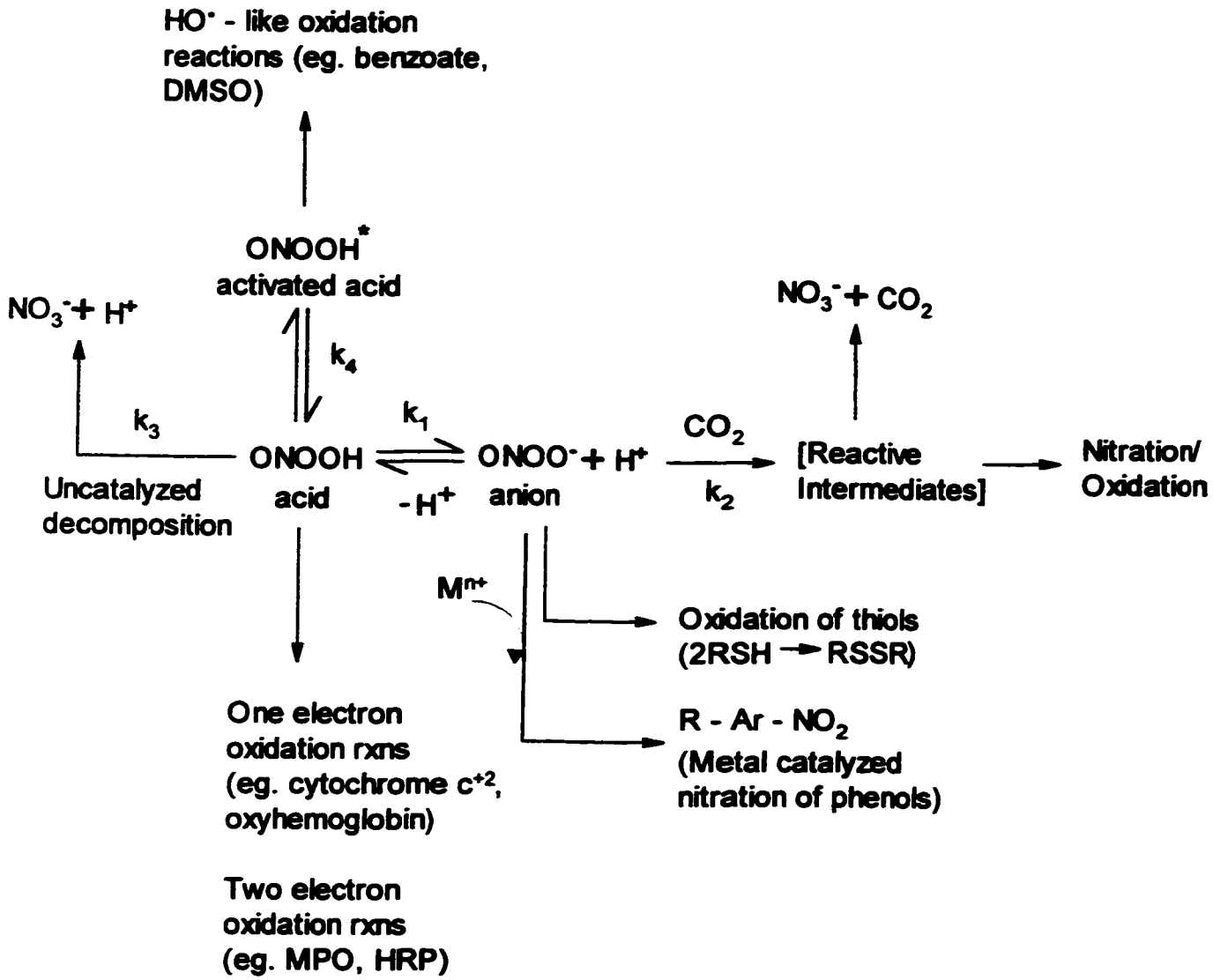

Scheme 3 Schematic representation of the proposed reactivity of peroxynitrite under physiological conditions (46, 47). Values of rate constants are given in Table 2.3.

Table 2.3 Rate constants for the reactions of peroxynitrite

Reactions			rate constants
1). ONOOH	$\longleftrightarrow$	$ONOO^- + H^+$	$k_1 = 2.21 \times 10^4\ s^{-1}$ $k_{-1} = 1.4 \times 10^{11}\ M^{-1}s^{-1}$
2). $ONOO^- + CO_2$	$\longrightarrow$	Reactive[a] Intermediates	$k_2 = 3 \times 10^4\ M^{-1}s^{-1}$
3). ONOOH	$\longrightarrow$	$NO_3^- + H^+$	$k_3 = 1.38\ s^{-1}$
4). ONOOH	$\longrightarrow$	$ONOOH^*$	$k_4 = 0.9\ s^{-1}$

[a] See Scheme 4.

the decay of peroxynitrite ($1.38\ s^{-1}$) (54, 55).

The rates of the reaction of the anion and the acid are dependent on the concentration of the biological target, (the opposite of the reaction of the activated acid, where it is zero-order in substrate) (54). Based on this analysis, most of the toxic effects of peroxynitrite *in vivo* should come from the reaction of the anion with CO_2, which is present at concentrations as high as 1 mM in tissues (Scheme 3 and 4). The nitrosoperoxicarbonate intermediate produced from this reaction is a much more potent nitrating agent than either $ONOO^-$ or $NO^\cdot$ (54, 56, 57). CO_2 reacts preferentially with the anion, $ONOO^-$, with a rate constant of $3 \times 10^4\ M^{-1}s^{-1}$ at physiological pH. The pH-independent value is $5.8 \times 10^4\ M^{-1}s^{-1}$, which gives a reactivity product for $[CO_2] = 1$ mM

of 58 s^{-1} (54, 55, 58). Scavengers that react directly with $ONOO^-$ must match or exceed the reactivity product of CO_2. Since most scavengers reach toxic levels at concentrations $\geq$ 1mM, in order to trap $ONOO^-$ they must do so with a second-order-rate constant higher than 10^4 $M^{-1}s^{-1}$. None of the common antioxidants available *in vivo* (eg, urate, ascorbate or glutathione) can compete with CO_2 for peroxynitrite. Only ebselen, a synthetic seleno compound with peroxidase activity, can compete with CO_2 since it is shown to react with $ONOO^-$ with a rate constant equal to 2 x 10^6 $M^{-1}s^{-1}$ at pH 7.4, 37 °C (59).

The products of the reaction of CO_2 with $ONOO^-$ could attack biological molecules and nitrate tyrosines by two possible routes (54). One involves a radical mechanism and the other a non-radical mechanism. Since the radical mechanism is more consistent with the observed yields of nitrotyrosine, it is considered as the most probable route for nitrotyrosine formation, and for this reason, is presented in Scheme 4. Homolysis of the O-O bond of the nitrosoperoxycarbonate intermediate yields $NO_2^{\cdot}$ and $CO_3^{\cdot-}$ as caged radicals. These can escape and $^{\cdot}NO_2$ can nitrate phenolic groups as presented in Scheme 4 (54). Reduction of these radicals would explain some of one-electron oxidations that have been attributed to $ONOO^-$, such as sulfhydryl oxidation and lipid peroxidation. Another reduction pathway for the nitrosoperoxycarbonate intermediate is rearrangement to form nitrocarbonate which further hydrolyzes to nitrate, the uncatalyzed decomposition product of peroxynitrite (Scheme 4).

Transition metals may also be important catalysts of nitration of phenolic groups by $ONOO^-$. Metal ions, more electropositive than the hydrogen ion, pull electron

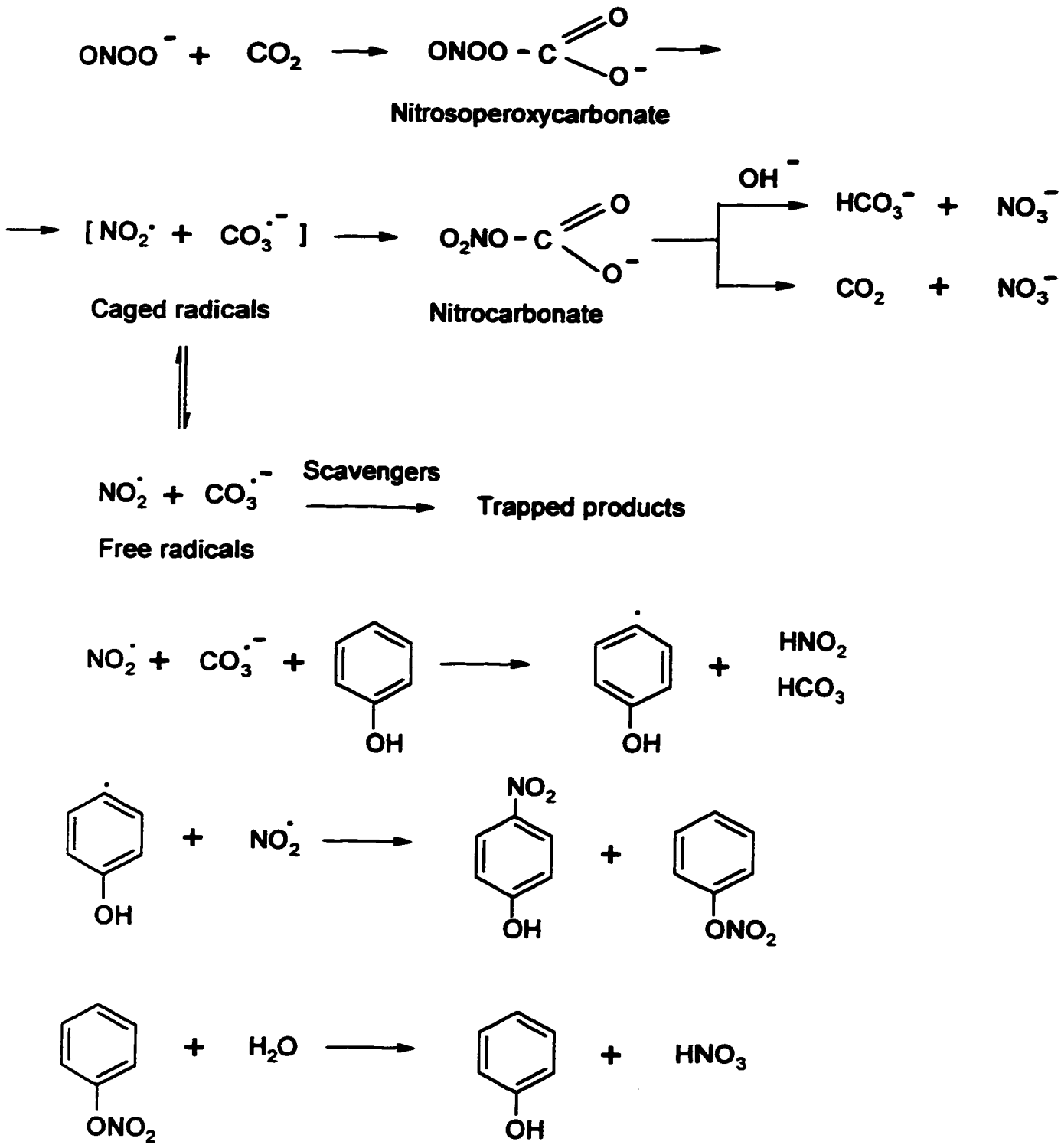

Scheme 4 Reaction of peroxynitrite anion with CO_2 and subsequent reactions of nitrosoperoxidase (54).

density towards them which will favor heterolytic cleavage of the O-O bond (9, 52). The nitronium ion produced will nitrate phenols or tyrosines (eqns 24-25).

$$Mn^{+} + ONOO^{-} \longrightarrow Mn\text{-}O^{\delta-}\cdots ONO^{\delta+} \qquad (24)$$

$$Phenol + NO_2^{+} \longrightarrow Phenol\text{-}NO_2^{+} \longrightarrow$$

$$\longrightarrow Nitrophenol + H^{+} \qquad (25)$$

Metal centers bound in proteins can catalyze nitration by $ONOO^{-}$. For example, it was shown that Cu,Zn SOD catalyzes the nitration of phenols with a rate constant of 1×10^5 $M^{-1}s^{-1}$ at 37° C (pH 7.4), which should compete with the reaction between CO_2 and $ONOO^{-}$ *in vivo* and hence contribute to the apparent toxicity of SOD in high dosages to the ischemic heart (52).

To summarize, of the three forms of peroxynitrite in Scheme 3, the activated acid is not of biological importance due to its slow formation. Thus, the acid and the anion forms are these that need to be scavenged. The acid reacts faster than the anion with most cellular antioxidants and peroxidases [eg, ferrocytochrome c (60), MPO, HRP (46), methionine, cysteine, ascorbate, tryptophan (59)]. Conversion of the anion to the toxic nitrosoperoxycarbonate intermediate is fast [$k_2 = 3 \times 10^4$ $M^{-1}s^{-1}$ (58)], and the search for possible scavengers that compete with CO_2 *in vivo* lead to glutathione peroxidase (GPx), since ebselen, a mimic of GPx, was shown to scavenge $ONOO^{-}$ very efficiently (59). Sies et al. (61) suggested that GPx protects the cell from peroxynitrite toxicity whereas Padmaja et al. (62) postulated that peroxynitrite inactivates GPx. Despite contradicting conclusions, both groups agree that the reaction of peroxynitrite with GPx generates a form of the enzyme that is not an intermediate in the normal catalytic cycle of the

enzyme. The second-order rate constant for the reaction of GPx with peroxynitrite at pH 7 is close to the rate of CO_2 adduct formation [$1.8 \pm 0.1 \times 10^4$ $M^{-1}s^{-1}$ (62) vs 3×10^4 $M^{-1}s^{-1}$(58), respectively] but the concentration of GPx in cells is ~ 1 μM, 10^3 times lower than that of CO_2. Thus, GPx is unlikely to effectively scavenge peroxynitrite *in vivo*.

The only biotargets identified so far that can compete with CO_2 for peroxynitrite are heme-containing proteins such as hemoglobin (63), or peroxidases such as MPO, LPO and HRP which react with peroxynitrite with apparent second-order rate constants equal to 6.2×10^6, 3.3×10^5 and 6.4×10^5 $M^{-1}s^{-1}$, respectively, at pH 7.4 (eqns 26-29) (46):

$$MPO + ONOOH \longrightarrow MPO\text{-}I - - NO_2^- \qquad (26)$$

$$MPO - - NO_2^- \longrightarrow MPO\text{-}II + NO_2^{\bullet} \qquad (27)$$

These rate constants are highly pH dependent since the acid form (ONOOH) actually binds to heme peroxidases (46).

Upon reaction with peroxynitrite, MPO is assumed to form compound I. The nitrite produced stays in the active site and quickly reduces compound I to compound II (eqns 26, 27) (46). The $NO_2^{\bullet}$ formed is as toxic as peroxynitrite but such an end product is not undesirable since MPO has an established role in the defensive mechanism of the cell (36 ,64). The $NO_2^{\bullet}$ released in reaction 27 can nitrate tyrosines (Scheme 4). Nitrotyrosine formation is a phenomenon linked to many human diseases and inflammation (9). It is interesting to note that a recent study has shown that MPO also nitrates tyrosines via $NO_2^{\bullet}$ formed from free NO_2^- (Scheme 5) (65). Extracellular or

intracellular NO_2^- can be used by MPO in activated neutrophils or macrophages to convert compound II into native MPO with the release of $NO_2^{\cdot}$. Furthermore, HOCl, the product of Cl^- oxidation by MPO compound I, reacts with free NO_2^- to generate NO_2Cl which is a very potent chlorinating agent. These results indicate that nitrotyrosine should not be considered a specific marker of peroxynitrite formation, but as an indicator for the involvement of RNS (65). With these findings, MPO is again shown to be a defensive rather than protective enzyme in the cell.

HRP also forms compound I and NO_2^- upon reaction with peroxynitrite, but NO_2^- escapes the active site before returning to undergo one-electron oxidation with consequent formation of compound II and the release of $NO_2^{\cdot}$ (eqns 28 ,29) (46):

$$\text{HRP} + \text{ONOOH} \xrightarrow{\text{fast}} \text{HRP-I} + NO_2^- \qquad (28)$$

$$(NO_2^- + H^+ \longrightarrow \text{HONO}) \qquad (29)^1$$

$$\text{HRP-I} + \text{HONO} \xrightarrow{\text{slow}} \text{HRP} + NO_2^{\cdot} + H^+ \qquad (30)$$

Based on its observed *in vitro* reactivity (46), HRP is unlikely to protect the cell from the toxicity of peroxynitrite.

[1] pK_a of HONO is 3.15 therefore, most of NO_2^-/HONO will be in the anion form at physiological conditions.

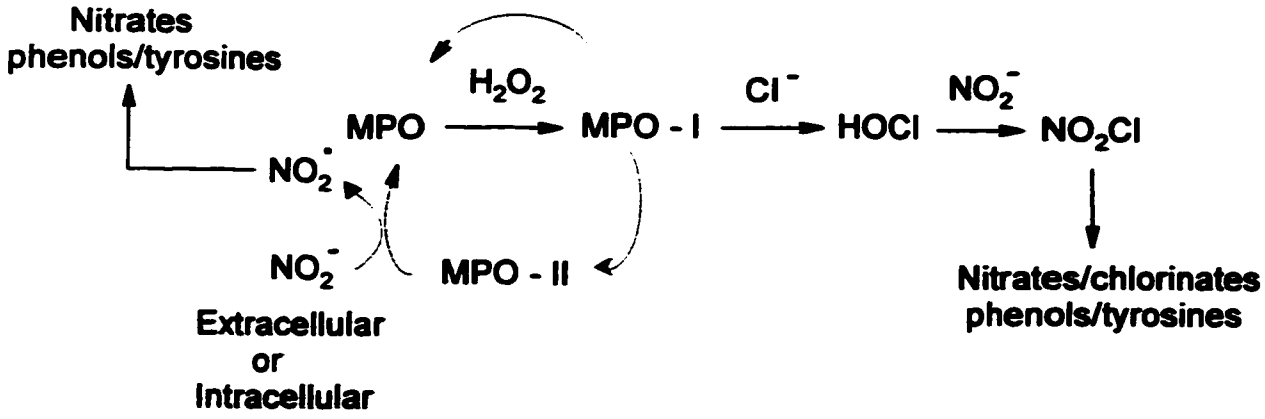

Scheme 5 Reactions showing how free NO_2^- enhances the nitrating/chlorinating effect of MPO (65).

2.1.3 Role of CCP in the cell

Interest in oxidative stress originates from our need to understand the role of oxidants in diseases such as cancer, reperfusion injury and even aging. It is known that defense mechanisms have evolved to allow high concentrations of oxygen to be tolerated. A better understanding of how these mechanisms are regulated upon oxidative stress and which enzymes are involved in the protective response of the cell against oxidant exposure will help us to understand the functioning of the cell under such conditions and will allow us to develop ways to overcome disease states when necessary.

Bacterial studies have focused attention on transient adaptive responses to high

doses of H_2O_2. These responses involve induction of a series of defense and repair enzymes (66). Some studies were also performed in yeast, which represents an ideal eukaryotic model to study cellular redox control and ROS metabolism because it has the same defense mechanisms as higher eukaryotes and most importantly, because of the availability of the complete sequence of its genome (67).

Saccharomyces cerevisiae, when pretreated with small doses of H_2O_2, adapts and protein synthesis is induced. This allows the cell to become resistant to higher H_2O_2 concentrations, which under normal conditions would have been lethal to the cell (68). Yeast mutants deficient in SOD or catalase, or with low glutathione levels, all important scavengers of H_2O_2, showed the same behavior as wild-type strains upon oxidative stress suggesting that the mutant yeast strains examined have compensatory antioxidant mechanisms other than the ones already established (69).

Our suspicion was that CCP is one such compensatory mechanism (6). Even though the function of CCP in the cell is still debated, it was found that upon incubation of *S. cerevisiae* with H_2O_2, the levels of CCP increased (38), which underlines its role as a primary antioxidant defense enzyme. Other proteins directly related to the cellular antioxidant defense (eg. glutathione reductase, cytosolic catalase and Cu/Zn and Mn SOD's), together with heat shock proteins, proteases, proteasome subunits, and enzymes involved in carbohydrate and amino acid metabolism were also over-expressed. This indicates that there is a H_2O_2 stimulon in yeast that coordinates the regulation of all these proteins in response to the peroxide concentrations in the cell, and that these proteins are important in the redox-control mechanisms of the cell (38). The fact that a catalase-negative yeast strain was able to decompose H_2O_2, and at the same time possessed high

CCP activity, suggests that mitochondrial peroxide decomposition occurs via CCP (11). In a very recent study in our lab, the growth curves of a CCP-deficient *S. cerevisiae* strain were compared to those of the wild-type strain (12), and it was found that indeed CCP protects *S. cerevisiae* from H_2O_2-induced stress throughout the growth cycle. In exponential phase, CCP protection is shown to be direct, but in stationary phase, CCP seems to protect the cell indirectly by controlling the regulation of antioxidant enzymes such as catalase and GPx (12).

With increasing evidence that peroxynitrite is toxic, interest in identifying possible peroxynitrite reductases has increased. Studies to date have focused on peroxidases as possible peroxynitrite scavengers (46, 51, 52, 61, 62, 70), and reveal that MPO, HRP and LPO all possess peroxynitrite-reducing activity (46). Bearing in mind the role that CCP plays in the cell, it is interesting to determine whether CCP will also behave as a peroxynitrite reductase. We considered this highly likely since the other heme peroxidases, most notably HRP, react with peroxynitrite (46). HRP and CCP have very similar active sites and catalytic mechanisms (6). In addition, peroxynitrite (O=N-O-O-H) can be considered an inorganic peroxide which suggests that it should bind to ferric form of CCP, unless the substitution of H by NO results in steric repulsion. Assuming that the latter is not the case, we expect that upon titration of CCP with peroxynitrite, compound I or compound II will be detected.

Possible reactions are:

$$\text{CCP} + \text{ONOO(H)} \longrightarrow \text{compound I} + NO_2^- \quad (31)$$

$$\text{compound I} + NO_2^- \longrightarrow \text{compound II} + NO_2^{\cdot} \quad (32)$$

Or if compound II is directly formed upon reaction of CCP with peroxynitrite (eqn 33),

$$CCP + ONOO(H) \longrightarrow \text{compound II} + NO_2^{\bullet} \quad (33)$$

$NO_2^{\bullet}$ would be released. Since $NO^{\bullet}$ is a strong nitrating and oxidating agent (Scheme 4) reaction (33) would not be consistent with the protective role of CCP in the cell. If compound I is observed (eqn 31) then the question is whether (and how fast) it oxidizes NO_2^- (eqn 32). On reaction with peroxynitrite, MPO does not release NO_2^- and compound II is observed rather than compound I (eqns 26-27) (46). This is not surprising since Cl^- is a reducing substrate for MPO, indicating that an anion binding site exists close to the enzyme active site, and $NO_2^{\bullet}$ production supports its function as a defensive enzyme in the cell. HRP, which is not considered a defensive enzyme, was shown to also release $NO_2^{\bullet}$ upon reaction with peroxynitrite (46). However, NO_2^- is first released from the active site with compound I formation, but the protonated form (HONO) returns to the active site and reduces compound I to compound II with the release of $NO_2^{\bullet}$ (46). Therefore, the possibility that CCP compound I will behave the same way as HRP can not be excluded. Thus, the goal of the research outlined below is to determine whether CCP is a protective enzyme against nitrosative stress.

2.2 EXPERIMENTAL SECTION

2.2.1 Materials

Sephadex G25 resin, horse heart cytochrome c (type III) and blue dextran were purchased from Sigma. Potassium ferricyanide [$K_3Fe(CN)_6$], sodium dithionite ($Na_2S_2O_4$) and 30%

(w/w) hydrogen peroxide (H_2O_2) solution were obtained from Fisher Scientific. Diethylenentriamine pentaacetic acid (DTPA), ethylenediaminetetraacetic acid (EDTA) were from ICN, sodium nitrite ($NaNO_2$) from Anachemia Chemicals and sodium nitrate ($NaNO_3$) from Allied Chemical. All buffer salts were purchased from Sigma. Peroxynitrite was purchased from Calbiochem in solid form as the tetramethylammonim salt ($N(CH_3)_4[ONOO^-]$) and from Cayman as sodium salt (NaONOO) in 0.3 M NaOH solution. Yeast cytochrome c peroxidase was a generous gift from professor James Erman (Northern Illinois University). All other reagents were of analytical grade. All solutions were prepared using distilled water (specific resistance 18 MΩ) from a Barnstead Nanopure system.

2.2.2 Methods

A Cytochrome c peroxidase

CCP samples had a purity index ($A_{408\ nm}/A_{280\ nm}$) of 1.25 – 1.30 in 0.1 M potassium phosphate buffer, pH 7.0 (71). The 408/380-nm and 620/647-nm absorptivity ratios were always in the range of the reported values, 1.54 ± 0.06 and 0.78 ± 0.04, respectively, characteristic of a 5-coordinate, high-spin enzyme (72). The concentration of CCP was determined spectrophotometrically with $\varepsilon_{408\ nm} = 98.0\ mM^{-1}\ cm^{-1}$ (73) in 0.1 M potassium phosphate buffer, pH 7.0. All CCP stock solutions were made by dissolving lyophilized enzyme in 0.1 M phosphate buffer, pH 7.00.

B Ferrocytochrome c

A stock ferricytochrome c solution was prepared by dissolving lyophilized cytochrome c in 0.1 M potassium phosphate buffer, pH 7.0 and its concentration was determined both by weight (MW = 12,384 Da) and spectrophotometrically with $\varepsilon_{550\ nm} = 9.1\ mM^{-1}\ cm^{-1}$ (74). The cytochrome c was reduced with excess dithionite and passed through a Sephadex G-25 column in a glove box (MBRAUN model MB 120-G) under nitrogen to remove excess reducing agent. The concentration of stock ferrocytochrome c sample was determined spectrophotometrically with $\varepsilon_{550\ nm} = 27.7\ mM^{-1}\ cm^{-1}$ (74) before and after each experiment. In all experiments performed, cytochrome c was always ≥ 90 % reduced. The stock ferrocytochrome c solutions were stored in liquid N_2 for a one-month period maximum.

C Calibration of the Sephadex G-25 column

A gel filtration column (1 x 19 cm) was poured in the glove box using degassed Sephadex G-25 resin. The column was equilibrated with at least 3 column volumes of degassed 0.1 M potassium phosphate, pH 7.0 buffer. Calibration of the column was achieved with a sample that consisted of blue dextran (MW = 2 x 10^6 Da) and ferricyanide (MW = 329.26Da). The blue- and yellow-colored bands, seen when the test sample separated into its constituents (blue dextran and ferricyanide, respectively), allowed determination of the separation efficiency and the void volume of the column.

D Titration of CCP with peroxynitrite

The stock peroxynitrite solution (12.7 mM in 0.3 M NaOH) from Calbiochem was diluted to the appropriate concentration with ice cold distilled H_2O adjusted to pH 11.0 with NaOH pellets just prior to use. The concentration of peroxynitrite was determined

spectrophotometrically ($\varepsilon_{302\ nm}$ = 1670 $M^{-1}cm^{-1}$) (75). Approximately 15 mL buffer (100 mM potassium phosphate, pH 7.0 with 0.1 mM DTPA) was purged with N_2 gas for 30 – 40 min. A quartz cuvette fitted with a septum was also degassed for 5- 10 min and phosphate buffer and the stock solution of CCP were added to the cuvette using gas-tight (500-μL and 25-μL, respectively) Hamilton syringes. The final volume in the cuvette was 1 mL and the CCP concentration ranged between 4-10 μM. Peroxynitrite aliquots (10 μL) were added to the cuvette using a 25-μL Hamilton syringe and after each addition the spectrum of CCP was recorded over 250 –700 nm using a Hewlett Packard 8451A diode array spectrophotometer. The final pH of the solution in the cuvette remained at pH 7.0 since peroxynitrite solution added was at pH 11.0 which corresponds to only 1mM NaOH. The total volume of peroxynitrite added (50-120 μL) never reached the calculated volume of OH^- (23 ml necessary to change 1 pH unit), necessary to exceed the buffering capacity of the system. The CCP concentration after the peroxynitrite addition was corrected by multiplying each spectrum by the appropriate dilution factor. The spectrophotometer was initially blanked with the buffer alone and no more blanks were recorded since peroxynitrite forms compound I or decomposes to nitrate which has a very small molar absorptivity [$\varepsilon_{302\ nm}$ = 6.7 M^{-1} cm^{-1} (76)] within the range of interest. The syringes were washed with degassed 10 mM EDTA and rinsed with degassed distilled H_2O at pH 11.0, to adjust the pH inside the syringe. The difference spectrum (CCP compound I minus resting CCP) shows a maximum at 424 nm; thus, a plot of $\Delta A_{424\ nm}$ vs concentration of peroxynitrite added should reveal whether ONOO(H) reacts with CCP stoichiometrically.

E Titration of CCP with decomposed peroxynitrite

Stock peroxynitrite solution was prepared in 0.1 M potassium phosphate, with 0.1 mM DTPA, (pH 7.0) at the same concentration as in the previous titrations and was let stand at room temperature for 15 – 20 min to decompose. Titration of CCP with this solution containing decomposed peroxynitrite was performed under aerobic conditions so that CO_2 in the buffer would eliminate traces of any remaining peroxynitrite. After each addition (10 μL), the spectrum of CCP (250 – 700 nm) was recorded on the diode array spectrophotometer and again the CCP concentration was normalized to its initial value by multiplying the spectrum by the appropriate dilution factor.

F Determination of the number of oxidizing equivalents in CCP species formed on reaction with peroxynitrite

The same stock solution of peroxynitrite and set up as described in Section 2.2.2D, were used. With a Hamilton syringe, 10 μl of 0.8 mM peroxynitrite (8 nmol) was added to a 1-ml solution of 4 μM CCP (4 nmol) in a quartz cuvette fitted with a septum. Aliquots of ferrocytochrome c (5 μL) were added to the cuvette with a Hamilton syringe, and after each addition, the spectrum was recorded (250 – 700 nm). The focus was on the change in absorbance at 550 nm due to ferrocytochrome c oxidation. The α band of ferrocytochrome c at 550 nm decreases significantly [$\Delta\varepsilon_{550}$ = 18.5 mM^{-1} cm^{-1} (74)] when the Fe^{II} is oxidized to Fe^{III}. The instrument was referenced with buffer alone and the observed absorbance at 550 nm vs ferrocytochrome c concentration added was plotted. Again the CCP concentration was normalized after ferrocytochrome c addition. A Beckman DU 650 spectrophotometer set at a scan rate = 1200 nm / min, spectral

bandwidth ≤ 1.8 mm, was used for all data collection at room temperature.

G Titration of ferricyanide with ferrocytochrome c

A ferricyanide stock solution (10 mM) was prepared in 100 mM potassium phosphate buffer, pH 7.00, and this was diluted in a 1-mL quartz cuvette to a final concentration of 10 μM. Immediately after each addition of 7 μL of stock (0.152 mM) ferrocytochrome c to the cuvette, an absorption spectrum (250-700 nm) was recorded. The focus again was on the absorption at 550 nm and a plot of the observed absorbance at 550 nm vs μL ferrocytochrome c solution added allows the number of reducing equivalents obtained in the cytochrome c solution to be determined. To establish whether the number of reducing equivalents depended on the titration procedure, ferrocytochrome c (~10 μM) was titrated with ferricyanide (1 – 2 μM additions). The average of four titrations (two of each kind) was used to determine the number of reducing equivalents in the ferrocytochrome c stock solution. All measurements were performed at room temperature on a Beckman DU 650 spectrophotometer with scan rate of 1200 nm /min and a spectral bandwidth ≤ 1.8 nm.

H Nitrite as possible reducing agent of CCP compound I

Experiment 1.

A $NaNO_2$ stock solution (0.1 M) was prepared in 0.1 M potassium phosphate buffer pH 7.0. CCP stock solution (2.3 mM) was added to a cuvette in the same buffer to a final concentration of 11.5 μM and a 11.5 mM H_2O_2 solution, prepared in distilled H_2O from a 30% stock, was added to the cuvette, to give a final concentration equal to that of CCP. After detection of compound I spectrophotometrically, stoichiometric $NaNO_2$ was added

to the cuvette and spectra (250-700 nm) were measured at t = 30, 60, 90, 120 min after the addition of $NaNO_2$. The difference in absorbance of compound I minus native CCP, gives a maximum at 424 nm. 100% is taken to be the point where all of CCP has been converted to compound I. Thus, $\Delta A_{424\ nm}$ at each time point was compared to $\Delta A_{424\ nm}$ at t =0 to monitor any reduction of compound I. To correct for the normal decay of compound I over time, a sample without $NaNO_2$ was monitored over the same time intervals. The experiment was repeated with 10x $NaNO_2$ (i.e., $NaNO_2$/compound I = 10/1). All measurements were recorded on the Beckman DU 650 spectrophotometer.

Experiment 2.

Compound I was formed as in *Experiment 1*, and stoichiometric $NaNO_2$ was added to the cuvette. At t = 15 min, compound I was titrated with ferrocytochrome c as described in Section 2.2.2F. The experiment was repeated with a $NaNO_2$/compound I molar ratio of 2/1. The number of reducing equivalents of ferrocytochrome c consumed, which equals the number of oxidizing equivalents stored in compound I, was determined from change in absorbance at 550 nm.

RESULTS

2.3.1 Calibration of Sephadex G-25 column

A solution (0.5 mL) containing 1.5 mg $K_3Fe(CN)_6$ and 1.5 mg dextran blue (3 mg total) was loaded on top of the (1 x 19 cm) G-25 gel filtration column in the glove box, and eluted with 0.1 M potassium phosphate buffer, pH 7.0. The void volume of the column was found to be ~ 6 mL which corresponds to the elution volume of the blue dextran, and

the ferricyanide eluted at 9 mL. This column is expected to effect a clean separation of cytochrome c and excess dithionite and its oxidation products since the proteins elute in the void volume while the small molecules should elute at 9 mL like ferricyanide.

2.3.2 Titration of CCP with peroxynitrite from Calbiochem

Addition of equimolar amounts of peroxynitrite to CCP is expected to give a spectrum identical to that of compound I assuming that peroxynitrite behaves as a peroxide. Spectrophotometric titration of 4-10 μM CCP with peroxynitrite (~ 2 μM additions) under anaerobic conditions yields an absorption spectrum with a Soret maximum at 419 nm and charge-transfer bands at 530 and 560 nm (Figure 2.1a). The spectrum obtained is identical to the one we obtained for compound I formed with H_2O_2 (Figure 2.1b and Table 2.4) and in close similarity to the reported spectrum (77). The compound I minus resting CCP difference spectrum shows a max at 424 nm (77) and the absorbance increments at 424 nm are plotted vs the added peroxynitrite concentration in Figure 2.2. The plot exhibits an inflection point at 9.6 μM peroxynitrite when 6.0 μM CCP was titrated. Thus, the apparent stoichiometry between peroxynitrite and compound I was found to be 1.6, and a value of 1.65 ± 0.10 was obtained from the average of three titrations.

2.3.3 Estimation of the apparent k_2 for the reaction of CCP with peroxynitrite at pH 7.0

A stoichiometry of 1.65 for the reaction between peroxynitrite and CCP indicates that the rates of peroxynitrite decomposition and compound I formation are similar. There are three possible routes that peroxynitrite decay can follow in a solution at pH 7.0 that

a)

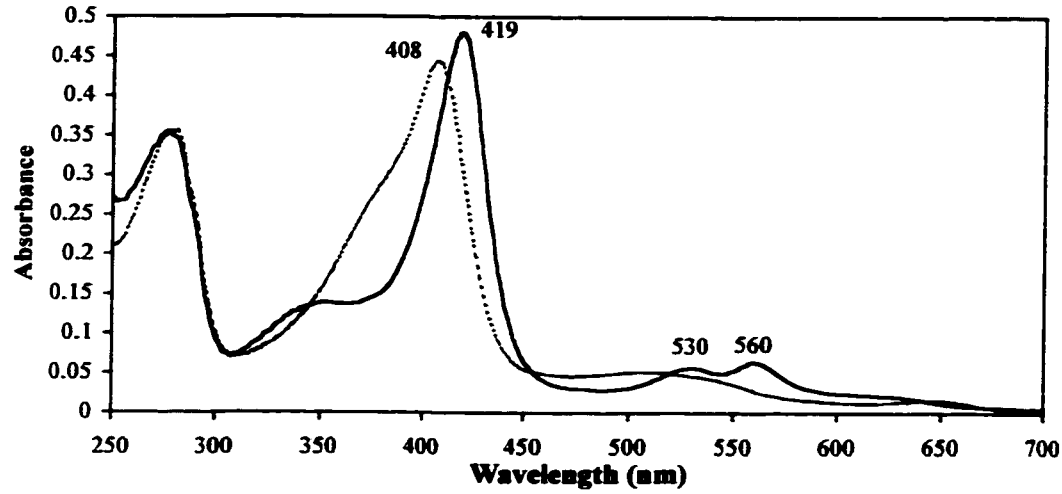

b)

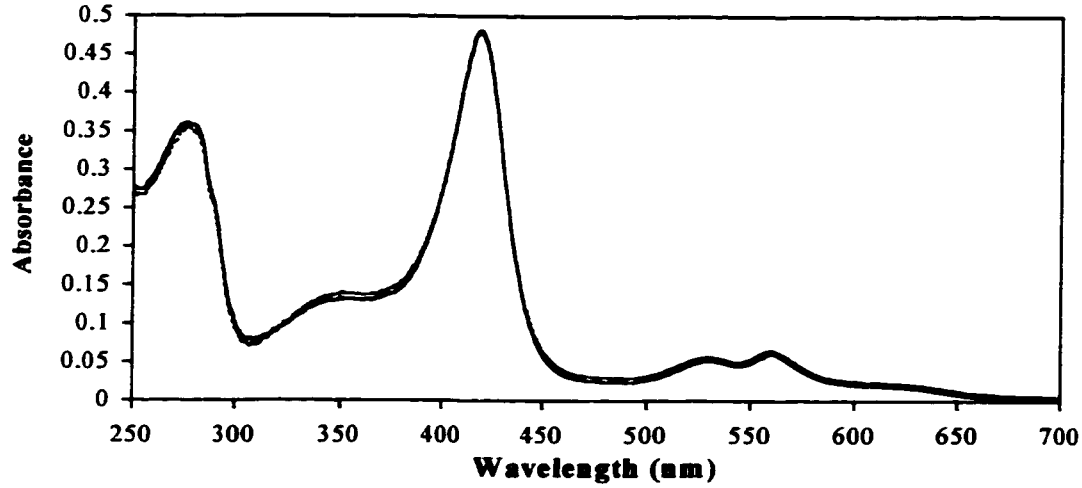

Figure 2.1 Spectral changes in CCP upon peroxynitrite addition.

(a) Spectrum of 4.52 μM resting ferric CCP (dashed line) in 0.1 M potassium phosphate buffer, pH 7.0, and spectrum formed when 1.65 molar equivalents of peroxynitrite (Calbiochem) are added to the cuvette (solid line). **(b)** Overlay of spectra of 4.52 μM CCP compound I formed on oxidation with H_2O_2 (solid line) and peroxynitrite (Calbiochem) (dashed line). The plotted spectra were normalized at the Soret maximum (419 nm).

Table 2.4 Molar absorptivities of the Soret and charge-transfer bands of CCP compound I formed on H_2O_2 and peroxynitrite oxidation

λmax (nm)	Molar absorptivity, ε (mM^{-1} cm^{-1})	
	Compound I (H_2O_2)[a]	Compound I (ONOOH)[b]
419	106	105.5
530 (α)	12.5	12.05
560 (β)	14.3	13.6
α/β ratio	1.14	1.13
	1.13[c]	
$\Delta\varepsilon_{424\ nm}$	47[d] ± 1	45[d] ± 1
(mM^{-1} cm^{-1})	41.5[e]	-
	49 ± 4[f]	-

[a] Compound I was formed by H_2O_2 oxidation of resting CCP in 0.1 M potassium phosphate buffer pH 7.0 with 0.1 mM DTPA, room temperature.

[b] Compound I was formed by peroxynitrite oxidation (Calbiochem) as in footnote a.

[c] Value reported in reference 78, 49% ethylene glycol, 49% 100 mM potassium phosphate pH 7.0, 2% isopropanol, 0.01% acetophenone and 0.1 nM catalase at -30°C.

[d] Values reported here are the average of four determinations. Molar absorptivity values are based on the ferric CCP concentration used and not on the H_2O_2 (1:1) or peroxynitrite (1.7:1) concentrations needed for the conversion of the enzyme to compound I.

[e,f] $\Delta\varepsilon_{424\ nm}$ values from reference 77 and 79, respectively. Conditions in both studies were: 0.1 M potassium phosphate, pH 6.0, 23°C.

contains CCP and CO_2 (Scheme 6). However, most of the CO_2 dissolved in phosphate buffer was removed by purging the solution with nitrogen gas for 30 – 40 min, and the titration was performed in a cuvette fitted with a septum to ensure that the system remains essentially CO_2-free. Therefore, route 1 (Scheme 6) is assumed to have been eliminated, such that the peroxynitrite will be distributed between routes 2 and 3. Thus, the apparent second-order rate constant (k_2; $M^{-1}s^{-1}$) for the reaction of peroxynitrite with CCP can be estimated by assuming simple competition kinetics between the proton-catalyzed isomerization of peroxynitrite to NO_3^- and oxidation of CCP to compound I. Thus, the ratio of the products of routes 2 and 3 is related to the ratio of their rate constants as:

$$\frac{[NO_3^-]}{[\text{compound I}]} = \frac{k_1\,[ONOO(H)]}{k_2[CCP]\,[ONOO(H)]} \qquad (34)$$

The concentration of compound I was estimated from the observed $\Delta A_{424\ nm}$ in the $CCP(Fe^{IV}=O) - CCP(Fe^{III})$ difference spectrum with $\Delta\varepsilon_{424\ nm} = 45\ mM^{-1}\ cm^{-1}$ (Table 2.4):

$$[\text{Compound I}]_{formed} = \Delta A_{424}/\Delta\varepsilon_{424} \qquad (35)$$

Assuming that the peroxynitrite not reduced by CCP forms nitrate (eqn 36), and that $k_1 = 1.38\ s^{-1}$ (54),

$$[NO_3^-]_{formed} = [ONOO(H)]_{added} - [\text{compound I}]_{formed} \qquad (36)$$

then k_2 can be estimated from eqn 34. A value for k_2 was determined after each 10-μL aliquot of peroxynitrite was added in the titration, and [ONOO(H)] in eqn 34 represents the formed peroxynitrite concentration ($[ONOO^- + ONOOH]$) added per aliqout. Since

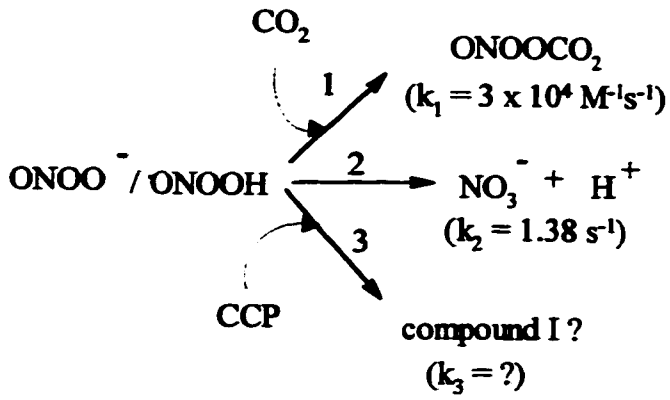

Scheme 6 Possible routes for the peroxynitrite in the cuvette.

6-10 aliquots of peroxynitrite were added per titration, 6-10 determinations of k_2 were performed and the average from three separate titrations gives a value of $6.9 \pm 2.2 \times 10^5$ $M^{-1}s^{-1}$ for k_2 at pH 7.0. The k_2 values ($M^{-1}s^{-1}$) for the other peroxidases at pH 7.2-7.4 are: 6.2×10^6 (MPO), 6.4×10^5 (HRP) and 3.3×10^5 (LPO) for their reaction with peroxynitrite (46). Our estimated k_2 for CCP oxidation by peroxynitrite at pH 7.0 is closest to that of HRP ($6.4 \times 10^5\ M^{-1}s^{-1}$) at pH 7.0 (46).

2.3.4 Titration of CCP with peroxynitrite from Cayman

Another source of peroxynitrite was also used in the titration of CCP. The experimental conditions were the same as in the titrations with peroxynitrite from Calbiochem, but the results were very different. When 12.4 μM CCP was titrated with a 0.135-mM peroxynitrite stock solution diluted from the Cayman stock, the $\Delta A_{424\ nm}$ vs peroxynitrite

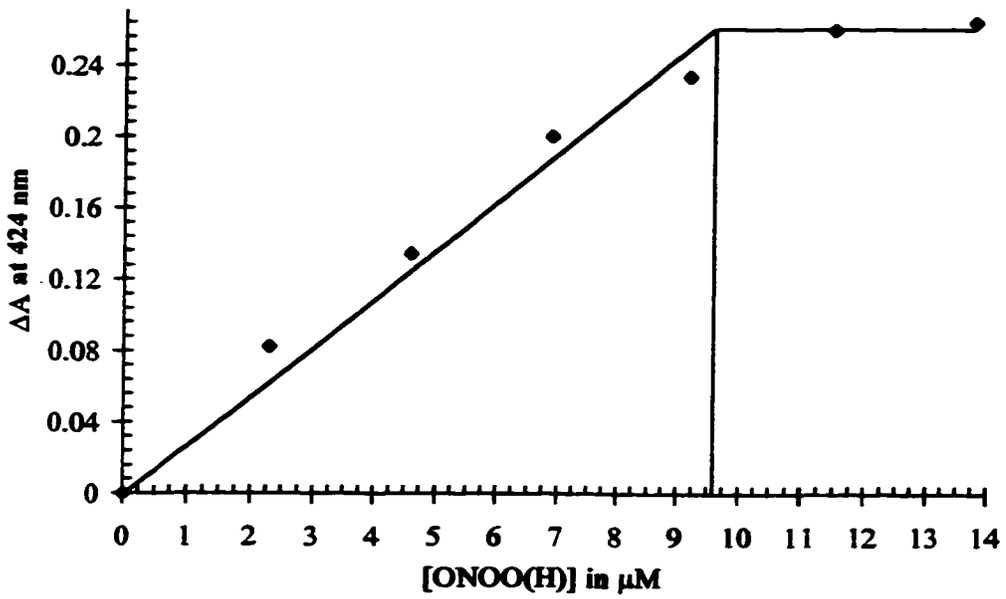

Figure 2.2 Titration of 6 μM CCP with peroxynitrite from Calbiochem in 0.1 M potassium phosphate, pH 7.0, with 0.1 mM DTPA, at room temperature. Formation of compound I is monitored by increments in $\Delta A_{424\ nm}$. The inflection point is at 9.6 μM peroxynitrite.

concentration plot (Figure 2.3) shows an inflection point at 9.76 μM peroxynitrite. This would correspond to a stoichiometry of only 0.79 mole of ONOO(H) to 1.0 mole of CCP. The same titration was repeated two more times and 0.79 was again found to be the stoichiometric ratio of peroxynitrite to CCP based on the concentration of peroxynitrite quoted by Cayman. However, a [ONOO(H)]/CCP ratio of <1.0 contradicts our assumption that a portion of peroxynitrite added in the cuvette decomposes to NO_3^- (Scheme 6).

Traces of H_2O_2 in the peroxynitrite sample will greatly affect the end-point determination in the titration of a peroxidase with ONOO(H). A stock solution of Cayman peroxynitrite was added to phosphate buffer at pH 7.0 and let stand at room temperature for 30 min to decompose. When it was used to titrate CCP, compound I formation was observed spectrophotometrically at the same ONOO(H)/CCP ratio as freshly-prepared peroxynitrite. Since the "decomposed" peroxynitrite from Cayman generated compound I (Figure 2.3b), we conclude that the sample is high in H_2O_2 and other stable oxidants. This must be the case when the Cayman peroxynitrite sample is freshly prepared (Figure 2.3a), and we conclude that the 0.79 ratio observed is not due to peroxynitrite oxidation but to H_2O_2 or some other oxidant impurities in the sample.

The presence of stable oxidants in the Calbiochem sample was also investigated. The solid peroxynitrite was dissolved in phosphate buffer, pH 7.0 to give an initial concentration of 0.154 mM, and the sample was let stand at room temperature to allow the peroxynitrite to decompose prior to its use in titration of CCP. Even with the Calbiochem sample, compound I formation was detected. The plot of $\Delta A_{424\ nm}$ vs "decomposed" [ONOO(H)] added (Figure 2.4), gives a ONOO(H)/CCP ratio of 5.6.

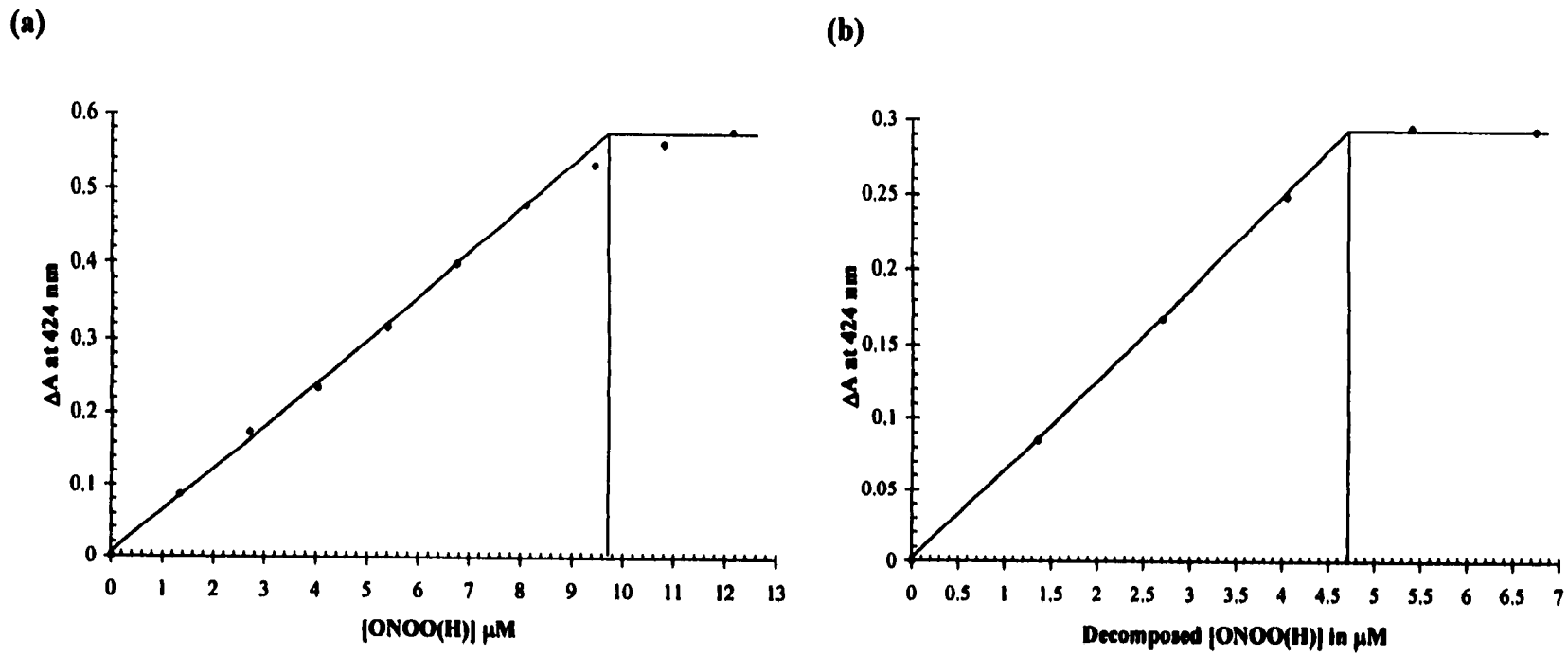

Figure 2.3 (a) Titration of 12.4 μM CCP in 0.1 M potassium phosphate, pH 7.0, 0.1 mM DTPA, with 0.135 mM Cayman peroxynitrite. The stock peroxynitrite was added in H_2O, pH 11.00 and immediately added to the cuvette. The inflection point is at 9.75 μM ONOO(H) which represents a [ONOO(H)]/CCP ratio of 0.79. **(b)** Titration of 6.55 μM CCP with 0.135 mM "decomposed" Cayman peroxynitrite. The peroxynitrite stock solution was added in 0.1 M potassium phosphate buffer, pH 7.00, containing 0.1 mM DTPA and was let stand at room temperature for 30 min prior to titration. The inflection point is observed at 4.73 μM ONOO(H) which represents a [ONOO(H)]/CCP ratio of 0.72.

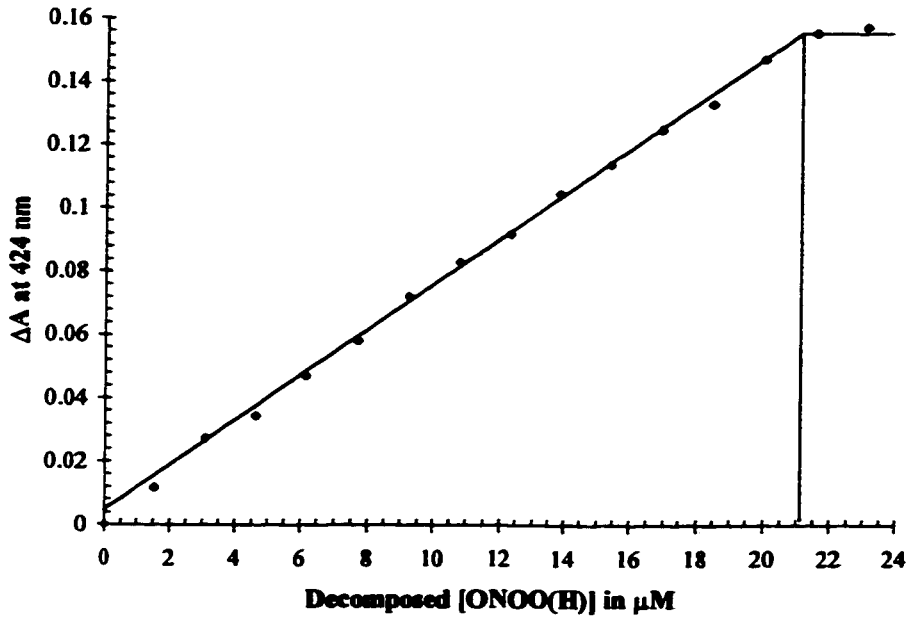

Figure 2.4 Titration of 3.8 μM CCP in 0.1 M potassium phosphate buffer, pH 7.0, 0.1 mM DTPA, with 0.145 mM "decomposed" Calbiochem peroxynitrite. Peroxynitrite stock solution was added to the buffer containing 0.1 mM DTPA, and was let stand at room temperature for 30 min prior to titration. The inflection point is observed at 21.2 μM ONOO(H) which represents a [ONOO(H)]/CCP ratio of 5.6.

Such a high ratio indicates that contaminating oxidants are present at a much lower level in the Calbiochem sample than in the Cayman sample.

2.3.5 Identification of the intermediate formed when CCP is titrated with peroxynitrite.

Compound I and compound II of CCP possess essentially identical spectral properties. This is because the Trp 191 radical found in compound I does not significantly perturb the electronic environment of the heme as measured by electronic absorption and MCD spectroscopy (78, 80). Thus, to determine the number of oxidizing equivalents in the intermediate formed upon reaction of CCP with ONOO(H), ferrocytochrome c titration is necessary. Bearing in mind the catalytic cycle of CCP (eqns 4 – 6), the number of reducing equivalents of ferrocytochrome c used in the titration will establish the identity of the intermediate formed. To determine the number of reducing equivalents in the ferrocytochrome c sample prepared, 10.0 μM ferricyanide was titrated using ferrocytochrome c as titrant. The plot of observed absorbance at 550 nm vs the concentration of ferrocytochrome c added (Figure 2.5a) shows an inflection point at 9.6 μM ferrocytochrome c which reveals that the latter solution contains 1.04 reducing equivalents per 1.00 mol ferrocytochrome c. Using ferricyanide as titrant (Figure 2.5b) 1.12 moles of titrant were necessary to oxidize 1.00 mole of ferrocytochrome c. The overall average of four titrations (2 with ferricyanide as titrant, 2 with ferrocytochrome c as titrant) revealed that the cytochrome c sample prepared contains 1.13 ± 0.08 reducing equivalents per 1.00 mole of protein. The additional reducing equivalents are taken into consideration in the titration of the CCP intermediate vs ferrocytochrome c shown in

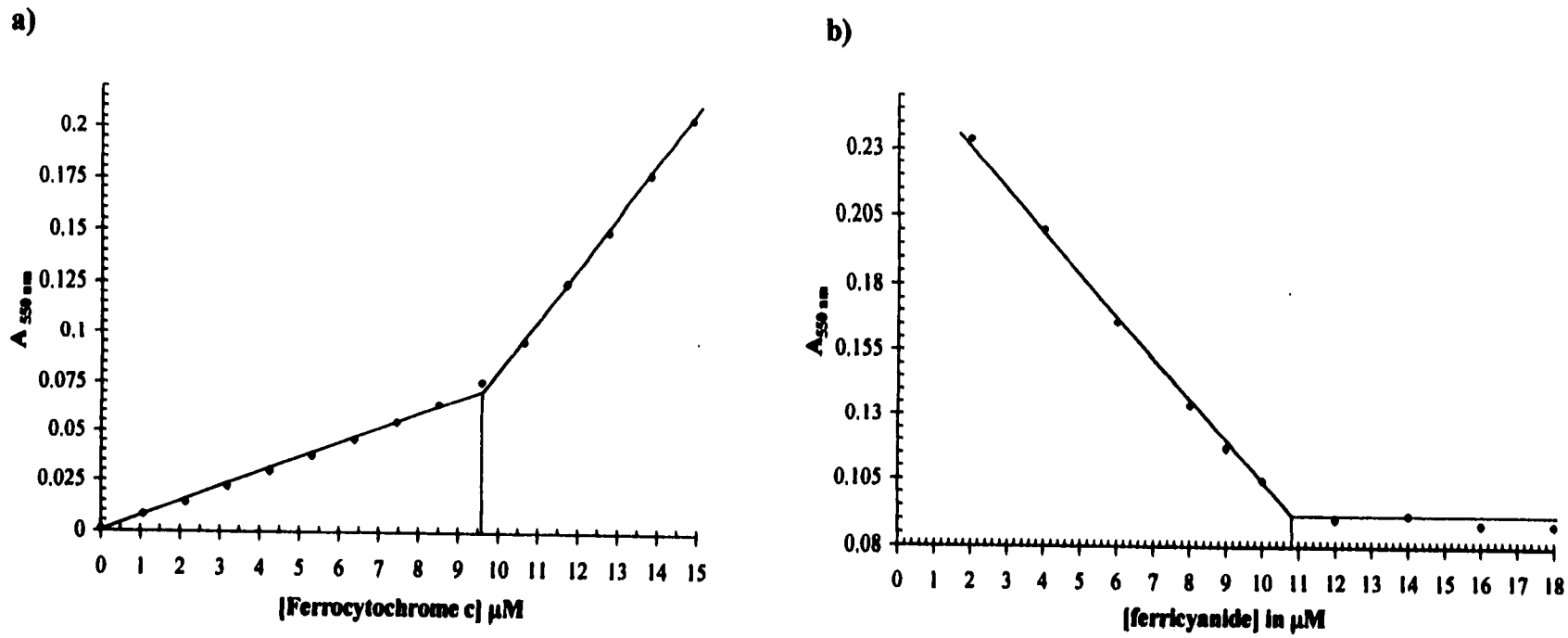

Figure 2.5 **(a)** Titration of 10 μM ferricyanide with ferrocytochrome c in 0.1 M potassium phosphate buffer, pH 7.0. The oxidation of the added ferrocytochrome c was monitored at 550 nm, and an inflection point is observed at 9.6 μM ferrocytochrome c added. **(b)** Titration of 9.65 μM ferrocytochrome c with ferricyanide. The 550-nm absorbance shows an inflection point at 10.8 μM ferricyanide added.

Figure 2.6. An inflection point at 7.47 μM in the titration of 4 μM CCP intermediate, identifies the latter as CCP compound I with 1.87 oxidizing-equivalents stored between the heme and polypeptide.

2.3.6 Effect of nitrate and nitrite on the spectra of resting CCP and compound I

As shown in Section 2.3.5, peroxynitrite reacts with CCP to yield compound I. This reaction is competitive with peroxynitrite isomerization to nitrate (Scheme 6). To probe any reaction between NO_3^- and either resting CCP or compound I, 1x, 10x and 100x excess nitrate were added to both forms of the enzyme. From the spectra recorded, even 100x NO_3^- appears to undergo no reaction with either resting CCP or compound I (Figure 2.7). The effect of NO_2^- on compound I was also examined and spectral changes consistent with reduction of compound I were observed (Figure 2.8). To quantitate the reduction of compound I upon addition of NO_2^-, spectra were recorded at time intervals of 30 min. Compound I spectra without NO_2^- were also recorded as a control and the results are summarized in Table 2.5. Clearly, NO_2^- accelerates the decay of compound I. For example, in the presence of 10x NO_2^- only ~ 50% compound I remains after 60 min, whereas, ~ 76% remains in its absence. However, NO_2^- will not compete with ferrocytochrome c as a reducing substrate for CCP compound I *in vivo*. This is seen when we add NO_2^- to compound I and then titrate within 15 min with ferrocytochrome c. Both 1x and 2x NO_2^- do not alter the number of reducing equivalents required for

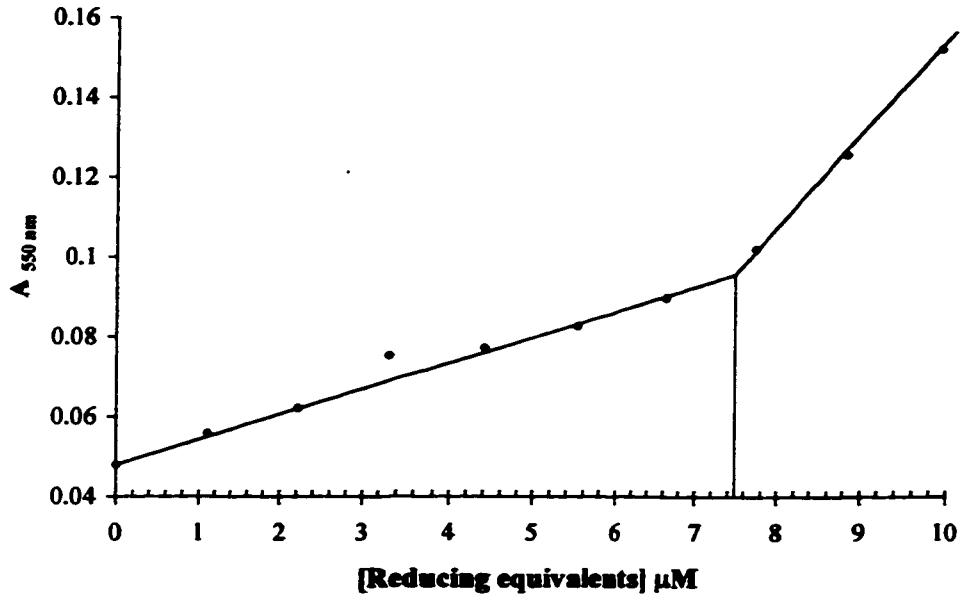

Figure 2.6 Titration of 4.0 μM CCP intermediate with ferrocytochrome c in 0.1 M potassium phosphate, pH 7.0, 0.1 mM DTPA. Approximately 8 μM peroxynitrite was added to 4.0 μM resting CCP to ensure complete formation of the intermediate as detected spectrophotometrically (Figure 2.1a). The CCP intermediate formed was titrated immediately with ferrocytochrome c, and the observed absorbance at 550 nm plotted vs the number of reducing equivalents in ferrocytochrome c solution added. An inflection point is observed at 7.47 μM reducing equivalents, indicating that 1.87 oxidizing equivalents are stored in the CCP intermediate.

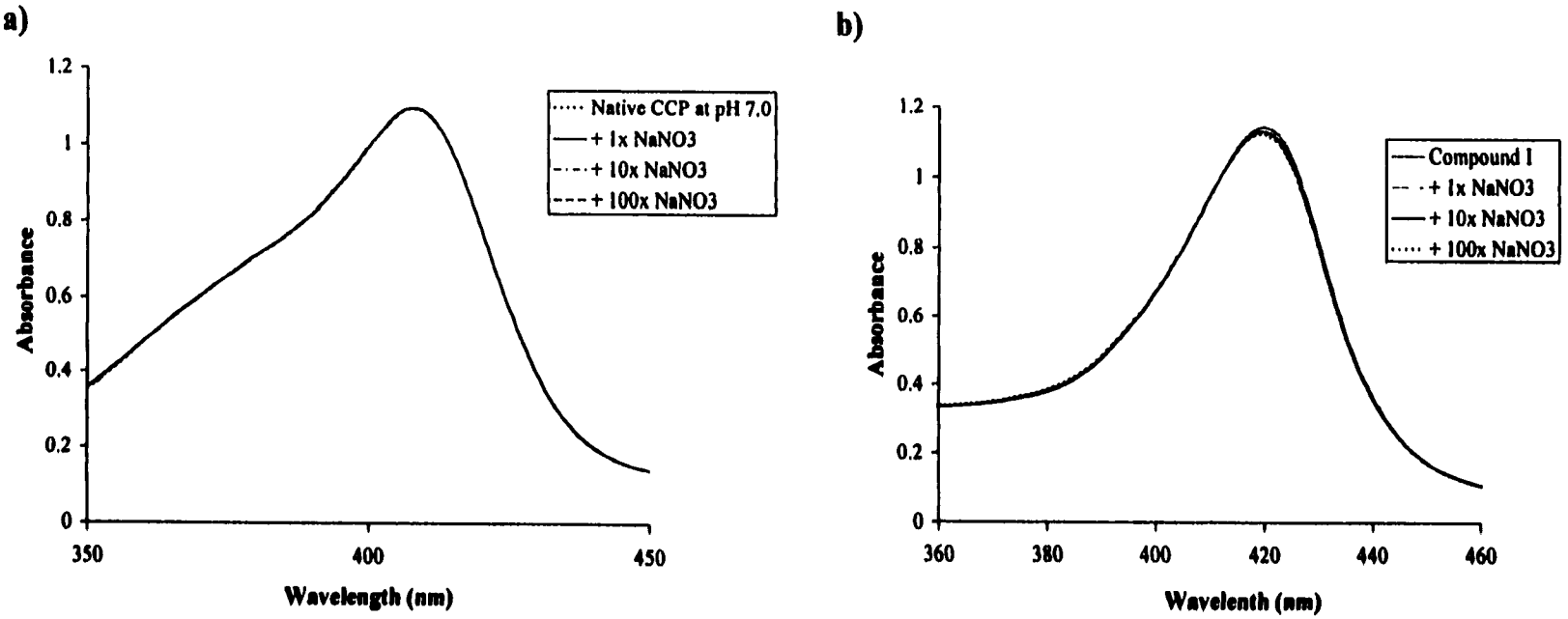

Figure 2.7 **(a)** Effect of NO_3^- on the spectrum of resting ferric CCP. 1x, 10x and 100x NO_3^- were added to 11.1 μM CCP and the spectrum of CCP was recorded. Note that even 100x NO_3^- does not alter the Soret band of CCP. **(b)** Effect of NO_3^- on the CCP compound I spectrum. Equimolar H_2O_2 was added to form compound I followed by 1x, 10x and 100x NO_3^-, and the specta were recorded immediately after each addition. Only 100x NO_3^- seem to slightly alter the Soret band of compound I. Spectra were recorded at 23°C on a Cary 1 spectrophotometer using a 1.00 SBW (nm) at 30 nm/min scan rate.

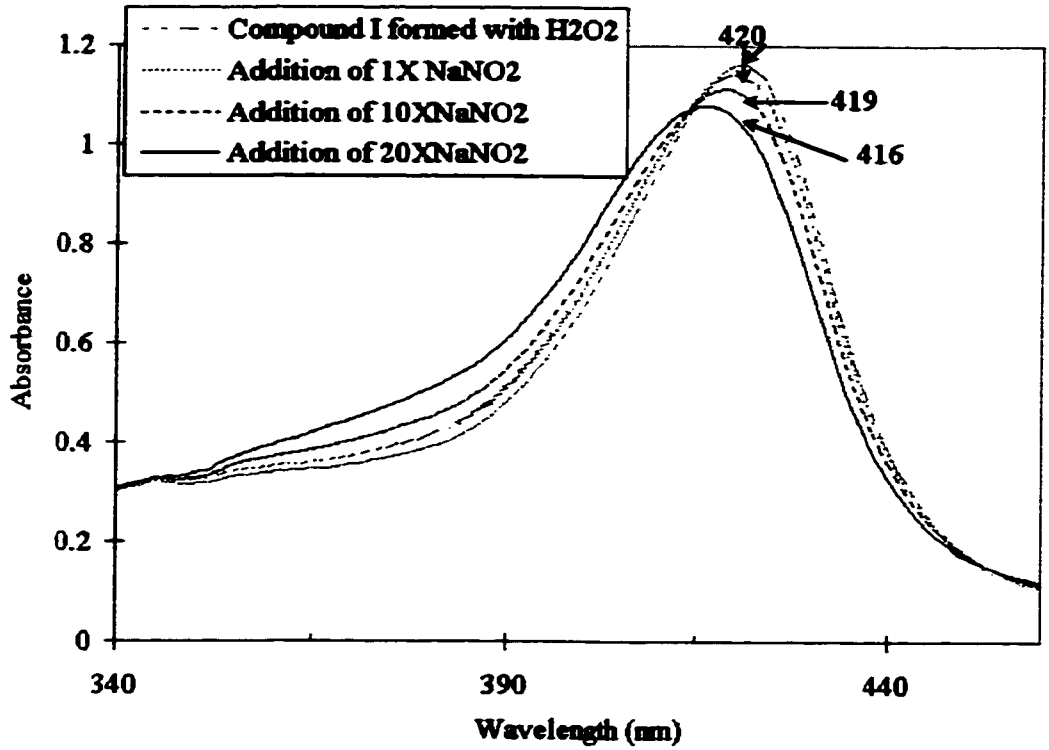

Figure 2.8 Effect of NO_2^- on the spectrum of CCP compound I. Resting CCP (11.5 μM) in 0.1 M potassium phosphate, pH 7.0, was converted to compound I by the addition of equimolar H_2O_2 followed by 1x, 10x and 20x NO_3^-. Immediately after each addition, the spectrum of compound I was recorded at 23°C in a Cary 1 spectrophotemeter using 1.00 nm SBW at 30 nm/min scan rate.

Table 2.5 Reduction of CCP compound I as a function of time and NO_2^- concentration[a].

% Compound I Remaining				
Time interval (min)[b]	0	1x NO_2^-	10x NO_2^-	10x NO_2^- corrected[c]
0	100	90.4	96.8	96.8
30	86	79.6	72.7	83.7
60	76.2	69.6	52.5	68.9
90	66.7	N.D.	36.8	55.2
120	58.2	N.D.	28	48.1

[a] 9.0 μM CCP in 0.1 M potassium phosphate, pH 7.0, room temperature.

[b] Time elapsed between each recorded spectrum of CCP compound I after NO_2^- addition.

[c] Corrected for the spontaneous decay of compound I given in column 2.

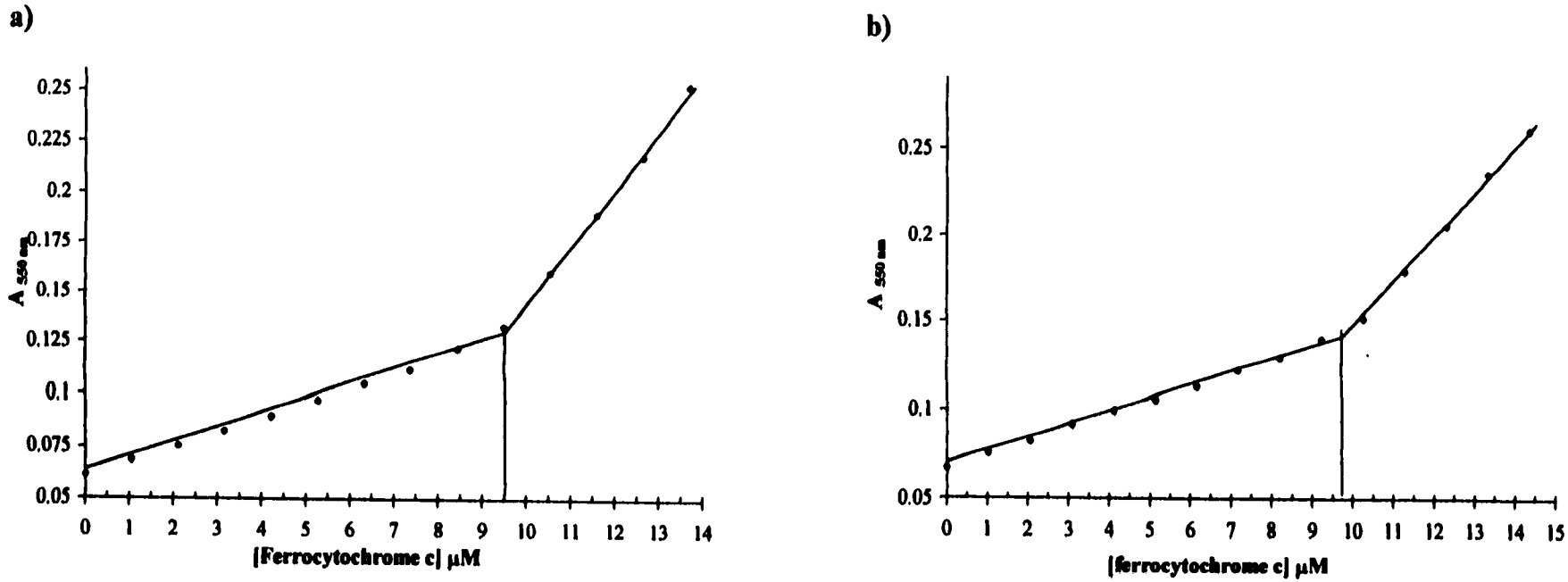

Figure 2.9 **(a)** Titration of 5.46 μM CCP compound I and 1x NO_2^- with ferrocytochrome c. CCP compound I was formed with H_2O_2 and titrated with ferrocytochrome c 15 min after the addition of 1x NO_2^-. The inflection is at 9.52 μM ferrocytochrome c which represents a ferrocytochrome c/compound I ratio of 1.74. **(b)** Titration of 5.88 μM CCP compound I and 2x NO_2^- with ferrocytochrome c. CCP compound I was titrated with ferrocytochrome c 15 min after the addition of 2x NO_2^-. The inflection point is at 9.89 μM ferrocytochrome c which represents a ferrocytochrome c/compound I ratio of 1.68.

compound I reduction (Figure 2.9) since their addition to compound I results in ratios of 1.74 and 1.68, respectively, between compound I and the number of cytochrome c reducing equivalents. When compound alone was titrated with ferrocytochrome c 15 min after its formation, a ratio of 1.65 was obtained (data not shown) which is essentially identical to that obtained in the presence of NO_2^-. The spontaneous decay of compound I over 15 min due to intramolecular reduction of the heme (81), gives rise to a lower ratio (1.65) than that observed (1.87, Figure 2.6) when compound I is titrated immediately with ferrocytochrome c.

To test for trace impurities in the $NaNO_2$ sample used, 1x and 2x NO_2^- were added to ferricyanide solutions and these were titrated with ferrocytochrome c (data not shown). The average of 4 titrations (2 with 1x NO_2^- and 2 with 2x NO_2^-) gave a ferrocytochrome c/ferricyanide ratio of 1.02 ± 0.04, indicating that no impurities were present in the nitrite solution that reduce ferricyanide.

2.4 DISCUSSION

2.4.1 Reaction of peroxynitrite with CCP

Peroxynitrite produced from $NO^{\bullet}$ and $O_2^{\bullet-}$ (48) in activated neutrophils and macrophages during the inflammatory response is of great interest due to its potential toxicity. It was shown *in vitro* that peroxynitrite reacts with a variety of substrates, most of them important biological molecules such as lipid membranes and DNA (80), causing

strand breaks and mutations. Its reaction with phenols such as tyrosine to form nitrotyrosine is also of great interest since substantial amounts of nitration were observed around macrophages and neutrophils in lung specimens from humans with respiratory distress syndrome or pneumonia (9). With growing information on peroxynitrite toxicity, the search for possible scavengers of peroxynitrite *in vivo* has begun (46, 51, 52, 59-62, 70). Heme peroxidases, including MPO, LPO and HRP have been shown to possess peroxynitrite-reducing activity (46). In this thesis CCP is the enzyme being investigated for such activity.

The titration of CCP with peroxynitrite yields an intermediate species that has an identical spectrum to compound I formed when the enzyme reacts with H_2O_2 (Figures 2.1a and b). Since compound I and compound II of CCP possess identical spectra (77, 79), titration of the peroxynitrite-CCP reaction product with ferrocytochrome c was performed. Figure 2.6 shows that 1.87 reducing equivalents are needed for the conversion of the intermediate to resting form of CCP so we conclude that peroxynitrite oxidizes CCP to compound I. The lower than 2.0 stoichiometric ratio observed could be because compound I spontaneously decays back to the ferric enzyme during the titration process. One might also assign the discrepancy to the presence of impurity in the CCP preparation; however, the purity index (408/280 nm) was 1.25 – 1.3, and the 408/380 nm and 620/647 nm ratios were in the range of the reported values, 1.54 ± 0.06 and 0.78 ± 0.04, respectively, characteristic of highly pure CCP in its native 5-coordinate, high spin state (72). Supporting evidence that compound I is indeed formed comes from the molar absorptivity values of its charge-transfer bands. The ratio of the α (560 nm) to β band (530 nm) for the compound I is reported to be 1.13 whereas for compound II these bands

are nearly equal with a ratio of $\alpha/\beta = 1.04$ (77). Comparing the 560/530 nm ratios for the species formed with H_2O_2 vs CCP-peroxynitrite (Table 2.4), we again arrive at the conclusion that compound I is formed in both cases.

From a plot of $\Delta A_{424\ nm}$ vs peroxynitrite from Calbiochem (Figure 2.2), it was shown that 1.6 mol of peroxynitrite are necessary to convert 1.0 mol of CCP to compound I. Based on Scheme 6 and on the fact that peroxynitrite quickly isomerizes to NO_3^- at the conditions employed here (pH 7.0, room temperature), not all of the peroxynitrite added will be available to form compound I and the 1.6 molar ratio is acceptable. When the same titration was performed with peroxynitrite from Cayman (Figure 2.3a), only 0.79 mol of peroxynitrite were presumably needed for the oxidation of 1.0 mol of CCP, which was unexpected. Titration of the enzyme with "decomposed" peroxynitrite from both Cayman and Calbiochem (Figures 2.3b and 2.4) shows that the low ratio of 0.79 can be attributed to high concentration of H_2O_2 contaminant in the Cayman peroxynitrite sample. Comparing Figure 2.3a and b, we can assume that H_2O_2 succesfully competes with peroxynitrite for the oxidation of CCP. In other words, the reaction of CCP with H_2O_2 is preferred over the reaction with ONOOH, which is consistent with the second-order rate constants for these two reactions [$3.91 \times 10^7\ M^{-1}s^{-1}$ (76, 77) vs $6.9 \pm 2.2 \times 10^5\ M^{-1}s^{-1}$ (this thesis), respectively].

The discrepancy in the molar ratios observed in the titrations performed with peroxynitrite from different sources establishes the importance of the method of peroxynitrite synthesis. Cayman peroxynitrite is synthesized from H_2O_2 and excess n-butyl nitrite in basic solution, according to the method of Uppu et al. (eqn 37) (78):

$$HOO^- + O{=}N\text{-}O\text{-}C_4H_9 \longrightarrow HOONO + C_4H_9O^- \qquad (37)$$

Hydrogen peroxide impurities can be lowered by passage of the solution through a manganese dioxide column (78), but as observed here, traces of H_2O_2 and other oxidants are unavoidably left behind. On the other hand, Calbiochem peroxynitrite is generated as the tetramethylammonium salt in solid form, by the reaction of tetramethylammonium superoxide with nitric oxide in ammonia solvent as reported by Bohle et al. (eqn 38) (76).

$$[(CH_3)_4N]^+ O_2^{\cdot-} + NO^{\cdot} \xrightarrow{NH_3(l)} [(CH_3)_4N]^+ ONOO^- \qquad (38)$$

This method is said to produce a pure form of peroxynitrite that does not contain contaminants such as nitrite, nitrate, metal ions or H_2O_2, which is critical when examining peroxynitrite reactions with peroxidases. However, as seen from Figure 2.4, "decomposed" peroxynitrite from Calbiochem also converts CCP to compound I at a ratio of ~ 6 mol "decomposed" ONOOH to 1.0 mol of enzyme. This shows that stable oxidants are also present in the Calbiochem preparation. Peroxynitrite isomerizes to nitrate, which does not seem to react with either resting CCP or its compound I (Figure 2.7a and b). Therefore, the spectral changes observed in Figure 2.4 can not be attributed to peroxynitrite isomerization products but to some unkown contaminants.

Using equations 34 – 36, and ignoring the effects of any oxidizing contaminants, the apparent second order-rate constant for the reaction of CCP with peroxynitrite at pH 7.0 was estimated to be $6.9 \pm 2.2 \times 10^5\ M^{-1}s^{-1}$. This is similar to the apparent second-order rate constants measured by stopped-flow for MPO ($6.2 \times 10^6\ M^{-1}s^{-1}$), LPO ($3.3 \times 10^5\ M^{-1}s^{-1}$) and HRP ($6.4 \times 10^5\ M^{-1}s^{-1}$) at pH 7.2 – 7.4 (46) but is ~ 2 orders of magnitude lower than the bimolecular rate constant [$3.91 \times 10^7\ M^{-1}s^{-1}$ (82, 83)] for compound I formation with H_2O_2 .

Nitrite is formed when peroxynitrite oxidizes CCP to compound I. Based on the mechanism proposed for the reactions of MPO and HRP with peroxynitrite (46), we questioned whether CCP compound I is also able to oxidize nitrite or nitrous acid. Addition of 20x NO_2^- to compound I resulted in a blue-shift in its Soret band from 420 to 416 nm (Figure 2.8), indicating reduction of compound I. The reduction of compound I by NO_2^- was followed over time (Table 2.5), and it was found that 52.5% remains after 60 min in the presence of 10x NO_2^-. If we correct this for the spontaneous decay of compound I (81), we find that 68.9% compound I remains when 10x NO_2^- is present. When 1x or 2x NO_2^- is added to compound I 15 min before titrating with ferrocytochrome c, molar ratios of 1.74 and 1.68 are obtained, respectively (Figures 2.8a and b), which are essentially identical to the 1.65 ratio observed when compound I alone is titrated 15 min after its formation with ferrocytochrome c (data not shown). Therefore, the deviation from the expected ratio of 2 (77) is attributed to the partial decay of compound I over 15 min rather than reduction by NO_2^-. The 15-min incubation of compound I with NO_2^- before titration with ferrocytochrome c was because NO_2^- was released in the reaction of HRP with peroxynitrite, was taken up again as HNO_2 (eqns 28-30). Since the pK_a of HNO_2 is 3.15, this reaction is expected to be slow around pH 7.0. Based on the results of Floris et al. (46) HNO_2^- reduces HRP compound I to compound II in 1-10 s, which is 100-1000-fold faster than the 15-min period allowed here for CCP compound I reduction by NO_2^-. Overall, we conclude that CCP is an efficient peroxynitrite reductase (eqn 31). Furthermore, CCP can be considered protective against

nitrosative stress, since $NO_2^{\bullet}$ formation (eqn 32) is unlikely to compete with ferrocytochrome c oxidation by compound I *in vivo*.

2.4.2 Biological significance

Recent studies on peroxynitrite have shown that CO_2 plays a catalytic role in the conversion of peroxynitrite anion into a much more aggressive species, nitrosoperoxycarbonate (Scheme 4), which can either react with biological substrates or decompose to nitrate (55, 85). It was shown that the presence of bicarbonate significantly enhanced peroxynitrite-mediated nitration of aromatics *in vitro* but, on the other hand, it partially inhibited the oxidation of thiols, dimethylsulfoxide, oxyhemoglobin and ferrocytochrome c, and totally inhibited the hydroxylation of benzoate (85). Therefore, the formation of nitrosoperoxicarbonate has been shown to redirect the reactivity of peroxynitrite.

However, the *reactivity product* is the parameter of importance *in vivo*. This is the second-order rate constant times the physiological concentration of a reactant (54). With ~ 1 mM CO_2 *in vivo* and a pH-independent rate constant of 5.8×10^4 M^{-1} s^{-1} (54), which corresponds to a reactivity product of 58 s^{-1}, it would be difficult for most peroxynitrite scavengers to compete with CO_2 unless they are present in very high concentrations in the cell. On the other hand, hemeperoxidases react rapidly with peroxynitrite; for example, MPO reacts with peroxynitrite with a pH-independent rate constant equal to 2×10^7 $M^{-1}s^{-1}$ (46). MPO is a defensive enzyme and even though it serves as a peroxynitrite reductance, the end product, $NO_2^{\bullet}$, is still toxic to the cell. We

have shown here that CCP is able to react with peroxynitrite with an apparent rate constant that is ~ $6.9 \pm 2.2 \times 10^5$ $M^{-1}s^{-1}$ at pH 7.0 and produce NO_2^- as the end product. These results suggest that CCP may scavenge peroxynitrite *in vivo* to protect the cell from its toxic effects.

Previous studies have shown that mitochondrial electon transport is susceptible to peroxynitrite (86). Peroxynitrite inactivates electron carriers of mammalian mitochondria, such as succinate dehydrogenase and NADH dehydrogenase, *in vitro* (86). The ability of peroxynitrite to cross biological membranes was also demonstrated (86) since inactivation of mitochondrial inner-membrane enzymes was evident even when intact mitochondrial preparations were used. Thus, even if peroxynitrite is synthesized in the cytosol it can diffuse into the mitochondria. Still another way that peroxynitrite can be found in mitochondria is from the diffusion of $NO^{\bullet}$ into the mitochondria and its reaction with mitochondrial-derived $O_2^{\bullet-}$. Finally, the reaction of $NO^{\bullet}$ with O_2 to form the nitrosodioxyl radical ($^{\bullet}ONOO$) could also lead to peroxynitrite formation in mitochondria. Because the nitrosodioxyl radical is a good one-electron oxidant ($^{\bullet}ONOO/ONOO^-$ = + 0.44 V), peroxynitrite formation is feasible due to electron leakage from the mitochondrial electron-transport chain (86).

In conclusion, it is believed that CCP is important in yeast mitochondria not only because it is able to protect the cell against oxidative stress but also because it likely defends the mitochondria against peroxynitrite damage.

3.0 PURIFICATION OF CCP AS A GST-FUSION PROTEIN

3.1 INTRODUCTION

3.1.1 Available recombinant forms of cytochrome c peroxidase

Altschul et al. (1) were the first to purify CCP from *Sacharomyces cerevisiae*, but their method was somewhat cumbersome and gave a poor yield (~ 3%, based on the concentration of enzyme in the original extract). Later on, Yonetani et al. (87) revised the purification procedure. The new protocol included ethyl acetate-induced lysis, water extraction and precipitation with ammonium sulfate, followed by chromatography on diethylaminoethyl cellulose (DEAE) column. Both the ethyl acetate-induced lysis and the mild chromatographic procedure increased the yield of CCP in the water extract and resulted in a final homogeneous preparation with no appreciable modification of the enzyme into enzymatically inactive hematin as was the case with the procedure of Altschul et al. (1, 88).

CCP is expressed as a precursor form in the cytoplasm. It is later transformed into the mature protein by proteolytic cleavage of 68 residues from the N terminus, either during or after post-translational translocation into the mitochondria (89). In order to create a system suitable for introducing site-directed mutations for structure-function studies, the cDNA for mature CCP was cloned into different vectors and transformed in *E. coli*. Three recombinant forms of CCP have been expressed so far, CCP, CCP(MI) and CCP(MKT).

CCP(MI), which was the first recombinant form prepared (13), has a methionine

residue inserted at the start of the mature gene sequence followed by a Ile residue. This ensured that only the mature protein was expressed, and also created a *Bcl* I site at the 5'-end of the sequence. This construct was then cloned into the *Bcl* I/*Pst* I sites in the multiple cloning site (MCS) of pUC 8 and transformed in *E. coli* cells. Purification of CCP(MI) was performed initially at UCSD (13) and later on in our lab using a revised protocol (Appendix IA), which involved growth of bacteria in TB media (Appendix II, 1A). The cells were lysed and the supernatant of the cell lysate subjected to gel-filtration chromatography (Sephadex G75) to remove most of the unwanted bacterial proteins, followed by addition of heme to convert apoCCP to holoCCP. Anion-exchange chromatography produced pure CCP and removed excess heme added. Finally, crystallization against dH_2O yielded 100% active enzyme. A typical yield of CCP from this purification method is ~ 400 mg/15 L of culture (Appendix I, A).

CCP(MKT) is the gene product of the cDNA enzyme cloned into pLACCP2-8 (14) and represents the mature sequence with a Met-Lys-Thr addition at the N-terminus. The addition of this sequence was done arbitrarily in an effort to increase the yield of protein expression, and CCP(MKT) was overexpressed in *E. Coli* using the plasmid pT7CCP, where expression is placed under the control of the T7 RNA polymerase. pT7CCP was constructed from the plasmid pLACCP2-8 by replacing the lac promoter with the T7 promoter (15). Induction with IPTG for 4 – 6 h was necessary to achieve high expression of CCP(MKT), and purification of the enzyme from bacterial cells involved similar steps as with CCP(MI). A typical reported yield is ~ 450 mg/15 L of culture (Appendix I, B). The wild-type mature sequence of CCP was also cloned in a vector to achieve hyperexpression. The vector used was pT7-7, and the CCP and lacZ

genes were fused to construct the pT7CCPZf1 plasmid (90). In this case, induction with IPTG for 4-5 h resulted in high-level expression of CCP. The purification procedure used is very similar to the CCP(MI) and CCP(MKT) protocols, and it produces 500 mg of crude secondary crystals/6 L of culture (ie, the first crystallization of CCP) (Appendix I, C).

All three methods discussed so far, and outlined in detail in Appendix I, yield sufficient CCP for structure-function studies. Additionally, the end products are highly pure and native-like in structure and function (13, 14, 90). However, problems are encountered when these recombinant enzymes are analyzed by electrospray mass spectrometry. Methionine aminopeptidase cleaves the initial methionine when the next residue has a radius of gyration of 1.29 Å or less (91). Threonine is the second residue in yeast CCP (1.24 Å) and recombinant CCP is isolated from *E. coli* with and without its initial methionine (91). Partial cleavage of the initial methionine is also encountered in CCP(MI), even though isoleucine has a radius of gyration of 1.56 Å, which exceeds that recognized by methionine aminopeptidase as substrate. Mixtures of CCP(MI) with and without the initial methionine were isolated from *E. coli* in our lab. Of the three different forms of recombinant CCP produced, only CCP(MKT) has an unprocessed initial methionine. While it is desirable for mass spectrometry studies to produce a recombinant form of uniform mass, oxidation of the initial methionine during isolation precluded this with the three recombinant forms available to date. Hence, it was desirable to produce recombinant CCP with no initial methionine. A faster purification method was also desirable because many CCP mutants are to be prepared in our lab in the future. Thus, we decided to express CCP as a fusion protein.

3.1.2 Overview of fusion protein systems

A fusion protein consists of a protein of interest linked to an affinity tag which may either be a small peptide or protein. Fusion protein expression is an easy solution to decrease proteolytic attack encountered in the purification of small proteins. Such systems are also used for purification of cytotoxic proteins, where a chemically inducible promoter provides strict control of protein expression. In most cases (and in our case too), fusion proteins are chosen because of their high level of expression and their ease of purification. A fusion protein can usually be purified to >90% in a single affinity-chromatography step, and recovered from the matrix under mild elution conditions which preserve its antigenicity and functionality. Furthermore, it is easy to monitor the fusion protein in each step of the purification procedure, since antibodies or activity assays are available for many affinity tags.

Of the common fusion tags commercially available, three were considered as potential candidates for our purpose: the His-tag, the FLAG-tag and the GST-tag. The His-tag is a sequence of six histidine residues placed either at the N- or C-terminus of the recombinant protein of interest. The FLAG tag is the octapeptide, N-Asp-Tyr-Lys-Asp-Asp-Asp-Asp-Lys-C, and it too can be added either upstream or downstream of the cDNA of interest. Finally, the GST system uses an enzyme, glutathione-S-transferase, as the affinity tag. Some of the mutants that our lab is planning to prepare are to be used in kinetic studies of electron transfer between the heme of CCP and a ruthenated-surface histidine residue (92). Because the ruthenation reaction is histidine-specific, the His-tag would have to be removed. This is often difficult to achieve since the sequence of six histidines can be hydrophobic and not always surface exposed, preventing access

by proteolytic enzymes. The presence of the His-tag would likely complicate the ruthenation reaction and yield a number of unwanted CCP derivatives.

Therefore, the choice was between the FLAG and the GST systems. The anti-FLAG M1 or M2 affinity gels (specific for the FLAG system), are six times more expensive than the glutathione Sepharose 4B (GS 4B) column used in the purification of the GST-fusion proteins. In addition, the binding capacity of GS 4B is estimated to be ≥ 8 mg of recombinant glutathione S-transferase (MW = 26 kDa) per ml of drained gel (93) whereas 1ml of either FLAG affinity gel, binds ~ 2.5 mg of FLAG fusion protein [eg, 50 nmol of FLAG-derivatized bacterial alkaline phosphatase (MW = 49 kDa) eluted from 1 ml of either anti-FLAG affinity gel] (94). Since the GST system is more economical, we decided to use this system. Another advantage of working with a GST- fusion protein over a FLAG-fusion protein is that cleavage of the former is efficient and easy to monitor by SDS PAGE due to the large difference in MW between the GST-CCP fusion protein and GST or CCP alone (fusion protein, 60 kDa; GST, 26kDa; CCP, 33.8 kDa]. By comparison, the FLAG peptide has a MW of only ~ 1 kDa which would make it difficult to distinguish between cleaved and uncleaved fusion protein by SDS PAGE.

A description of the three recombinant forms of CCP available to date was given above. Their purification from *E. coli* (Appendix I) and reported yields were also outlined. The scope of this study is to develop a new purification method for CCP that is faster and leads to a mature CCP sequence where the initial methionine has been eliminated. Since expression and purification as a fusion protein is a solution to both those goals, a brief introduction on the fusion proteins was given, as well as, the reasons for choosing the GST system.

3.2 EXPERIMENTAL SECTION

3.2.1 Materials

All restriction enzymes, their corresponding 10X buffers and dNTP's were purchased from Promega. All buffer salts were from Sigma. For other materials the company name is indicated in parenthesis. All primers were synthesized by BioCorp Inc.

3.2.2 Methods

A PCR mutagenesis

Usually, the PCR technique involves the amplification of a fragment of DNA whose length is determined by the set of primers used. The 5'-end of the primer can contain any sequence, preferentially one that is recognized by a specific restriction enzyme, but the 3'-end should be complementary to the DNA strand of interest. Therefore, if a mutation is to be incorporated into a gene, it has to be within the primer length and usually at the ends of the DNA fragment to be amplified (95). The technique used here (96) is more flexible, allowing us to introduce a mutation in the middle of the CCP gene and, at the same time, create appropriate sequences at the ends of the gene that are recognized by restriction enzymes.

The method involves two rounds of PCR and two sets of primers (Figure 3.1). The first PCR round involves two separate tubes with the full-length gene as template and primers A/B in one tube and C/D in a second tube. Primers A and D have 3'-ends complementary to the sequence to be amplified and their 5'-ends introduce restriction sites. Primers C and B are complementary to each other and to the template sequence except at the sites where the mutation is to be introduced. At the end of first step, two

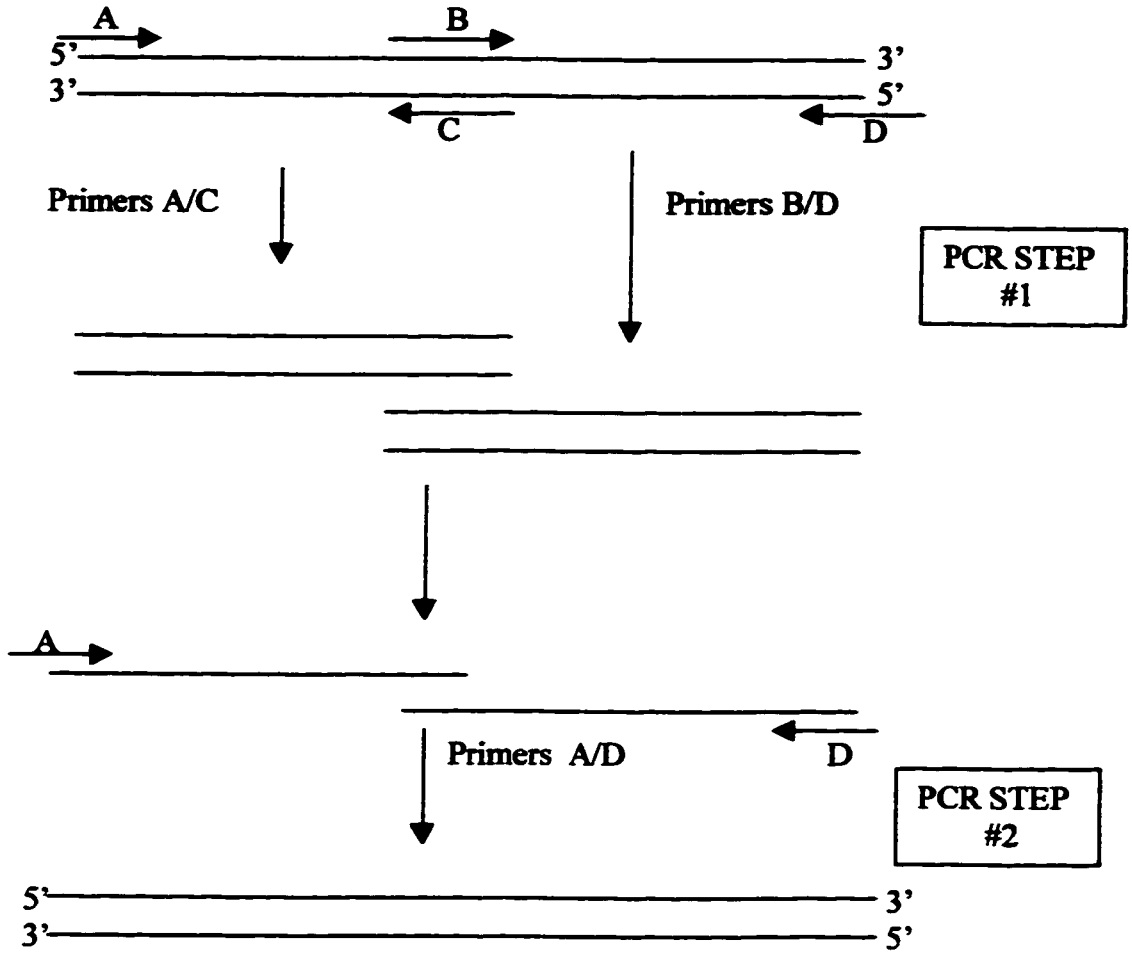

Figure 3.1 Addition of restriction sites to the 5'- and 3'-ends of a DNA fragment and mutation using PCR. In the first step, primers A/C and B/D are used to amplify approximately half the gene fragment, introduce the restriction sites and incorporate the mutation. In the second PCR step, the two halves are brought together with primers A/D, where they anneal to one another following denaturation, and the whole fragment is produced with the mutation incorporated.

PCR fragments are produced, A-C and B-D. When these fragments are brought together in the second step in the same reaction tube, they anneal to one another with the help of their complementary ends. Primers A and D are added to amplify the whole sequence.

The pUC8CCP(MI) vector, kindly provided by Dr. Mark Miller (UCSD), was the source of the CCP cDNA (87). Since the CCP cDNA was to be cloned into the *BamH* I-*EcoR* I site of the GST vector, pGEX-2T (Pharmacia), it was necessary to remove an internal *BamH* I site from the CCP gene. A *BamH* I-silent mutation was introduced into the CCP cDNA by a single base-pair change, T729C, so that the original *BamH* I sequence (G$^{\downarrow}$GATCC) was destroyed (GGACCC) with no effect on the CCP sequence since both GAT and GAC are codons recognized by Asp-tRNA.

The set of primers used for the PCR reactions (based on Figure 3.1) are:

PRIMER A: CCP-GEX-1EX

5' CGC GGA TCC ACA CCG CTC GTT CAT GTC GCC 3'
BamH I site

3'--- --- --- -- TGT GGC GAG CAA GTA CAG CGG --- --- 5' (CCP anticoding strand)

PCR using this primer inserts a *BamH* I site at the beginning of the CCP coding region in frame with the GST gene. The Met start codon and the first residue (Thr) after the Met start codon in wild-type CCP, were eliminated and substituted by Gly and Ser from the linker region from the C-terminal of the GST-tag. Hence, our recombinant protein is named CCP(GS) to indicate the presence of the additional N-terminal residues (Scheme 7).

PRIMER B: CCP-T729C-SEQ

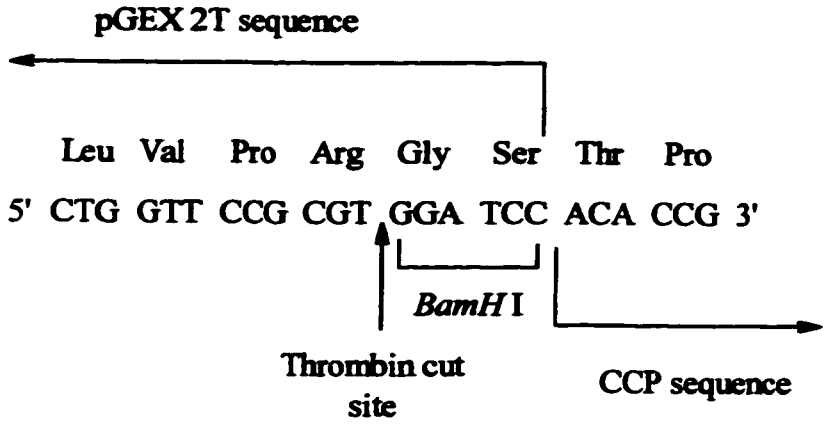

Scheme 7 Schematic representation of the creation of CCP(GS) sequence. Residues 1-4 of mature wild-type CCP are Met-Thr-Thr-Pro. In recombinant CCP(GS) the N-terminal Met-Thr is replaced by Gly-Ser.

5' CTT TGA TTC AGG ACC CCA AGT ACT TAA GC 3'

3' GAA ACT AAG TCC TAG GGT TCA TGA ATT CG --- --- 5' (CCP anticoding strand)

This primer introduces the silent mutation.

PRIMER C: CCP-T729C-ANTI

3' GA AAC TAA GTC CTG GGG TTC ATG AAT TCG 5'

5' CT TTG ATT CAG GAT CCC AAG TAC TTA AGC --- --- 3' (CCP coding strand)

This is the complementary antisence sequence to primer B.

PRIMER D: CCP-GEX-3EX

3' CTC CTT GTT CCA AAT ATC CAG TGA GAA TTC CGG 5'
EcoR I site

5' GAG GAA CAA GGT TTA TAG GTC ACT --- --- --- 3' (CCP coding strand)

Primer D inserts an *EcoR* I site at the end of the CCP coding sequence after the stop codon, TGA.

The PCR cycling conditions used for both PCR rounds were:

Cycle 1:	Cycles 2-21:	Cycle 22:
Denaturation	*Amplification*	*Extension*
5 min at 94°C	45 sec at 94°C	45 sec at 94°C
45 sec at 55°C	45 sec at 55°C	45 sec at 55°C
2 min, 30 sec at 72°C	2min, 30 sec at 72°C	10 min at 70°C

A typical PCR reaction consisted of the following in a reaction volume of 50 µl:

5 µL 10X reaction buffer (Stratagene)

4 µL of primer (2 µl of each primer at 25 pmol/µL)

1 µL of 10 mM dNTP mix

1 µL template (0.1 – 0.2 µg)

1 µL Pfu DNA polymerase (2.5 u/µL; Stratagene)

38 µL of distilled water (dH_2O)

To prevent evaporation, a drop of mineral oil was added on top of the reaction mixture.

B Cloning into the TA and GST vectors

Cloning into the TA vector

The PCR product was cleaned by passing it through a QIAquick spin column (QIAGEN) and eluted with 30 µL dH_2O. To add A overhangs prior to ligation into the

TA vector, 10 μL of cleaned PCR DNA (~ 4 μg) was incubated with 1 μL of Taq polymerase (5 u/μL); (Promega), 5 μL of 10X buffer, 1 μL of 10 mM dATP and 33 μL of dH_2O at 74°C for 30 min. The PCR product with A overhangs (3 μL, ~ 0.2 μg) was mixed with 1 μL of 10X ligation buffer, 2 μL (~ 50 ng) of PCR 2.1 vector, 0.5 μL of 10 mM dATP and 1 μL of T4 DNA ligase (4 u/μL) from the Original TA Cloning Kit (Invitrogen). dH_2O was added to make up a final volume of 10 μL. The reaction was left overnight at room temperature and 2 μL was used to transform INVαF' *E. coli* cells (TA Kit, Invitrogen), following the protocol given by Invitrogen. To screen for ampicillin resistance, and to allow blue-white selection, the transformed *E. coli* cells were plated on agar plates containing ampicillin (ICN Biochemicals) and Xgal (5-bromo-4-chloroindolyl-β-D-galactosidase; Promega) (Appendix II, 2A). White colonies contain the insert ligated in the middle of the lacZ gene which disrupts expression of β - galactosidase. Transformation of pUC 18 DNA (TA Kit, Invitrogen) in the INVα5F' *E. coli* cells was carried out as a positive control. Plates containing these transformants should produce only blue colonies since β galactosidase is expressed due to trans α-complementation with the INVαF' cells.

Analysis of plasmids from the white colonies

White colonies were chosen and used to inoculate LB-Amp liquid media (Appendix II, 1C). Cultures were grown overnight in an incubator-shaker at 37°C and 250 rpm. Plasmid DNA was extracted using the QIAGEN Miniprep kit and eluted with 50 μl dH_2O from the spin column. 10 μl DNA from each colony was digested with *EcoR* I. The digestion reaction was carried out using:

1 μg of vector, 1 μL of restriction enzyme, 2 μL of 10X buffer and X μL dH_2O to a final volume of 20 μL. Samples were incubated at 37°C for 1 h and analyzed on a 1% agarose gel (Appendix II, 4A). If the insert is present, we expect to see a 3.9 kb band corresponding to PCR 2.1 vector and a 902 bp band representing the insert. TA vectors containing the CCP insert are designated TA-CCP.

Cloning into the GST vector, pGEX 2T

The TA-CCP vector was digested with both *EcoR* I and *BamH* I. The digestion reaction mixture was similar to that described in *Analysis of plasmids from the white colonies* but two different enzymes were used which work efficiently at different salt concentrations. The sample was digested at 37°C for 1 h in the low salt 10X buffer; then the high salt buffer was added and the sample incubated for another hour at 37°C to complete the digestion. The mixture was analyzed on a 1% agarose gel (Appendix II, 4A) and the band corresponding to the insert (902 bp) was gel isolated using the QIAquick Gel Extraction kit from QIAGEN.

The pGEX 2T vector was also double digested with *EcoR* I and *BamH* I restriction enzymes and cleaned by passing it through a QIAquick spin column and eluting with 30 μl dH_2O. The cut vector was phosphorylated as follows: 2 μl of *Eco* RI/*BamH* I digested pGEX 2T was incubated with 1μl T4 kinase (Promega), 2μl 10X kinase buffer and 2μl 10 mM dATP. The volume of the reaction mixture was adjusted to 20 μl with dH_2O. The reaction tube was placed at 37°C for 1 h for phosphorylation to take place and then at 65°C for 10 min to inactivate the kinase.

Insert (~ 5 pmole; 1.5 μg in 7 μl) was mixed with 1 μl of cut pGEX 2T vector (1

pmole; 1.6 μg), and 1 μL T4 DNA ligase (Promega) was added together with 1 μL 10X buffer and 0.5 μL 10 mM dATP. After overnight ligation at room temperature, the ligase was inactivated by incubating the sample at 65°C for 10 min. *Sma* I (0.5μL and 1μL 10X buffer) was added to the ligation mixture and the sample was incubated for 2 h at 25°C to reduce background due to uncut pGEX 2T vector (*Sma* I site is present in the MCS of pGEX 2T, but not in vector digested with *BamH* I and *EcoR* I. Therefore, digestion with *Sma* I reduces background due to undigested pGEX 2T in the ligation mixture). The ligation mixture (3 μL) was used to transform 50 μL competent DH5α *E.coli* cells (GIBCO BRL). After addition of the foreign DNA, the bacterial cells were incubated for 30 min on ice. The vial was then placed at 37°C for 20 s and immediately on ice for 2 min. This heat-shock treatment ensures that the DNA is transformed into the bacterial cells. LB media (950 μL) was added to the cells and they were let grow for 1 h at 37°C with shaking (222 rpm). To screen for ampicillin resistant colonies, the transformed *E. coli* were plated onto agar containing ampicillin (Appendix II, 1E). pGEX 2T digested only with *Sma* I was also added to cells and the transformation procedure carried out as described. If *Sma* I digests efficiently, no colonies should be seen when the cells are plated on agar containing ampicillin since cut vector does not transform *E. coli*. Also, the DH5α cells will be sensitive to ampicillin if not transformed with foreign DNA with the ampicillin resistance gene.

Ten colonies were picked from a plate with DH5a cells transformed with the GST-CCP vector and plasmid DNA was extracted as previously described. The isolated plasmids were digested with both *BamH* I and *EcoR* I restriction enzymes and the digests were analyzed on a 1% agarose gel. Bands were expected at 4.9 kb and 902 bp

corresponding to pGEX 2T and the CCP insert, respectively.

C Summary of constructs prepared

TA-vector constructs

The pCR 2.1 vector was supplied digested at the *EcoR* I – *EcoR* I site with T overhangs at the 3'-end of each strand of the open vector (Invitrogen, Original TA Cloning Kit). pUC8CCP(MI) was the source of the CCP cDNA. PCR primers were designed to amplify only the mature CCP DNA sequence. An internal *BamH* I silent mutation was introduced in the middle of the CCP insert and A-overhangs were added to the mutant CCP DNA. Ligation of the 902 bp CCP DNA into the 3.9 kb TA-vector yields the 4.8 kb TA-CCP hybrid vector (Figure 3.2).

GST-vector constructs

The pGEX 2T vector was double digested with *BamH* I and *EcoR* I restriction enzymes. TA-CCP plasmid was digested with the same enzymes and the CCP DNA sequence excised. Ligation of the 902 bp single-mutant CCP DNA to the 4.9 kb pGEX 2T vector, yields the 5.8 kb GST-CCP plasmid (Figure 3.3).

D DNA sequencing

The GST-CCP construct was sent to the Sheldon Biotechnology Centre, McGill University, for sequencing. This was performed with Cy5 labelled dATPs by ALF (Pharmacia). Seven different primers (Scheme 8) were used for this purpose, four of which were used to sequence the anticoding strand of the CCP DNA.

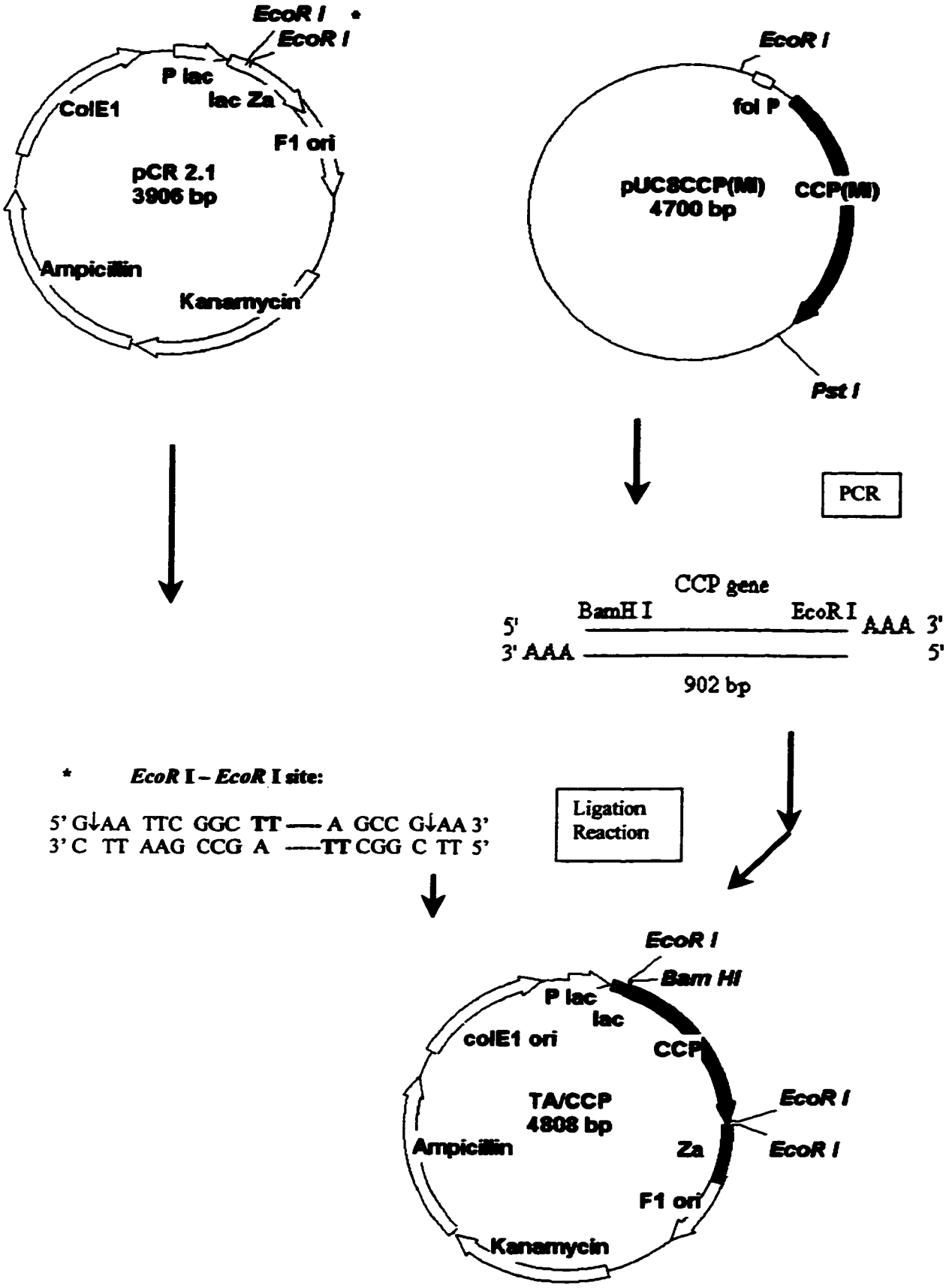

Figure 3.2 Construction of the TA-CCP vector.

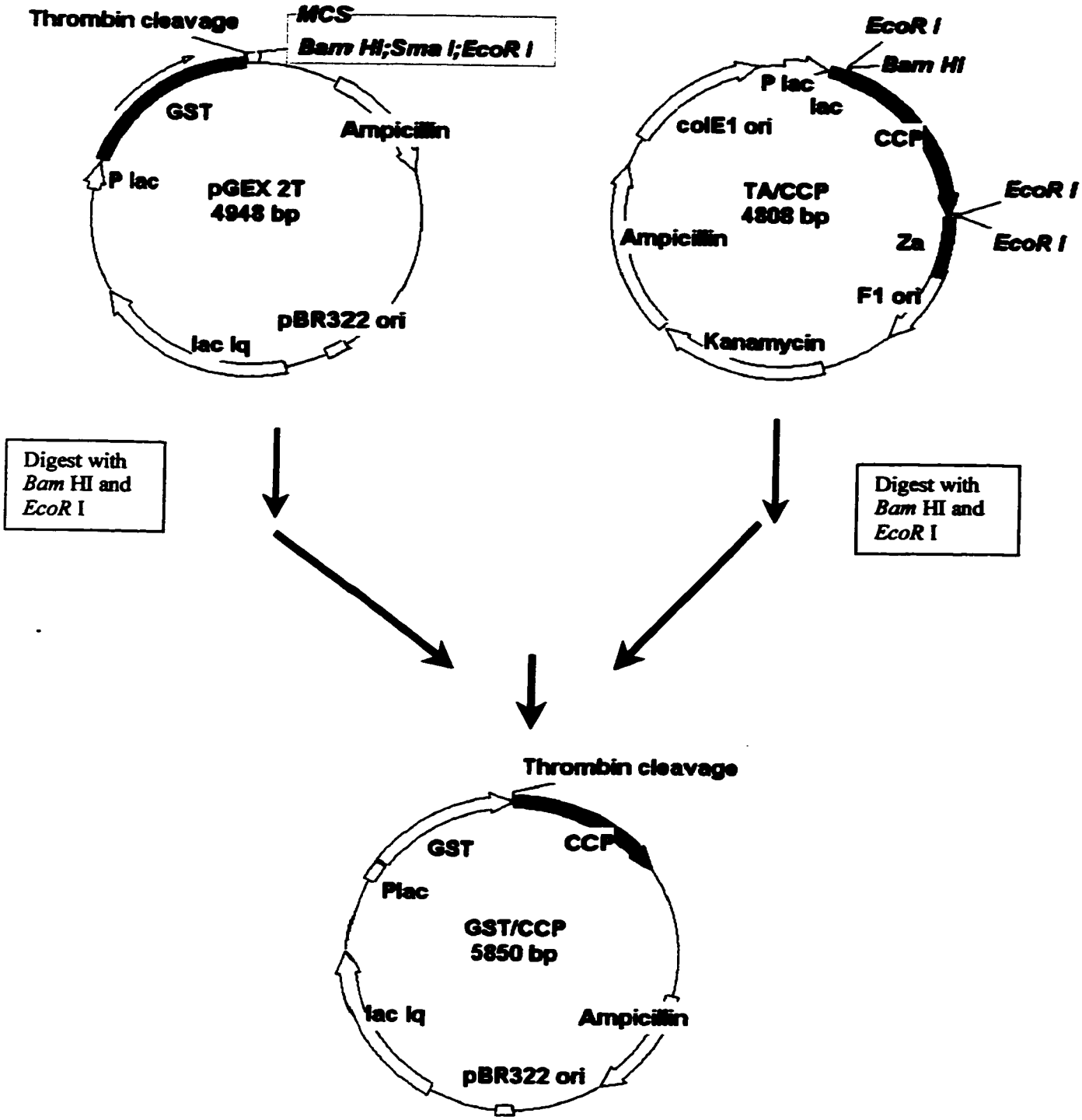

Figure 3.3 Construction of GST-CCP vector

The three primers that were used to read the coding sequence of the single-mutant CCP DNA are as follows:

Primer CCP-GEX-3EX:

3' CTC CTT GTT CCA AAT ATC CAG TGA GAA TTC CGG 5'
EcoR I site

5' GAG GAA CAA GGT TTA TAG GTC ACT CTT AAC 3' *(CCP coding strand)*. This primer was described in Section 3.2.2A.

Primer Y236H-CCP(2):

3' CGG GTG ACT AGT AAG AAA CTA AGT CC 5'

5' GCC CAC TGA TTA TTC TTT GAT TCA GG --- --- --- 3' (CCP coding strand)

Y236H-CCP(2) is complementary to primer CCP-Y236H-mut.

Primer CCP-H60Q-Mut-Anti:

3' CCC TGT TCG TCC TGT TAT GTC CGC 5'

5' GGG ACA AGC ACG ACA ATA CAG GCG --- --- 3' (CCP coding strand)

This primer is complementary to primer CCP-H60Q-Mut-Coding. The 4 primers that were used to sequence the anticoding strand of CCP are:

Primer SEQ 1A:

5' GCA AGT ATA TAG CAT GGC C 3'

3' CGT TCA TAT ATC GTA CCG G --- --- 5' (pGEX 2T anticoding strand)

This primer was used to sequence the start of the CCP gene, since it is complementary to the sequence of pGEX 2T close to the 5'-end of its MCS (bp 844 to bp 863).

Primer CCP-H60Q-Mut-Coding:

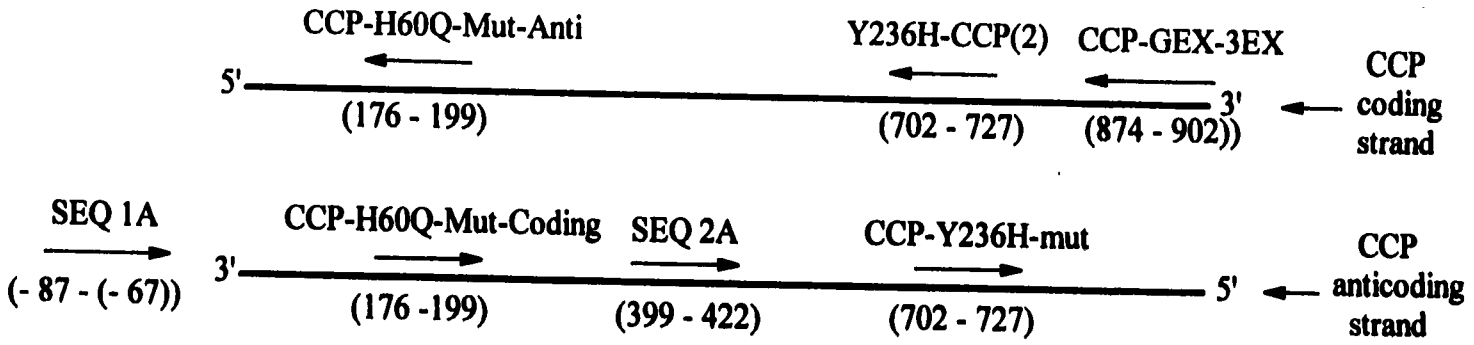

Scheme 8

Sequencing primers and their complementary sites (indicated by base-pair numbers) on the sequence of CCP(GS) gene.

5' GGG ACA AGC AGG ACA ATA CAG GCG

3' CCC TGT TCG TGC TGT TAT GTC CGC --- --- 5' (CCP anticoding strand)

This primer, which was synthesized to create the H60Q mutation by changing codon CAC to CAG, can also be used for sequencing purposes since the template sequence is read upstream of the primer-binding site.

Primer SEQ 2A:

5' CGA CAC GCC AGA GGA TAC TAC CCC 3'

3' GCT GTG CGG TCT CCT ATG ATG GGG --- --- 5' (CCP anticoding strand)

With this primer, we can sequence the middle of the CCP gene since it anneals at bp 399.

Primer CCP-Y236H-mut:

5' GCC CAC TGA TCA TTC TTT GAT TCA GG 3'

3' CGG GTG ACT AAT AAG AAA CTA AGT CC --- --- 5' (CCP anticoding strand)

This mutagenic primer, which was synthesized to create the Y236H mutation by changing codon TAT to CAT, can be used to sequence the 5'-end of the anticoding strand (Scheme 8).

E CCP(GS) expression and purification

The protocols provided by Pharmacia (97), with appropriate modifications, were followed for the expression and purification of CCP(GS) by affinity chromatography.

DH5α cells containing the GST-CCP plasmid were used to inoculate 3 mL of 2X

YTA liquid media (Appendix II, 1D). The culture was grown at 37°C and 250 rpm for 4-5 h until some turbidity was evident. An aliquot (200 µL) of this culture was used to inoculate 20 mL of 2X YTA in a 100 mL-Erlenmeyer flask. This culture was also grown at 37°C and 250 rpm for 2-3 h until slightly turbid. Finally, 1 mL of the latter culture was used to inoculate 1 L of 2X YTA in a 2-L Erlenmeyer flask. A total of twelve 2-L flasks were inoculated and the bacteria were grown under the same conditions as mentioned above, until the $OD_{600\ nm} = 2.0$ (~ 11-12 h). Expression of the GST-CCP fusion protein was induced by adding IPTG (Appendix II, 2F) to a final concentration of 0.5 mM, and growth was continued for another 4 h until $OD_{600\ nm} \sim 2.5$.

All subsequent steps were performed at 4°C. Cells were harvested by centrifugation at 7,700 x g for 15 min using a JA-10 rotor in a Beckman J2-HS centrifuge and resuspended in 36 mL 50 mM potassium phosphate (KPi) buffer, pH 6.0. (Note: volumes used depended on the weight of cell pellet. The volumes given here are appropriate for 50 – 60 g of cells.). Lysis buffer [36 mL; 100 mM KPi, pH 7.5 and 40.3 mM Na_2EDTA (Sigma)] and 6 mL lysozyme (Sigma) (17 mg/mL in 50 mM KPi, pH6.0) were added and cells lysed for 1 h with stirring every 15 min. To further disrupt the cell membranes, cells were frozen in a dry ice/ethanol bath and let thaw overnight at 4°C. Triton X-100 (Sigma) (1%) was added and the mixture was shaken for 30 min at 4°C, to solubilize the fusion protein. Lysis was completed by the addition of 10 mL 2 M $MgCl_2$, 1.8 mL Dnase I (Sigma) (~ 20 mg in 50 mM KPi, pH 6.0) and 60 µL Rnase A (Sigma) (12.5 mg/mL in dH_2O). 200 µL of the lysate was kept for analysis by SDS-PAGE gel (Appendix II4B) and CCP activity assay (Section 3.2.2F) so that the amount of fusion protein present can be determined. The lysate was cleared by centrifugation at 19,000 rpm using JA 20 rotor

in a Beckman J2-HS centrifuge for 35 min. The pellet is dissolved in ~ 80 mL of 50 mM KPi and BioRad Protein assay (98) was performed on the resuspended pellet, cell lysate and supernatant to establish the amount of total cell protein in each fraction. 60 μg of total cell protein in each fraction is loaded on an SDS-PAGE gel (Appendix II4B) to qualitatively detect the amount of fusion protein present.

The supernatant (~ 80 mL) was dialyzed [Spectrapor 2 dialysis tubing; 12 – 14 kDa MW cut-off] overnight against 4 L of 50 mM KPi, pH 7.5 to increase the pH of the supernatant from ~ 6.0 to 7.5. It is important to increase the pH for heme incorporation in the next step.

A 5 mM stock solution of bovine hemin, (Sigma, type I) was prepared in 0.1 N NaOH and the pH adjusted to pH 7.5 with 50 mM KPi, pH 7.5, just before use. A 5-fold molar excess of hemin relative to the CCP expected concentration (from small-scale trials) was added to the supernatant. From 12 L of culture, 300 mg CCP (~ 530 mg fusion protein) were expected so 28.7 mg of hemin (MW 651.9 Da) was dissolved in 1.5 mL of 0.1 N NaOH. This was diluted to 8.8 mL with 50 mM KPi, pH 7.5, and added immediately to the protein solution. The sample was incubated on ice for 1.5 h, with swirling every 15 min. Hemin solution (10 μL) was also added to an aliquot of cell lysate (100 μL) and the supernatant and cell lysate were assayed for CCP activity (Section 3.2.2F).

Following hemin incorporation, the fusion protein was purified by adding the GST-CCP solution (~100 mL) to 40 mL of 50% GS 4B beads (Pharmacia) and end-over-end mixing overnight at 4°C. The beads were pre-equilibrated in 50 mM KPi, pH 7.5 by washing at least 3 times with 10X bed volumes. The estimated capacity of the beads

(from small-scale purification trials) was 3-5 mg of GST-CCP per mL of 50% beads; hence, 120-200 mg of fusion protein is the expected yield for 40 mL of beads. The beads and cell supernatant were mixed in a 500-mL centrifuge bottle to facilitate the washing and cleavage steps.

The GS 4B beads with bound GST-CCP were washed at least 4 times with a 10X bed volume of 50mM KPi, pH 7.5. The buffer was added to the beads, mixed and centrifuged at 500xg using a JA 10 rotor in a Beckman J2-HS centrifuge at 4°C for 5 min, for the beads to settle. Fresh buffer was added and the procedure repeated 3-4 times. The amount of active fusion protein bound to the beads was estimated from that initially present in the cell supernatant minus the amount present in the wash solutions.

CCP was eluted from the beads by cleavage of the fusion protein with thrombin for 4 h at room temperature. One cleavage unit of Boehringer Mannheim thrombin (1 B.M. unit = 12.8 NIH units) was found to release 1.4 - 2.3 mg active CCP. Approximately 50 B.M.U of thrombin (30 U/mg) was dissolved in ~ 50 μL of 50 mM KPi, pH 7.5, just prior to use, and added to the washed beads with the bound fusion protein; 20 mL of 50 mM KPi, pH 7.5 was also added to make up a ~ 50% suspension. Centrifugation at 500xg for 5 min (4°C) allowed the supernatant containing CCP to be removed and the beads were washed with 1X bed volume of buffer. The wash was also combined with the supernatant and the 408/280 nm ratio was checked and found to be 1.25. The CCP solution was concentrated to 25 – 30 mg/mL by ultrafiltration using a 10-mL Amicon stirred-cell concentrator with a YM-10 membrane under 55 psi N_2. The concentration of active CCP(GS) was estimated by the CCP activity assay. The protein was dialyzed overnight in 50 mM KPi, pH 6.0 and then against ice-cold dH_2O to crystallize the protein.

The dH_2O was changed every 15 h and fine, powdery crystals appeared after three days. The crystals were collected by centrifugation at 3,020xg for ~ 3 min, washed in dH_2O and stored in liquid N_2. To prepare for recrystallization, samples were thawed on ice, resuspended in a minimal volume of 0.1 M KPi, pH 6.0 and dialyzed vs cold dH_2O without stirring. The crystals which appeared after 3-4 days were also fine and powdery-like whereas other groups report that recrystallization of CCP in dH_2O yields needle-like crystals [(71) and personal communication with Dr. Mark Miller (UCSD)]. The crystals were collected as before, washed with cold dH_2O, and suspensions in dH_2O stored in liquid N_2.

F CCP activity assay

Throughout the purification, the amount of catalytically active CCP present at each step was determined by measuring its activity. The assay is based on the fact that CCP catalyzes the reduction of H_2O_2 to H_2O by ferrocytochrome c:

$$2 \text{ cyt c } (Fe^{II}) + H_2O_2 + 2H^+ \xrightarrow{\text{CCP}} 2 \text{ cyt c } (Fe^{III}) + 2\ H_2O \qquad (39)$$

There is a large difference in the molar absorptivity at 550 nm ($\Delta\varepsilon_{550} = 19.5\ mM^{-1}cm^{-1}$) between the Fe^{II} and Fe^{III} states of cytochrome c; thus, reaction 39 can be easily monitored at 550 nm (77).

Ferricytochrome c (50 μM) was dissolved in 0.1 M KPi buffer, pH 7.0, so that $A_{550\ nm}$ was ~ 0.5. A few grains of solid dithionite were added to this solution to reduce cytochrome c which gives $A_{550\ nm}$ ~ 1.3-1.4. The ferrocytochrome c solution (500 μL) was mixed with 500 μL of assay mixture (0.1 M KPi, pH 7.0, 10 mM EDTA, 18 mM

H_2O_2) in a 1-mL cuvette. Absorbance at 550 nm was measured with a Hewlett Packard 8451A diode array spectrophotometer 10 s after mixing and this measurement is taken as the blank (no enzyme added). To determine the amount of active CCP, 5 μL of enzyme solution was added to 500 μL of assay mix and 500 μL of ferrocytochrome c was also added to the cuvette and was immediately inverted several times. The first measurement was taken 10 s after cytochrome c addition, and this value minus the blank is taken as $\Delta A_{550\,nm}$. Since it has been established previously that $\Delta A_{550} = 1.0$ for 5 μL of 20 μM CCP in 1000 μL assay solution (84, 99), the amount of active CCP (in mg) can be determined from:

$$\text{mg CCP} = \Delta A_{550} \times 34 \times 20 \times V \qquad (40)$$

where V = total volume of the CCP sample in liters, 34 is the MW of CCP in kDa, and 20 corresponds to the μM concentration of active CCP necessary to give $\Delta A_{550} = 1$ over 10 s.

G Physical characterization of CCP(GS)

Determination of MW of purified CCP(GS) by mass spectrometry

A small crystalline sample of CCP(GS) was dissolved in 0.1 M KPi, pH 6.0 to yield a ~ 20-μM CCP(GS) solution, assuming $\varepsilon_{408\,nm} = 98\ mM^{-1}\ cm^{-1}$ (73). The sample was desalted on a 1-cm C_{18} cartridge (Michrom BioResources) attached to a HP model 1090 HPLC system. 20 μL were added to the cartridge and eluted with a step gradient [10% B (acetonitrile in 0.05% TFA) for 5 min followed by 65 % B for 10 min] at a flow rate of 40 μL/min, and directly infused into the ESI source of a mass spectrometer (Finnigan SSQ 7000) for MW determination. (The LC-MS was performed by Angelo

Filosa).

Titration of CCP(GS) with KCN and NaF

A 0.1-M NaF stock solution was prepared by dissolving 0.4198 g NaF (ICN) in 100 mL 0.1 M KPi, pH 6.0 and the final pH of the solution was adjusted to pH 6.0 with 5N NaOH. A 0.1-M KCN solution was prepared by dissolving 0.651 g KCN (BDH Chemicals) in 0.1 M KPi, pH 6.0. The final pH of the solution was adjusted to pH 6.0 with concentrated HNO_3. CCP(GS) concentration was estimated as described in Chapter 2, Section 2.2.2A. The spectrum of 8.85 μM CCP(GS) was recorded from 250 to 700 nm, and 10X NaF was added to the cuvette and the spectrum re-recorded immediately. The same procedure was carried out for 100X and 1000X NaF, and also for titration of the CCP with 10X, 100X and 1000X KCN. Spectra were recorded at 23°C on a Cary 1 spectrophotometer, with 1.0-nm signal band width (SBW), 1.0-s signal averaging time, 0.25 data interval and 15 nm/min scan rate. All spectra were multiplied by the appropriate factor to correct for the dilution in CCP concentration due to additions of either NaF or KCN.

3.3 RESULTS

3.3.1 Cloning into the TA and GST vector

The goal of this study was to express and purify baker's yeast CCP as a GST-fusion protein. The crystal structure of CCP reveals that the N-terminal Thr residue is

disordered (4). Therefore, we can assume that a high degree of flexibility at the amino terminus is an inherent property of the molecule, not only in the crystal, but also in the enzyme's normal physiological environment. For this reason, fusing a tag to the N-terminus should not alter the structure of CCP. The pGEX 2T vector was chosen from the GST fusion systems available (93) because the GST tag is fused to the N-terminus of the protein of interest.

The cDNA for CCP was cloned into the *BamH* I and *EcoR* I site in the MCS of pGEX 2T. A PCR technique was used to introduce these sites at the 5'- and 3'-ends of the CCP sequence. Since there is an internal *BamH* I site in the sequence of CCP starting at bp 725, a set of mutagenic primers was used to introduce a silent mutation to eliminate the *BamH* I site. The first PCR step yielded the expected 725- and 177-bp fragments (Figure 3.4a), and the combination of these two fragments in the second PCR step yielded the full-length CCP DNA which is 902 bp (Figure 3.4b). The codon for Thr in wild-type yeast CCP was substituted by Gly and Ser codons in the CCP fusion since the thrombin cut site introduces the codons for these residues (Section 3.2.2A, Scheme 7). Hence, our recombinant CCP is designated CCP(GS).

The next step would be to clone the 902-bp PCR fragment from PCR step 2 into the pGEX 2T vector. However, cleavage by restriction enzymes at sites near or at the ends of DNA is often inefficient (100). This was confirmed in our lab since direct cloning of the digested 902-bp PCR DNA into the open pGEX 2T vector was not achieved. Thus, the PCR fragment was subjected to the action of Taq polymerase to add A overhangs and ligated into the TA vector. INVα5F' *E. coli* transformants were grown overnight on LB-Amp-Xgal plates, six white colonies picked and *EcoR* I single

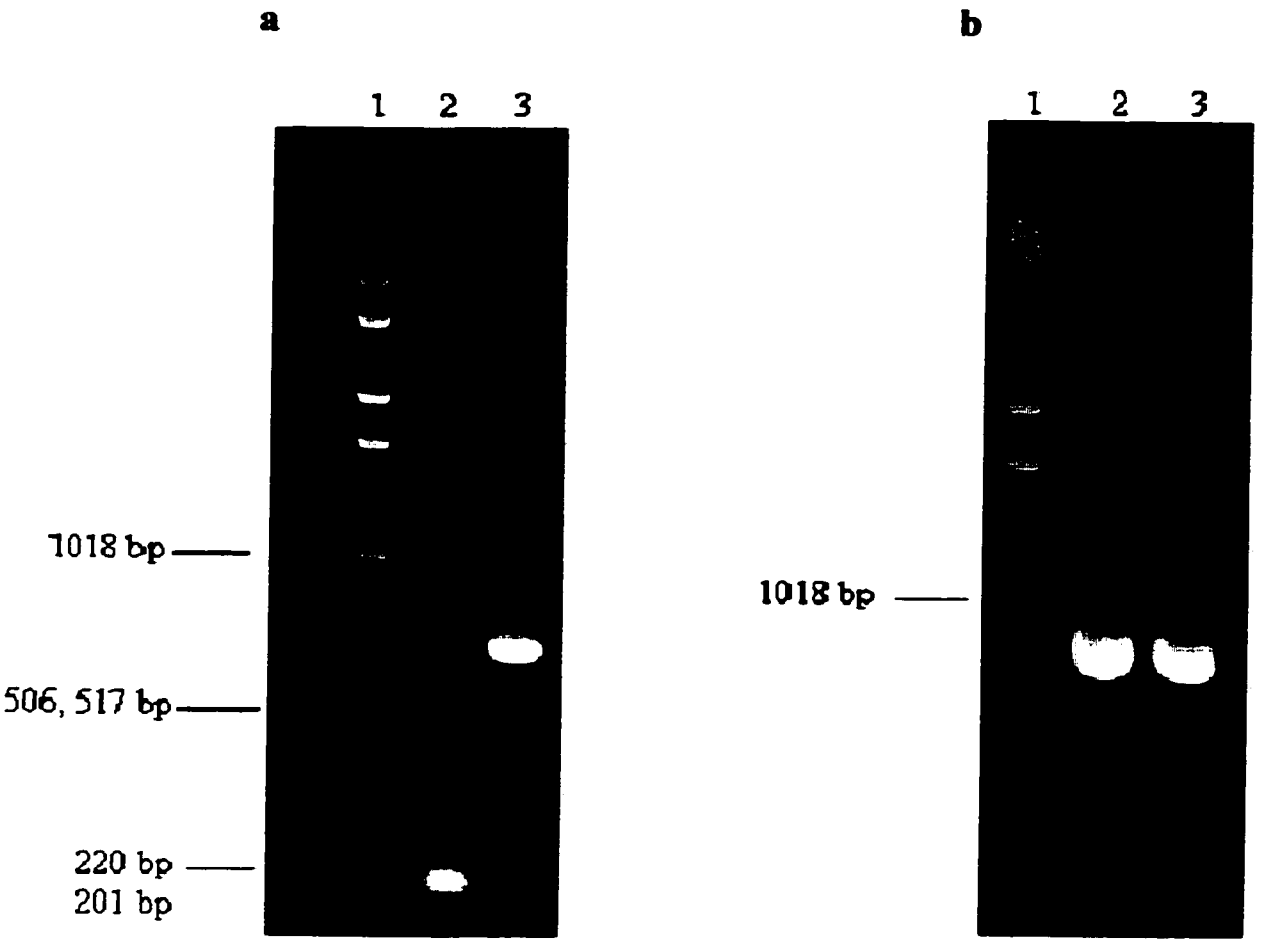

Figure 3.4 Analysis of the DNA fragments from PCR steps 1 and 2 outlined in Figure 3.1. **(a)** Lane 1 contains the MW markers (GIBCO BRL), lane 2 the 177-bp PCR product and lane 3 the 725-bp product from PCR step 1. **b)** Lane 1 contains the MW markers, and lanes 2 and 3 the 902-bp PCR product from step 2. Experimental conditions: 1% agarose gel (Appendix II, 4A) run at 75 – 85 volts for ~ 1 h was used to analyze the PCR products, and the DNA bands were detected under UV light in a transilluminator (Mode FBTIV-816; Fisher Scientific) and a photograph was taken with a photo-documentation camera (Model FB-PDC-34; Fisher Scientific). The photographs were scanned with a UMAX Astra 1220P scanner.

digestion and *EcoR* I – *Hind* III double digestions performed. *EcoR* I digestion cuts the TA-CCP vector at two sites corresponding to the 5'- and 3'-ends of CCP sequence, and the expected 3.9-kb and 902-bp bands were produced corresponding to the PCR 2.1 vector and CCP insert respectively (Figure 3.5). The *Hind* III site is at bp 797 of the CCP insert; therefore, double digestion with *EcoR* I and *Hind* III should produce a 3.9 kb band containing PCR 2.1, and the 797-bp and 105-bp bands of the CCP insert. Such bands were observed (Figure 3.5).

DNA from one of the colonies that contain the expected insert was further analyzed by digestion with *BamH* I and *EcoR* I. This should also excise the insert since these sites were introduced at the 5'- and 3'-ends of the CCP cDNA by PCR. The expected 902-bp band was gel isolated and ligated into the pGEX 2T vector. DH5α *E. coli* transformants were grown overnight in LB-Amp plates and 10 colonies were picked. All contained the desired construct as is evident from the *BamH* I – *EcoR* I, *BamH* I – *EcoR* I – *Hind* III, and *Apa* I restriction analysis (Figure 3.6). *BamH* I – *EcoR* I digestion releases the insert from the vector so two bands are observed at 4.9 kb and 902 bp (Figure 3.6a) corresponding to the pGEX 2T vector and CCP insert, respectively. *BamH* I – *EcoR* I – *Hind* III digestion produced the expected 4.9-kb, 796-bp and 106-bp bands (Figure 3.6b), which confirms that we have the correct insert since the *Hind* III site is at bp 796 of the CCP DNA. Finally, *Apa* I digestion provides further confirmation that the desired construct was obtained since it cuts the CCP insert (137 bp) and pGEX 2T (3854 bp), producing the expected 3.7-kb and 2.2-kb fragments (Figure 3.6c).

3.3.2 CCP(GS) purification

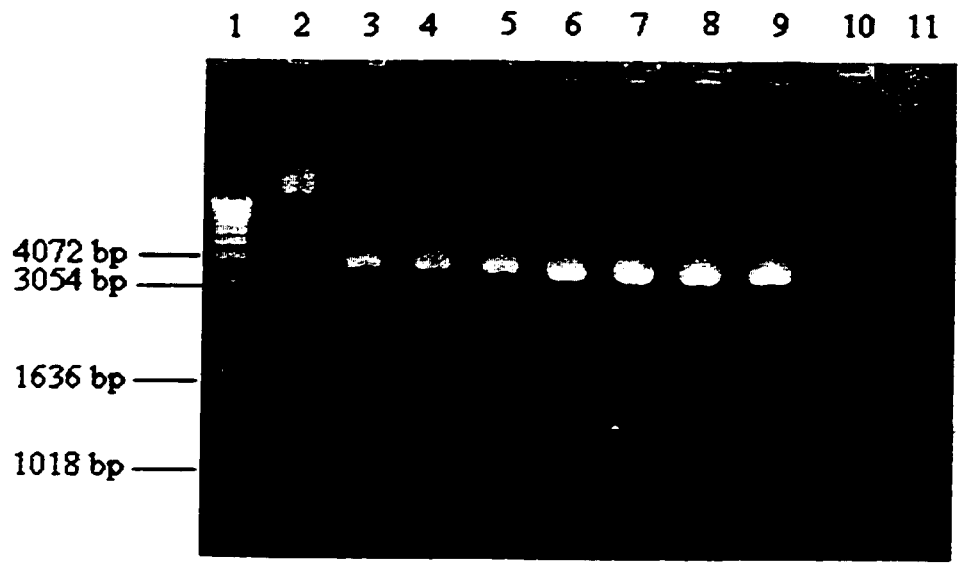

Figure 3.5 Restriction Analysis of the TA-CCP constructs. MW markers (GIBCO BRL) are in lane 1; lanes 2-7 contain *EcoR* I digests of DNA from white colonies. Only colonies contained in lanes 6 and 7 seem to have the correct construct, since digestion with *EcoR* I should excise the 902-bp CCP insert. The large DNA fragment is the PCR 2.1 vector (~ 3.9 kb). The PCR fragment was loaded in lane 11 and the bands below 1 kb in lanes 6 and 7 are identical in size to that in lane 11, confirming that the correct construct was obtained. Lanes 8-9 contain DNA from the same as lanes 6 and 7 but digested with *EcoR* I and *Hind* III, which digests CCP at bp 796, and three bands are produced. In this figure, only the 3.9-kbp and 796-bp bands are shown since the 106 bp band was very faint. As a positive control, PCR DNA was also digested with *EcoR* I and *Hind* III and, as can be seen in lane 10, the same 796-bp band is detected. The experimental conditions are given in Figure 3.4.

Figure 3.6 Restriction Analysis of the GST-CCP constructs.

a) *BamH* I – *EcoR* I digestion. In lane 1, the PCR product from step 2 (Figure 3.4) was loaded as a control. Lanes 2-11 contain DNA from ten different colonies, and all possess the desired insert since the expected 4.9-kb and 902-bp bands are present.

b) *BamH* I – *EcoR* I – *Hind* III digestion. *BamH* I and *EcoR* I excise the insert and *Hind* III digests it into two fragments; therefore, the desired construct produces three fragments. *BamH* I – *EcoR* I – *Hind* III digests of DNA from the same ten colonies were run in lanes 1-10, and the PCR product, digested under the same conditions, is run as a control in lane 11. The expected 4.9-kb, 796-bp and 106-bp bands are present.

c) *Apa* I digestion. *Apa* I digests both the CCP sequence and pGEX 2T. In lane 2, MW markers were loaded. *Apa* I digests of DNA from the same 10 colonies as in (a) and (b) were loaded in lane 1 and lanes 3-10. The presence of the expected bands at 3.7-kb and 2.2-kb confirm that the insert contains the CCP sequence. Experimental conditions: digestions were carried out with 1 – 2 μg DNA, 1 μL of each of the restriction enzyme and 2 μL of 10X buffers were added to give 20 μL digestion. Samples were incubated at 37°C for 2 h, except for the *Apa* I digestions which were carried out at 30°C. (see Section 3.2.2B and Appendix II, 4A for further details). The gel was run as given in Figure 3.4.

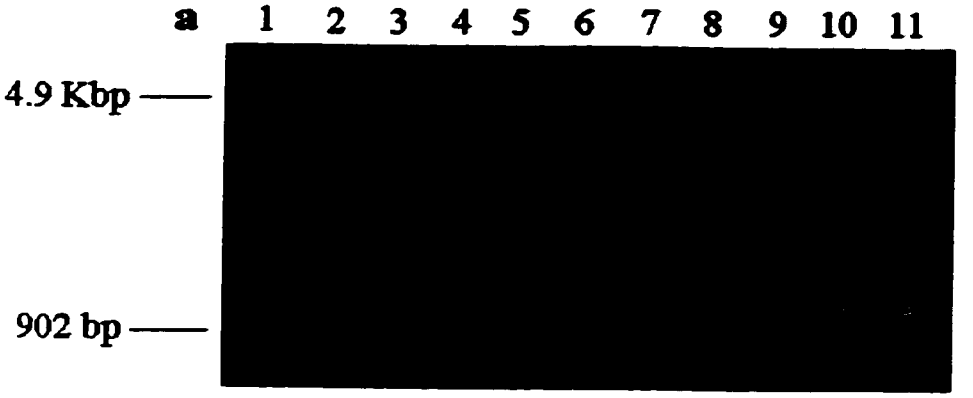
a
1 2 3 4 5 6 7 8 9 10 11
4.9 Kbp
902 bp

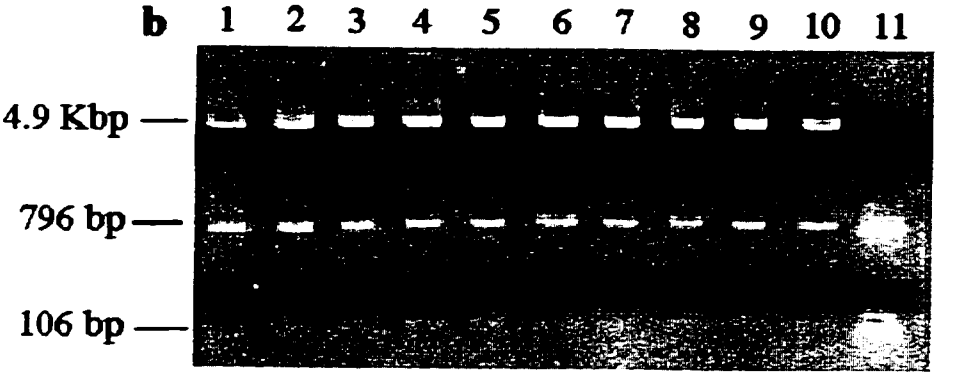
b
1 2 3 4 5 6 7 8 9 10 11
4.9 Kbp
796 bp
106 bp

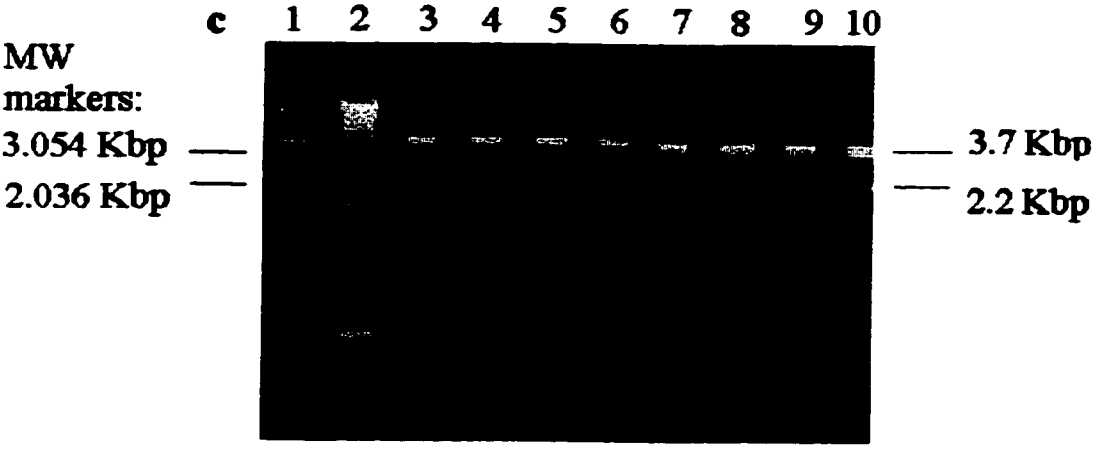
c
1 2 3 4 5 6 7 8 9 10
MW
markers:
3.054 Kbp
2.036 Kbp
3.7 Kbp
2.2 Kbp

DH5α cells transformed with GST-CCP vector were used to inoculate 12 L of 2X YTA media. The culture was grown and induced with IPTG to express the fusion protein as outlined in Materials and Methods (Section 3.2.2E). The cells were harvested by centrifugation, and 48 g of cell pellet was obtained. Cells were resuspended in phosphate buffer and lysed with lysozyme, Dnase I and Rnase A. After centrifugation proteins in the lysate, pellet and supernatant were analyzed by SDS PAGE (Figure 3.7a). Most of the fusion protein is present in the supernatant as expected for a soluble protein such as CCP.

The CCP activity assay was used to monitor the amount of CCP present at each step of the purification and the results are summarized in Table 3.1. Fusion protein bound to the GS 4B resin was cleaved with thrombin and highly pure CCP was eluted as can be seen from Figure 3.7b. In summary, 12 L of culture produced 300 mg of CCP (which corresponds to ~ 530 mg of fusion protein since the MW of CCP is 34 kDa and that of GST is 26 kDa) in the cell lysate. Predicted fusion-protein yields with the GST system range from 1 to 10 mg/L of culture, with an average yield of 2.5 mg/L of culture (97, 101). Based on this estimate, our yield of 44 mg GST-CCP/L culture is much more than expected. From the 300 mg active CCP in the cell lysate, 270 mg remains soluble in the supernatant (Figure3.7a, Table 3.1), and 50 mL of 50% GS 4B beads bound 135 mg of CCP (240 mg fusion protein). This corresponds to a binding capacity of 6 mg of fusion protein/mL, which exceeds the capacity estimated in our lab from small- scale purification trials (3-5 mg GST-CCP protein/mL of 50% beads). Such a high binding capacity was unexpected since it was shown that the saturation of GS beads is dependent on both the MW and the bulkiness of the fusion protein (102). Based on the reported size

Figure 3.7 SDS-PAGE Analysis of the GST-CCP protein purification. **(a)** Lane 1 contains the MW markers (BioRad). Lane 2 contains 1.12 μL of cell lysate, lane 3, 0.87 μL of supernatant and lane 4, 0.9 μL pellet of the cell lysate resuspended in buffer as discussed in Section 3.2.2E. In lane 5, bovine serum albumin was loaded as an additional marker (MW = 66 kDa). Experimental conditions: The total cell protein was estimated using the Biorad assay. 60 μg of proteins was loaded per lane. A 12% SDS-PAGE was prepared and run as described in Appendix II, 4B. **(b)** Lane 1 contains the MW markers, lanes 2 and 3 contain 7 μL and 5 μL, respectively, of the concentrated, cleaved-CCP solution prior to crystallization. The high purity of CCP solution is evident since bands due to contaminating proteins are much less intense compared to the CCP-containing bands in lanes 2 and 3. Lane 4 contains bovine serum albumin as a marker (MW = 66 kDa).

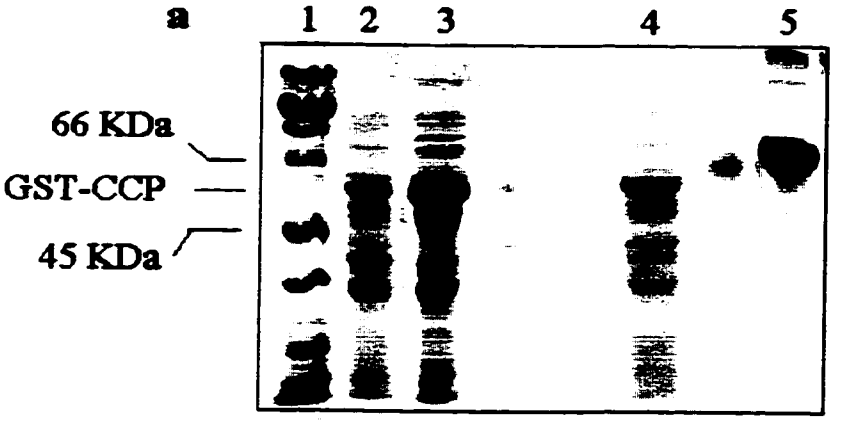
a
1
2
3
4
5
66 KDa
GST-CCP
45 KDa

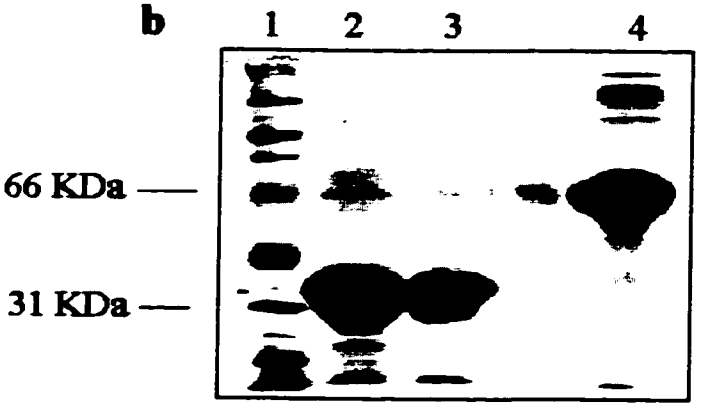
b
1
2
3
4
66 KDa
31 KDa

Table 3.1 Active CCP present at each step of the purification procedure[a]

Purification step	Active CCP (mg)	% Activity[b]
Cell lysate	300	100%
Supernatant[c]	270	90%
Total CCP in bead wash[d]	135	45%
CCP bound to GS 4B beads[e]	135	45%
Cleaved CCP [f]	100	33%
Recrystallized CCP	60	20%

[a] CCP assay, as described in Section 3.2.2F, was performed on each fraction.

[b] %Activity is relative to the cell lysate.

[c] Supernatant from cell lysate.

[d] Combined run-off from four washing of the GS 4B beads.

[e] Active CCP bound to 40 mL of 50% GS 4B beads suspended in 50 mM KPi, pH 7.5. The estimated capacity of the beads is 68-113 mg CCP based on 3-5 mg GST-CCP per mL (see Section 3.2.2E).

[f] 50 B.M.U of thrombin dissolved in ~ 20 mL of 50 mM KPi, pH 7.5 were added to the beads 4 h to cleave the fusion protein.

selection imposed by the beads, we expected ~ 0.3 mg of the 60-kDa GST-CCP fusion protein to to bind to 1 mL of 50% beads since it was estimated that an average of 3 μg of a 70 kDa-fusion protein bound to 5 μL of Pharmacia GS 4B beads (101), which corresponds to 0.3 mg/mL of 50% beads. In fact, the GST-CCP capacity is closer to GST only capacity (4 mg/mL of 50% beads) of GS 4B indicated by Pharmacia.

After four washings and cleavage with thrombin, we recovered 100 mg of active CCP from the 135 mg bound to the beads (Table 3.1). Thrombin does not show as a contaminant, in Figure 3.7b because the MWs of thrombin and CCP are close (38 and 34, respectively). A test of the purity of CCP is the ratio of absorbances (R) at 408 nm and 280 nm. If CCP is in its native state and highly pure, R is in the range of 1.2-1.3 (see Section 2.2.2A) (77). Despite the fact that thrombin has high 280-nm absorption [$\varepsilon_{280\ nm}$ = 74.1 $mM^{-1}\ cm^{-1}$ (103)], the purity index of cleaved CCP was found to be 1.26. The 1.66 mg of thrombin add per 100 mg CCP(GS), did not alter the spectrum of CCP (data not shown). This cleaved CCP(GS) was concentrated to 25-30 mg/mL and dialyzed against dH_2O to induce crystallization. Very fine powdery crystals appeared which had a purity index of 1.34, and recrystallization did not increase the size of the crystals. The CCP(GS) concentration estimated from its Soret absorption [assuming $\varepsilon_{408\ nm}$ = 98 $mM^{-1}cm^{-1}$ as for yeast CCP (73)] revealed that CCP(GS) was only 61.5 % as active as yeast CCP.

3.3.3 Sequence of CCP(GS) gene

The sequence of the CCP(GS) DNA (Appendix II) was found to be identical to the published yeast CCP sequence (89) except for the changes we introduced. The initial

codons that correspond to Met and Thr were replaced by Gly and Ser codons and the silent T to C mutation at base 725.

3.3.4 MW determination of CCP(GS)

The MW of CCP(GS) purified from DH5α cells was estimated by electrospray mass spectrometry (Figure 3.8a). As can be seen from Figure 3.8b, the MW of CCP(GS) is 33,532 ± 2 Da, which agrees very well with the value of 33,529 Da, predicted from the translated sequence of CCP(GS) gene, and within the 0.01% error expected for ESI-MS measurements.

3.3.5 Fluoride and Cyanide complex of CCP(GS)

Although the recombinant CCP(GS) purified from DH5α cells transformed with the GST-CCP vector possesses the predicted MW, its activity is only 61.5% that of yeast CCP. To identify possible reasons for the low activity, the spectral properties of CCP(GS) and its adducts were examined since the Soret and charge-transfer bands are sensitive to the coordination state of the iron in heme proteins. The spectrum of unligated CCP(GS) (Figure 3.9a and b, Table 3.2) is similar to that of yeast CCP (72, 73, 104, 105) with maxima at 408, 508 and 642 nm and a purity index (408/280) of 1.32. The latter value, however, can be influenced by the preparation conditions [ie., a R value of 1.5 does not indicate a more pure enzyme preparation but is due to the formation of 6-coordinate high-spin heme in certain buffers (72)]. The ratios of the 408/380 and 620/647 absorbancy provide a sensitive indicator of the coordination state of ferric iron in CCP (72, 73), and based on the work of Yonetani and Anni (73), both of these ratios

a)

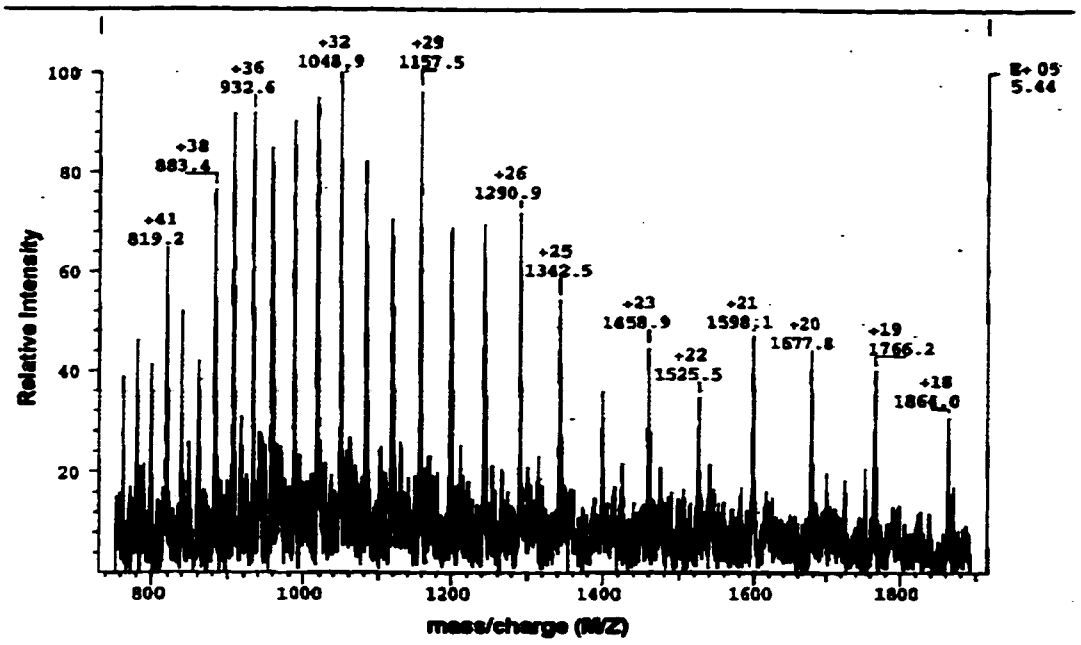

b)

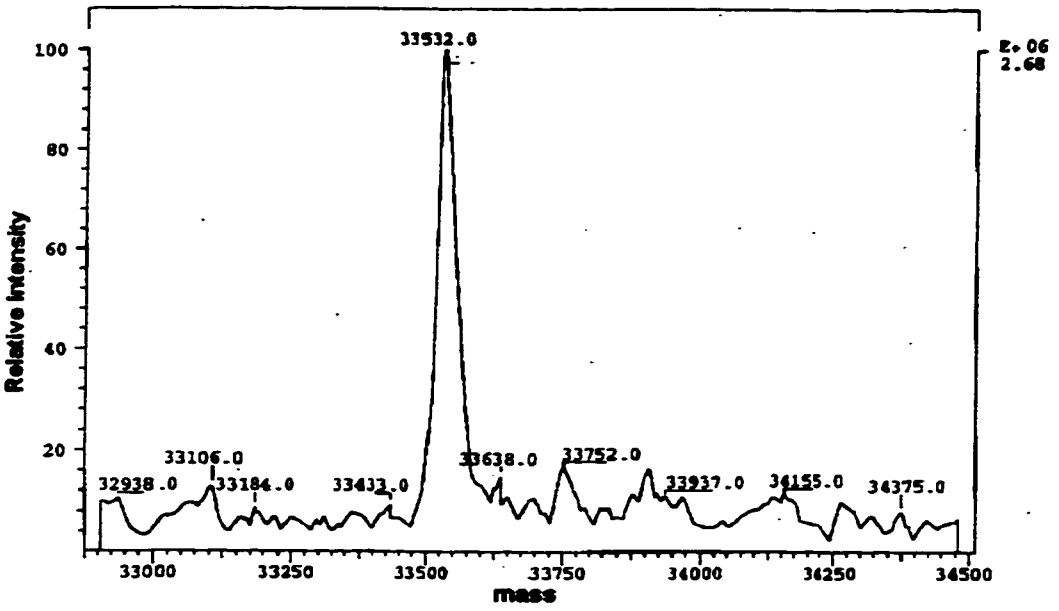

Figure 3.8 Mass spectrum of CCP(GS).

a) ESI mass spectrum of CCP(GS) (average of 30 scans). For experimental conditions see Section 3.2.2G. **b)** The deconvoled mass spectrum. MW is 33532 ± 2.2 Da.

a)

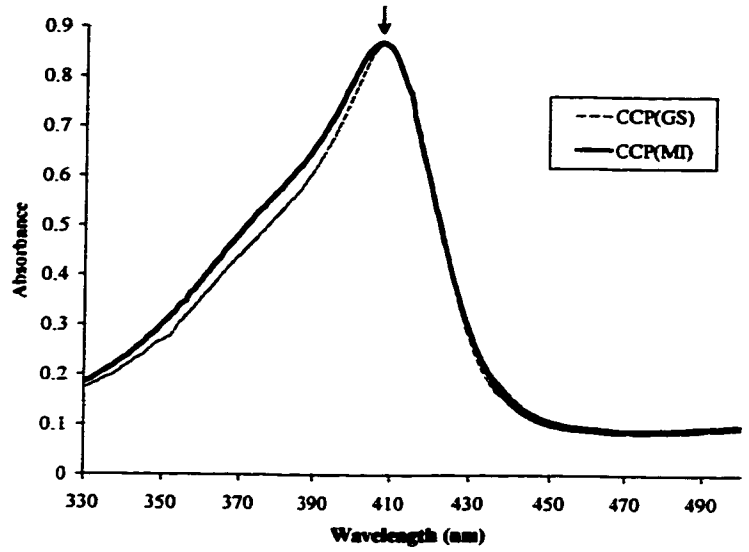

b)

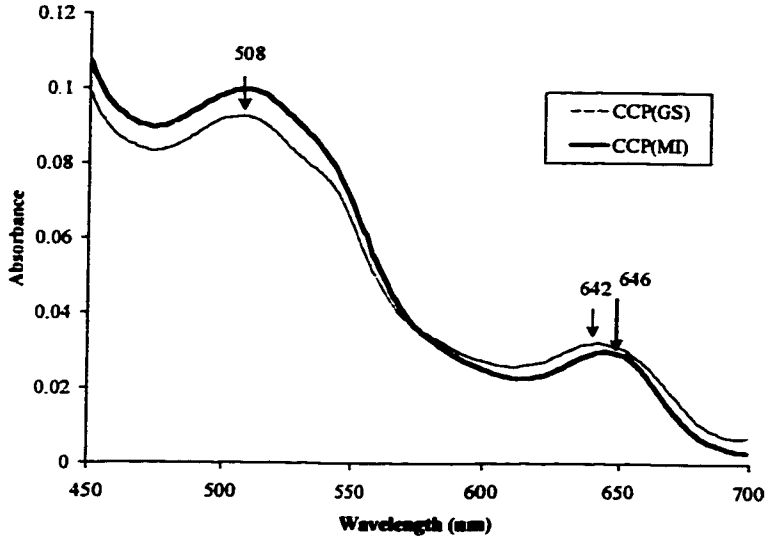

Figure 3.9 Overlay of the absorption spectrum of 8.85 μM CCP(GS) and CCP(MI). **(a)** The Soret region where the arrow indicates the maximum at 408 nm for both forms of CCP. **(b)** The visible region where the arrows indicate the maxima in the charge-transfer bands at 508 nm and 642 nm for CCP(GS). 646 nm band corresponds to CCP(MI).

Table 3.2 Electronic absorption maxima of CCP(GS) at 0.1 M KPi, pH 6.0 and comparison with the reported values for yeast CCP

CCP	λ max (nm)	ε (mM^{-1} cm^{-1})	408/380 nm	620/647 nm	F^- Complex (λ max)	CN^- Complex (λ max)
CCP(GS) (pH 6.0)	408 508 642	98[a] 10.5 3.6	1.66	0.85	407 620	424 542.5
YCCP	408[b] 507.5[b] 645[b]	98[b] 10.6[b] 3.0[b]	-	-	407[e] 620[e]	426[h] N.D.
	408[c] 507[c] 646[c]	99[c] 11.4[c] 3.4[c]	1.54±0.06[c]	0.78± 0.04[c]	407[f] 610[f]	424[f] 530[f]
	- 506[d] 646[d]	- 11.4[d] 3.4[d]	-	-	407[g] 617[g]	424[g] 540[g]

[a]This value was taken to be the same as wild-type CCP value reported by Yonetani et al. (0.1 M phosphate or Mes buffer, pH 7.0) (73).

[b]Values reported by Pond et al. (0.1 M sodium acetate buffer, pH 5.0) (105).

[c]Values reported by Vitello et al. (two buffer systems at pH 7.0 were used: 0.1 M KPi and 10 mM KPi with KNO_3 to adjust the ionic strength to 0.1 M) (72).

[d]Values are the average of previously reported estimations in different buffering systems (pH 7.0) as outlined by Vitello et al. (104).

[e]Values reported by Yonetani et al. (0.1 M Mes buffer, pH 5.0) (73).

[f]Values reported by Yonetani et al. (50 mM sodium acetate buffer, pH 6.0) (87).

[g]Values reported by Yonetani et al. (0.1 M sodium acetate buffer, pH 6.0) (106).

[h]Value reported by Erman (0.01 M sodium acetate buffer, pH 6.0 adjusted to 0.15 M ionic strength with KNO_3) (107).

increase with the aging of CCP (72, 73). The 408/380 and 620/647 absorptivity ratios for recrystallized CCP(GS) were found to be 1.66 and 0.85, respectively (Table 3.2), values close to 8% higher than those reported for 5-coordinate, high-spin CCP (72) (see Section 2.2.2A) and indicate the presence of a small portion of aged or 6-coordinate, high-spin CCP(GS) in our preparation.

The fluoride and cyanide adducts of CCP(GS) were also formed, and these adducts are purely 6-coordinate, high- and low-spin, respectively. The formation of the fluoride adduct of CCP is characterized by the intensification of the Soret band, the loss of the high-energy shoulder, and a blue-shift of the 645-nm charge-transfer band (73, 87, 106). The same spectral features are evident in the spectrum of the fluoride complex of CCP(GS) (Figure 3.10a and b). Upon 1000X F^- addition to CCP(GS) [$K_D = (0.6 \pm 0.4) \times 10^{-4}$ M (108)] the Soret band shifts to 407 nm with a molar absorptivity increase from 98 to 128.4 $mM^{-1}cm^{-1}$ (Figure 3.10a) and the 642-nm band of the native enzyme seen in Figure 3.9, is now replaced by a 620-nm band (Figure 3.10b). These absorbance maxima correspond to previously reported values (Table 3.2) (73, 87, 106). The CN^- adduct of CCP is characterized by red-shifting of the Soret, the loss of the high-energy shoulder, substitution of the 507-nm charge-transfer band by the β-band at 540 nm, and complete loss of the 645-nm band (87, 106, 107). The spectrum obtained for the strong-field CN^- adduct of CCP(GS) is shown in Figure 3.11. Upon addition of 1000X CN^- to CCP(GS) [$K_D = 3.0 \pm 0.2$ μM (87)], the Soret band shifts to 424 nm ($\varepsilon_{424\ nm} = 103\ mM^{-1}\ cm^{-1}$), which is identical to the previously reported value (107) and the β band is observed at 542.5 nm (Table 3.2).

a)

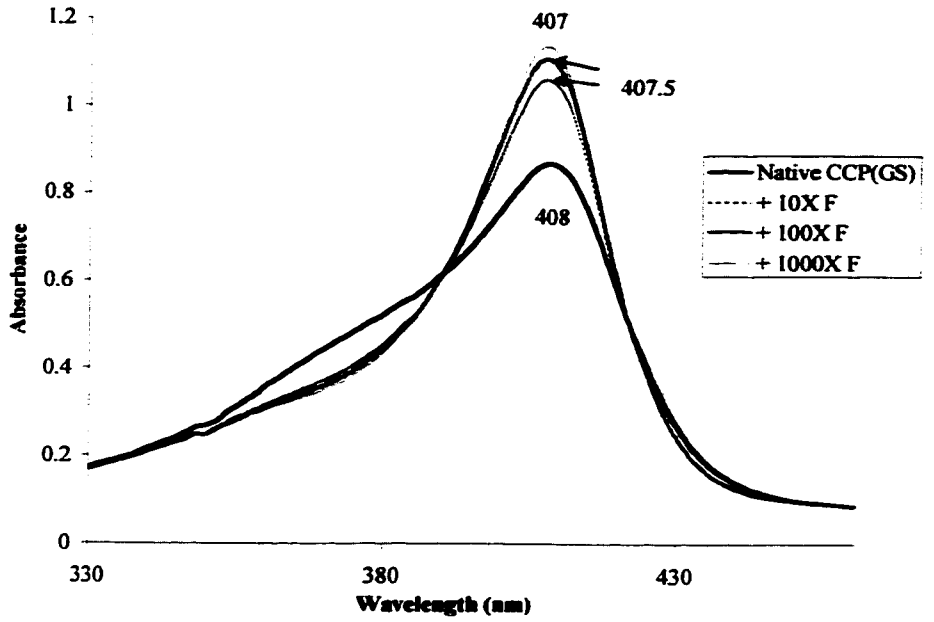

b)

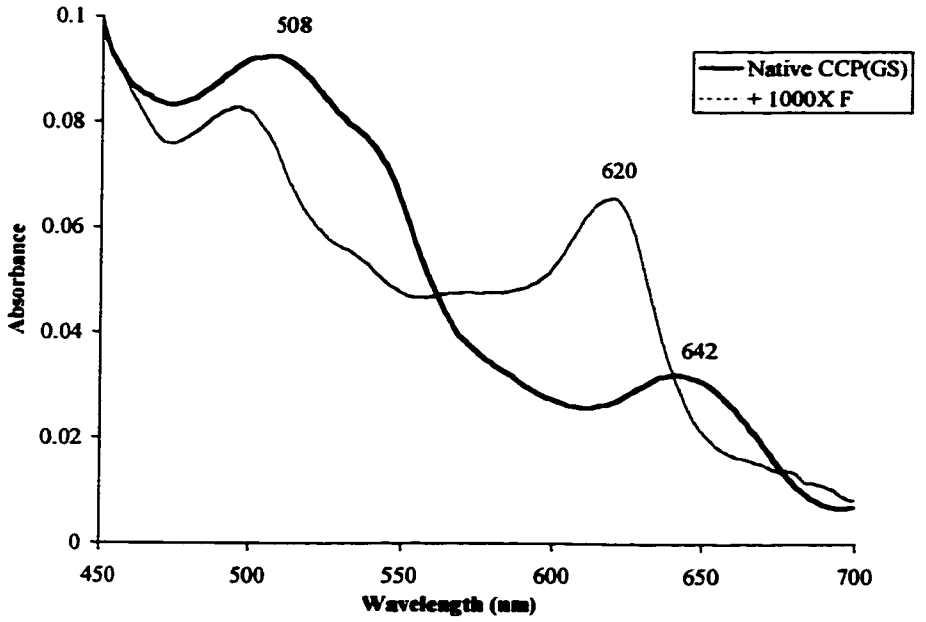

Figure 3.10 Electronic absorption spectrum of the fluoride adduct of 8.85 μM CCP(GS) at pH 6.0, 23°C. **(a)** The change in the Soret maximum and **(b)** the shift in the charge-transfer band are shown when CCP(GS) binds F^-.

a)

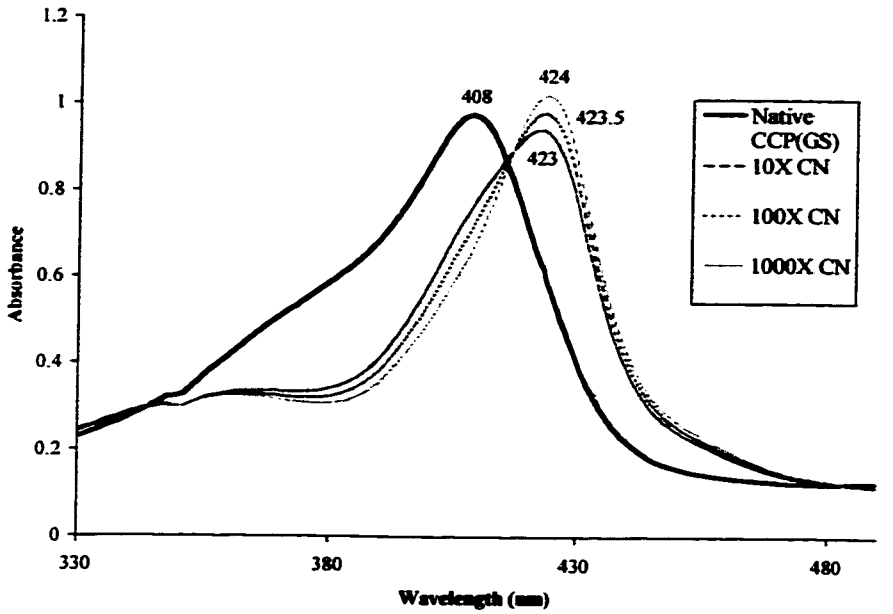

b)

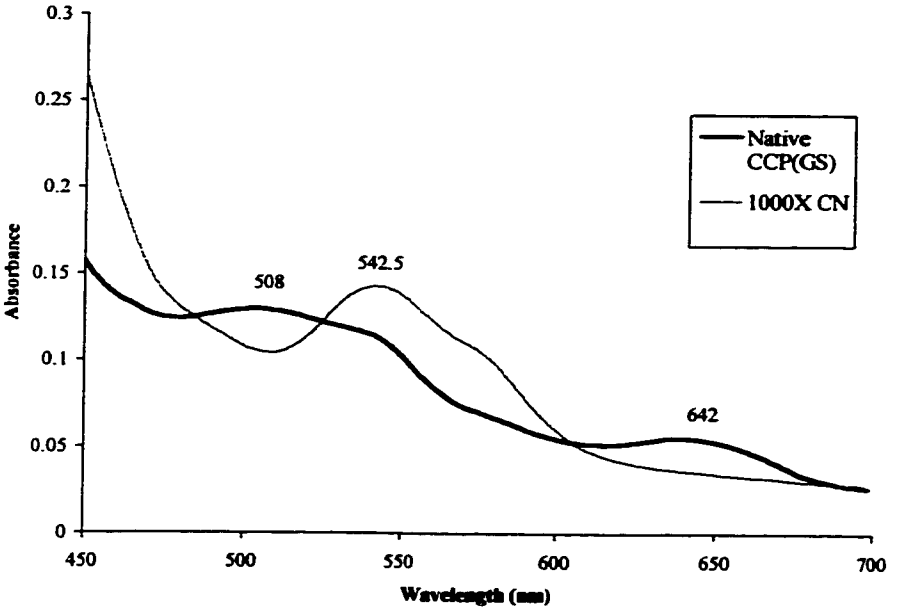

Figure 3.11 Electronic absorption spectrum of the CN^- adduct of 9.96 μM CCP(GS) at pH 6.0, 23°C. The change in the Soret maximum **(a)** and the charge-transfer bands **(b)** are shown when CCP(GS) binds CN^-.

3.4 DISCUSSION

Three successful methods have been developed for the purification of recombinant yeast CCP from *E. coli*: CCP (90), CCP(MI) (13) and CCP(MKT) (15). Yields as high as 400-500 mg of highly pure enzyme with 100% activity per 15 L of culture grown were produced (personal communication, Professors A. Grant Mauk and Tom Poulos). Here we describe a method which combines both high-level production and fast-affinity purification of CCP. Also, using this method, we were able to express and purify CCP without its initial Met. The method involves cloning a modified CCP cDNA downstream of the GST gene in the pGEX 2T vector. After expression, the GST-CCP fusion protein is purified by affinity chromatography.

The published purification procedures for the recombinant forms of CCP are almost the same (Appendix I). After lysis of the cells and centrifugation, the supernatant is dialyzed in phosphate buffer containing EDTA, passed through a gel filtration column and the apo-CCP fractions are converted to holo-CCP, by addition of a 5X hemin solution. Further purification is achieved by anion exchange chromatography, the CCP fractions are pooled and concentrated, and CCP is crystallized by dialysis against ice-cold dH_2O. The purification of CCP(MKT) involves the same steps except that a 1:1 hemin solution is added to concentrated apo-CCP after the anion exchange step, the holoenzyme is first dialyzed against phosphate buffer (pH 6.2) and then against dH_2O to induce crystallization.

All three published protocols require about the same amount of time to purify CCP. In our hands the CCP(MI) protocol takes about 2 weeks and produces ~ 400 mg/ 15 L of culture grown. With the method described here, a single affinity chromatography

step is sufficient to purify the GST-CCP fusion protein. Cleavage of this fusion protein with thrombin yields CCP(GS) as revealed by ESI-MS (Section 3.3.4). Also, sequencing of the CCP insert in pGEX 2T vector (Sections 3.2.2A and D, Appendix III) confirm that CCP(GS) was expressed.

Typical expression yields cited for the GST-system range from 1 to 10 mg of fusion protein per liter of culture; therefore, our yield of 530 mg GST-CCP per 12 L of culture is unexpectedly high. An even higher expression level was obtained when we increased the induction time from 4 to 8 h after IPTG addition. However, this reduces the solubility of the GST-CCP as revealed from small-scale trials; where most of GST-CCP was found in the lysate pellet.

Thrombin cleavage was monitored over time and SDS-PAGE and CCP activity assays revealed that 4-16 h cleavage time at room temperature yields approximately the same amount of free CCP(GS). Excess heme, added to apo-GST-CCP prior the affinity chromatography step, binds to the GS 4B beads. In an attempt to avoid this, the fusion protein was passed through a BSA affinity chromatography column after the heme incorporation step. Although hemin reportedly binds to BSA (109), this step did not affect the free hemin content of the GST-CCP solution, and was thus eliminated from the procedure.

Our final yield was 100 mg of cleaved, active CCP(GS) per 12 L of culture (Table 3.2). After recrystallization, 60 mg of CCP(GS) (Table 3.2) was recovered which is a low yield compared to these obtained for the other recombinant forms of CCP. For example, we were able to purify up to 400 mg of CCP(MI) from a 15 L culture. The relatively low binding capacity of the GS 4B affinity gel and the efficiency of thrombin

cleavage of the GST-CCP limit the scale-up of our method. Since we estimate that 6 mg of GST-CCP is bound per ml of 50% beads, to extract all the GST-CCP from the supernatant of the cell lysate, ~ 100 mL of 50% beads would be necessary to recover all the CCP. Also, more thrombin (~ 135 U) would have to be added to the beads. These changes would greatly increase the cost of the purification. Since the purification is so rapid, it is recommended that the cell paste be stored and purified as required in smaller amounts (eg, ~ 10g of cell paste vs the 48g used here).

The major problem that we encountered with this new protocol is that the CCP(GS) obtained is only 61.5% active relative to yeast CCP, assuming that CCP(GS) possesses the same Soret absorptivity [$\varepsilon_{408\ nm} = 98\ mM^{-1}cm^{-1}$ (73)]. The MW of CCP(GS), as determined by mass spectrometry (Figure 3.8 a and b), is 33,532 ± 2.2 Da, which is within experimental error of the theoretical value (33,529.4 Da) predicted from the gene sequence. Therefore, the low activity of CCP(GS) is not due to unspecific cleavage by thrombin. The thrombin used to cleave the fusion protein remains in solution with CCP(GS) but should be eliminated after the recrystallization step since thrombin does not crystallize in dH_2O (110). The purity index of CCP(GS) after recrystallization was found to be 1.32 which is indicative of a pure CCP preparation [1.2-1.3 represents highly pure enzyme (71)].

The Soret and charge-transfer absorption bands are sensitive to the coordination state of the ferric heme iron in CCP. Yeast CCP has a 408-nm Soret maximum and 506-508 and 645-646 nm charge-transfer bands (Table 3.2). The electronic absorption of CCP(GS) (Figure 3.9) is similar to that of yeast CCP (Table 3.2). However, the blue end shoulder of the Soret is not so intense in CCP(GS) as in CCP(MI) and the lower energy

charge-transfer band of CCP(GS) is blue-shifted to 642 nm, which is indicative of aged CCP (6-coordinate, high-spin) but, complete conversion to a 6-coordinate, high-spin heme (such as the F^- adduct) gives rise to an absorption band at 620 nm; therefore, the amount of aged CCP in our sample must be small. The 408/380 and 620/647 absorptivity ratios are also indicative of the spin state of CCP (72 ,73). For native CCP, the values of these ratios are 1.54 ± 0.06 and 0.78 ± 0.04, respectively (72) whereas, the values found for CCP(GS) are 1.66 and 0.85, respectively (Table 3.2). An 8% increase in both values is a clear indication that there is indeed some small portion of aged (or 6-coordinate, high-spin) CCP(GS) present in our purification. Aged CCP(GS), is expected to show decreased activity (72), but the low concentration of aged CCP(GS) predicted from the spectra cannot account for the ~ 40% lower activity observed. A possible reason for the low activity is that the CCP(GS) sample was crystallized too rapidly. For example, stirring of the water during crystallization may have induced crystals to form too fast. Also, freezing and thawing of the crystals prior recrystallization may have induced the aging of CCP(GS). The fact that, even after recrystallization, we did not obtain needle-like crystals characteristic of CCP (71) may account for the lower activity of CCP(GS) purified to date. The crystallization steps appear to be important in converting CCP to its fully-active form [(71) and personal communication with Dr. Mark Miller].

The fluoride and cyanide adducts of CCP(GS) were formed to characterize the 5- and 6-coordinate high- and low-spin ferric enzyme as carried out previously for yeast CCP (73, 87, 106). Addition of 1000X F^- to CCP(GS) yielded the characteristic spectrum of 6-coordinate, high-spin CCP (Figure 3.10, Table 3.2). A purely 6-coordinate, low-spin spectrum was observed upon addition of 1000X CN^- to CCP (Figure

3.11, Table 3.2). These results revealed that the adducts of CCP(GS) possess the spectral properties of the wild-type adducts.

Overall, it is anticipated that 100% active CCP(GS) sample could be prepared if slow stirring is applied during the first crystallization step and the crystals are recrystallized immediately. In the large-scale trial presented here, freezing and thawing of the crystals prior to recrystallization may have negatively affected the structure of the final crystals. It is also possible that the concentration of CCP(GS) (25-30 mg/mL as estimated by the activity assay) was too high and promoted rapid crystal formation. Typically concentrations of ~ 20 mg/mL are used in CCP crystallizations (personal communication, Dr. Tom Poulos) and the CCP concentration is measured using its Soret absorption. Finally, this affinity purification procedure can yield double the amount of recrystallized CCP(GS) given in Table 3.2 (60 mg). Appropriate amounts of GS 4B beads and thrombin need to be used or alternatively, as recommended above, smaller-scale CCP(GS) isolations can be performed.

4.0 SUMMARY AND SUGGESTIONS FOR FURTHER STUDY

Chapter 2

Titration of CCP with peroxynitrite reveals that a species with a similar spectrum to compound I/II is formed. Titration of this species with ferrocytochrome c identifies this species as compound I. Since nitrite is not an efficient reductant of compound I, $NO_2^{\cdot}$ is unlikely be the end-product of the reduction of peroxynitrite by CCP *in vivo*; instead nitrite is produced. The ability of CCP to reduce toxic peroxynitrite to water and nitrate categorizes this enzyme as protective against nitrosative stress.

An attempt was made to estimate the rate of the reaction of CCP with peroxynitrite. Since peroxynitrite is unstable at pH 7.0 ($k = 1.38\ s^{-1}$) and, at the same time, atmospheric CO_2 catalyzes its decomposition to nitrate, the bimolecular rate constant, $6.9 \pm 2.2 \times 10^5\ M^{-1}\ s^{-1}$, for compound I formation with peroxynitrite might be not accurate. Determination of this rate constant by stopped-flow instrument should be carried out to confirm our results.

Peroxynitrite from both Cayman and Calbiochem stock solutions was shown to contain peroxide or other stable oxidants as impurities. Since the reaction of H_2O_2 with CCP is favored over that with peroxynitrite (3.91×10^7 vs $6.9 \pm 2.2 \times 10^5\ M^{-1}s^{-1}$, respectively) it is possible that the compound I observed is in part due to peroxide impurities in the peroxynitrite sample. More accurate titration data may be obtained if SIN-1 were used as a peroxynitrite source. When SIN-1 is added to a high pH (> 5) solution, it decomposes to $NO^{\cdot}$ and $O_2^{\cdot -}$, which rapidly combine to form peroxynitrite with no other oxidizing impurities present.

Finally, it was shown that LPO and MPO react much faster with peroxynitrite in acid conditions with a $pK_a \sim 6.8$, which underlines their preference for the protonated form of peroxynitrite. A pH study using stopped-flow would determine which form of peroxynitrite is preferred by the CCP active site.

Chapter 3

Using the GST-fusion system we were able to purify CCP(GS) as a GST-fusion protein. This method involved a single affinity chromatography step which enabled us to purify the enzyme in a much shorter time than the 2-week period usually needed with the other purification procedures available. Even though the R value of CCP(GS) was 1.32, the enzyme was only 61.5% active. We suggest that a slower rate of crystallization would enhance the activity of the preparation.

Finally, it has been suggested that CCP(GS) should be purified without the use of Triton X-100 (personal communication, Professor Justin Powlowski, Concordia U). Triton X-100 binds tightly to proteins and is very difficult to remove in the later steps of the purification. This might affect the activity of the purified protein and could be the reason why CCP(GS) was only 61.5% active.

REFERENCES

1. Altschul, A.M., Abrams, R., Hogness, T.R., (1940) J. Biol. Chem. 136, 777.
2. Goodhew, C.F., Wilson, I.B.H., Hunter, D.J.B., Pettigrew, G.W., (1990) Biochem. J. 271, 707.
3. Campos, E.G., Smith, J.M., Prichard, R.K., (1995) Comp. Biochem. Physiol. 111b, 371.
4. Finzel, B.C., Poulos, T.L., Kraut, J., (1984) J. Biol. Chem., 259, 13027.
5. Poulos, T.L., Finzel, B.C., (1984) In Peptide and Protein Reviews (Hearn, M.T.L., ed) vol 4, p.115. Dekker, New York.
6. English, A.M., Tsaprailis, G., (1995) In Advances in Inorganic Chemistry vol 43, p. 79.
7. Sayle, R.A., (1995) Trends Biochem. Sci., 20, 374.
8. Darley-Usmar, V., Wiseman, H., Halliwell, B., (1995) FEBS Letts., 369,131.
9. Beckman, J.S., (1996) Chem. Res. Toxicol. 9, 836.
10. Tsai, J.-H. M., Harrison, J.G., Martin, J.C., Hamilton, T.P., van der Woerd, M., Jablonsky, M.J., Beckman, J.S., (1994) J. Am. Chem. Soc. 116, 4115.
11. Verduyn, C., van Wijngaarden, C.J., Scheffers, W.A., van Dijken, J.P., (1991) Yeast 7, 2, 137.
12. Sephard, T.R., Wright, M., English, A.M., *In preparation.*
13. Fishel, L.A., Villafranca, J.E., Mauro, J.M., Kraut, J., (1987) Biochemistry 26, 351.
14. Goodin, D.B., Davidson, M.G., Roe, J.A., Mauk, A.G., Smith, M. (1991) Biochemistry 30, 4953.

15. Fitzgerald, M.M., Churchill, M.J., McRee, D.E., Goodin, D.B. (1994) Biochemistry 33, 3807.

16. McCord, J.M., Fridovich, I., (1977) Superoxide and Superoxide Dismutase (Michelson, A.M., McCord, J.M., Fridovich, I., eds) Academic Press, New York.

17. McCord, J.M., Keele, B.B.Jr., Fridovich, I., (1971) Proc. Natl. Acad. Sci. USA 68, 1024.

18. Mann, T., Keilin, D., (1938) Proc. Roy. Soc. (London) B126, 303.

19. Mohamed, M.S., Greenberg, D.M., (1953) J. Gen. Physiol. 37, 433.

20. Markowitz, H., Cartwright, G.E., Wintrobe, M.M., (1959) J. Biol. Chem. 234, 40.

21. McCord, J.M., Fridovich, I., (1968) J. Biol. Chem. 243, 5753

22. Klug, D., Rabani, J., Fridovich, I., (1972) J. Biol. Chem. 247, 4839.

23. Martinez-Cayuela, M., (1995) Biochimie 77, 147.

24. Basaga, H.S., (1990) Biochem. Cell. Biol. 68, 989.

25. Chow, C.K., (Eds) (1988) Cellular Antioxidant Defense Mechanisms, Vol II CRC Press, Boca Raton, Florida.

26. Tarr, M., Sampson, F., (Eds) (1993) Oxygen Free Radicals in Tissue Damage Birkhauser, Boston.

27. Jonata, E., Schuler, R.H., (1982) J. Phys. Chem. 86, 2078.

28. Weiss, S.J., (1989) N. Engl. J. Med. 320, 365.

29. Stendahl, O., Molin, L., Dahlgren, C., (1978) J. Clin. Invest. 62, 214.

30. Halliwell, B., Gutteridge, J.M.C., (1984) Biochem. J. 219, 1.

31. Haber, F., Weiss, J., (1934) Proc. R. Soc. London Ser. A 147, 332.

32. Fridovich, I., (1983) Annu. Rev. Pharmacol. Toxicol. 23, 239.

33. Esterbauer, H., (1986) In Free Radicals in Liver Injury (Poli, G., Cheesman, K.H., Dianzani, M.U., Slater, T.F., ed) p. 29 IRL Press Ltd, Oxford, England.

34. Webster, N.R., Nunn, J.P., (1988) Br. J. Anaesth. 60, 98.

35. Davies, K.J.A., Delsignore, M.E., Lin, S.W., J. Biol. Chem. (1987) 262, 9902.

36. Everse, J., Everse, K.E., Grisham, M.B., (1991) In Peroxidases in Chemistry and Biology Vol I, CRC Press, Boca Raton, Florida.

37. Everse, J., Everse, K.E., Grisham, M.B., (1991) In Peroxidases in Chemistry and Biology Vol II, CRC Press, Boca Raton, Florida.

38. Godon, C., Lagniel, G., Lee, J., Buhler, J-M., Kieffer, S., Perrot, M., Boucherie, H., Toledano, M.B., Labarre, J., (1998) J. Biol. Chem. 273, 34, 22480.

39. Harris, D.C., (1991) In Quantitative Chemical Analysis 3rd Ed, (Freeman W.H. and Company ed.), New York.

40. Pryor, W.A., Squadrito, G.L., (1995) Am. J. Physiol. 268, L699.

41. Koshland, D.E.Jr., (1992) Science 258, 1861.

42. Alberts, B., Bray, D., Lewis, J., Raff, M., Roberts, K., Watson, J.D., (1994) Molecular Biology of The Cell, 3rd ed, Garland publishing, Inc. New York & London.

43. Palmer, R.M.J., Ferrige, A.G., Moncada, S., (1987) Nature 327, 524.

44. Garthwaite, J., Charles, S.L., Chess-Williams, R., (1998) Nature 336, 385.

45. Furchgott, R.F., Mechanisms of Vasolidation Vol IV, Vanhoutte P.M. ed, Raven, New York.

46. Floris, R., Piersma, S.R., Yang, G., Jones, P., Wever, R., (1993) Eur. J. Biochem., 215, 767.

47. Lowenstein, C.J., Snyder, S.H., (1992) Cell 70, 705.

48. Huie, R.E., Padmaja, S., (1993) Free Radical Res. Commun. 18, 195.

49. Cudd, A., Fridovich, I., (1982) J. Biol. Chem. 257, 11443.

50. Radi, R., Beckman, J.S., Bush, K.M., Freeman, B.A., (1991) J. Biol. Chem. 266, 4244.

51. Crow, J.P., Beckman, J.S., McCord, J.M., (1995) Biochemistry 34, 3544.

52. Beckman, J.S., Ischiropoulos, H., Zhu, L., van der Woerd, M., Smith, C., Chen, J., Harrison, J., Martin, J.C., Tsai, M., (1992) Arch. Biochem. Biophys. 298, 438.

53. Crow, J.P., Spruell, C., Chen, J., Gunn, C., Ischiropoulos, H., Tsai, M., Smith, C.D., Radi, R., Koppenol, W.H., Beckman, J.S., (1994) Free Rad. Biol. Med., 16, 3, 331.

54. Squadrito, G.L., Pryor, W.A., (1998) Free Rad. Biol. Med. 25, 392.

55. Pryor, W.A., Lemercier, J-N., Zhang, H., Uppu, R.M., Sqadrito, G.L., (1997) Free Rad. Biol. Med. 23, 2, 331.

56. Denicola, A., Freeman, B.A., Trujilo, M., Radi, R., (1996) Arch. Biochem. Biophys. 333, 1, 49.

57. Uppu, R.M., Squadrito, G.L., Pryor, W.A., (1996) Arch. Biochem. Biophys. 327, 2, 335.

58. Lymar, S.V., Hurst, J.K., (1995) J. Am. Chem. Soc. 117, 8867.

59. Masumoto, H., Kissner, R., Koppenol, W.H., Sies, H., (1996) FEBS Letts. 398, 179.

60. Thomson, L., Trujillo, M., Telleri, R., Radi, R., (1995) Arch. Biochem. Biophys. 319, 2, 491.

61. Sies, H., Sharov, V.S., Klotz, L.O., Brivida, K., (1997) J. Biol. Chem. 272, 44, 27812.

62. Padmaja, S., Squadrito, G.L., Pryor, W.A., (1998) Arch. Biochem. Biophys. 349, 1.

63. Alayash, A.I., Ryan, B.A.B., Cashon, R.E., (1996) Arch. Biochem. Biophys. 333, 482.

64. Chow, C.K., (Eds) (1988) Cellular Antioxidant Defense Mechanisms, Vol III CRC Press, Boca Raton, Florida.

65. Eiserich, J.P., Hristova, M., Cross, C.E., Jones, A.D., Freeman, B.A., Halliwell, B., van der Vliet, A., (1998) Nature 391, 393.

66. Demple, B., Halbrook, J., (1983) Nature 304, 466.

67. Saccharomyces Genome Database Website: http://genome-www.stanford.edu/saccharomyces/

68. Davies, J.M.S., Lowry, C.V., Davies, K.J.A., (1995) Arch. Biochem. Biophys. 317, 1.

69. Fortuniak, A., Jakubowski, W., Bilinski, T., Bartosz, G., (1996) Biochem. Mol. Biol. Int. 38, 1271.

70. Grace, S.C., Salgro, M.G., Pryor, W.A., (1998) FEBS Letts. 426, 24.

71. Yonetani, T., Chance, B., Kajiwara, S., (1966b) J. Biol. Chem. 241, 2981.

72. Vitello, L.B., Huang, M., Erman, J.E., (1990) Biochemistry 29, 4283.

73. Yonetani, T., Anni, H., (1987) J. Biol. Chem. 262, 9554.

74. Margoliash, E., Frohwirt, N., (1959) Biochem. J. 71, 570.

75. Hughes, M.N., Nicklin, H.G., (1968) J. Chem. Soc. (A), 450.

76. Bohle, D.S., Glassbrenner, P.A., Hansert, B., (1996) Meth. Enzymol. 269, 302.

77. Yonetani, T., (1965) J. Biol. Chem. 240, 11, 4509.

78. Pond, A.E., Bruce, G.S., English, A.M., Sono, M., Dawson, J.H., (1998) Inorg. Chim. Acta 275 – 276, 250.

79. Coulson, A.F., Erman, J.E., Yonetani, T., (1971) J. Biol. Chem. 246, 917.

80. Ho, P.S., Hoffman, B.M., Kang, C.H., Margoliash, E., (1983) J. Biol. Chem., 258, 4346.

81. Erman, J., Yonetani, T., (1975) Biochim. Biophys. Acta, 393, 350.

82. Balny, C., Anni, H., Yonetani, T., (1987) FEBS Letts. 221, 349.

83. Wilcox, S.K., Jensen, G.M., Fitzerald, M.M., McRee, D.E., Goodin, D.B., (1996) Biochemistry 35, 4858.

84. Uppu, R.M., Pryor, W., (1996) Methods Enzymol. 269, 322.

85. Denicola, A., Freeman, B.A., Trujillo, M., Radi, R., (1996) Arch. Biochem. Biophys. 333, 1, 49.

86. Radi, R., Rodriguez, M., Castro, L., Telleri, R., (1994) Arch. Biochem. Biophys. 308, 1, 89.

87. Yonetani, T., Ray, G.S., (1965) J. Biol. Chem. 240, 4503.

88. Abrams, R., Altschul, A.M., Hogness, T.R., (1942) J. Biol. Chem. 142, 303.

89. Kaput, J., Goltz, S., Blobel, G., (1982) J. Biol. Chem. 257, 15054.

90. Darwish, K., Li, H., Poulos, T. L., (1991) Prot. Eng. 4, 701.

91. Sherman, F., Stewart, J.W., Tsunasawa, S., (1985) BioEssays 3, 27

92. Fox, T., English, A.M., Gibbs, B.F., (1994) Bioconjugate Chem. 5, 14.

93. Pharmacia Biotech product catalogue.

94. Sigma Chemicals product catalogue.

95. Mullis, K., Faloona, F., (1987) Methods Enzymol. 155, 335.

96. Horton, R.M., Cai, Z., Steffan, N.H., Larry, R.P., (1990) Biotechniques 8, 528.

97. Pharmacia Biotech, GST Gene Fusion System, 3rd ed, Revision 1.

98. Bio-Rad Protein Assay manual, BioRad

99. Yonetani, T., (1970) Adv. Enzymol. Relat. Areas Mol. Biol. 33, 309.

100. Stoker, A.W., (1990) Nucleic Acid Res. 18, 4290.

101. Smith, D.B., Corcoran, L.M., (1990) Current Protocols in Molecular Biology, Vol II, Ausubel, F.M. et al. eds, John Wiley & Sons, New York.

102. Frangioni, J.V., Neel, B.G., (1993) Anal. Biochem. 210, 179.

103. Winzor, D.J., Scheraga, H.A., (1964) Arch. Biochem. Biophys. 104, 202.

104. Vitello, L.B., Erman, J.E., Miller, M.A., Mauro, J.M., Kraut, J., (1992) Biochemistry 31, 11529.

105. Pond, A.E., Sono, M., Elenkova, E.A., McRee, D.E., Goodin, D.B., English, A.M., Dawson, J.H., (1999) J. Inorg. Biochem. *In Press.*

106. Yonetani, T., Wilson, D.F., Seamonds, B., (1966b) J. Biol. Chem. 241, 5347.

107. Erman, J., (1974) Biochemistry 13, 39.

108. Erman, J., (1974) Biochemistry 13, 34.

109. Wilchek, M., (1972) Anal. Biochem. 49, 572.

110. Windholz, M., Budavari, S., Blumetti, R.F., Otterbein, E.S., (1983) The Merck Index, (3rd Ed.) Merck & Co., Inc., Rahway, N.J., U.S.A.

111. Sambrook, J., Fritsch, E.F., Maniatis, T., (1989) Molecular Cloning, a Laboratory Manual, Vol III, (2nd Ed.) CSH Press, U.S.A.

APPENDIX I

LITERATURE PURIFICATION PROCEDURES FOR CYTOCHROME C PEROXIDASE

A. Protocol for the purification of CCP(MI)

The procedure given here is that of (13) as modified slightly in our lab.

Step1: Starter culture: 250 mL of TB media (Appendix II, 1A) with 250 μg/mL Amp is inoculated from a 20% glycerol stock of SK383 *E. coli* cells transformed with pUC8CCP(MI) vector and let grow for 14 h at 37°C, with shaking (250 rpm).

Step 2: 4 L of 4X TB media are prepared and sterilized. Also, 12 L of dH_2O are sterilized in a 16-L fermentor. The media and the starter culture are poured into the fermentor and grown at 37°C, 210 rpm for 32 – 36 h or until $OD_{600\ nm} = 2.5$ and pH ≥ 8.

Step 3: Harvesting the cells: 500-mL centrifuge bottles are used to centrifuge the culture at 5K rpm, 10 min, 4°C (Sorvall GSA rotor). The supernatant is discarded.

From this point on, all steps are performed in 4°C and all volumes are for a 60-g cell pellet.

Step 4: Lysing the cells: (a) The cell pellet is resuspended in a total of 36 mL of 50 mM potassium phosphate, pH 6.0. (b) 36 mL of 1X lysis buffer (Appendix II, 3A) and (c) 6 mL of lysozyme solution (Appendix II, 2D) are added and the mixture is let to stand for 1 h with mixing every 15 min. (d) The cells are frozen in a dry-ice/ethanol bath and thawed for 10-12 h at 4°C. (e) After addition of 25 mL of 5% Brij 58, the cells are

shaken gently for 1.5 h. (f) 10 mL of 2 M $MgCl_2$, 1.8 mL Dnase I and 60 μL Rnase A solutions (Appendix II, 2B, 2C) are added and the shaking is continued for another hour until the solution is no longer viscous. (g) The lysate is pipeted into 25-mL centrifuge bottles and centrifuged for 35 min at 19K rpm in a JA 20 rotor in a Beckman J2-HS centrifuge. The pellet is discarded and the supernatant is kept on ice.

Step 5: The supernatant is dialyzed for 6 – 12 h in 4 L of ice cold 50 mM KPi/1mM Na_2EDTA, pH 6.0. Spectrapor #2 dialysis tubing (MW cut-off 12-14 kDa) is used in this step and some of the unwanted cellular proteins precipitate during dialysis.

Step 6: The dialyzed supernatant is centrifuged at 19K rpm, 4°C, in a JA 20 rotor for 20 min to remove the precipitated material.

Step 7: If the volume of the supernatant is greater than 170 mL, an Amicon stirred concentrator (180-mL capacity) with a PM-10 (or YM-10) membrane is used to reduce it to ~ 170 mL.

Step 8: SDS-PAGE (12% gel; Appendix II, 4B) analysis checks for CCP overproduction and relative yields in the cell lysate, supernatant and cell pellet.

Step 9: A 2.5-cm X 180-cm Sephadex G75 column is prepared and equilibrated with 50 mM KPi, pH 6.0. The supernatant from step 7 is added to this column and eluted with the same buffer.

Step 10: 15-mL fractions are collected and every other fraction is checked on by SDS-PAGE for CCP content.

Step 11: All CCP-containing fractions are pooled and the volume is reduced to 50 mL in an Amicon concentrator as in *step 7.*

Step 12: Heme insertion: (a) The pH of the solution is increased to 7.5 by dialysis vs 4 L

of ice-cold 50 mM KPi, pH 7.5.

All steps from this point on should be performed in the dark.

(b) A 5X molar excess of hemin (MW = 651.9 Da) is added to apoCCP. For 400 mg CCP:

(0.4 g CCP x 5) / 34,000 g/mol = 5.88×10^{-5} mol hemin

5.88×10^{-5} mol hemin / 5×10^{-3} M = 11.8 mL

5.88×10^{-5} mol hemin x 651.5 g/mol = 38.4 mg hemin

11.8 mL of hemin solution (Appendix II, 2E) is added and the mixture is let stand in the dark for 90 min with constant swirling of the flask, and dialyzed against 4 L of ice-cold 20 mM KPi, pH 6.0.

Step 13: (a) The solution from *step 12* is loaded on a 8.5-cm X 12.5-cm DEAE-cellulose column equilibrated with 10 mM KPi, pH 6.0; (b) CCP is eluted from the column using a 50-500 mM KPi (pH 6.0) gradient. This column separates holo-CCP from protein impurities and removes excess hemin which remains bound to the top of the DEAE column. (c) The purity index (R = 408/280) is checked in all fractions, and those with R $\geq$ 1.1 are pooled and concentrated to 30 mg/mL in an Amicon concentrator.

Step 14: The concentrated solution is dialyzed vs ice-cold dH_2O to induce crystallization of CCP. The dH_2O is changed every 10-15 h. This step can take up to three days.

Step 15: Once crystals are formed the suspension is centrifuged for 10 min, 5K rpm, at 4°C in JA 20 rotor. The supernatant is checked for CCP by measuring the 408/280 nm ratio. If the ratio is < 1.1, the supernatant is discarded and the crystals are resuspended in dH_2O and spun again.

Step 16: Recrystallization of CCP: crystals collected from *step 15* are dissolved in ice

cold 0.1 M KPi, pH 6.0, and dialyzed vs dH_2O to induce recrystallization without stirring. Needle-like CCP crystals are formed with a purity index of 1.2-1.3 within 1-2 days. Typical yield of CCP from this procedure is ~ 400 mg/15 L of culture based on our results, whereas an average yield of more than 120 mg/15 L has been reported (13).

B. Protocol for purification of CCP(MKT)

This procedure was provided by Professor A. Grant Mauk (UBC) and is a more detailed description of the procedure published in (15).

Step 1: Starter culture: 3 mL of superbroth/amp media (Appendix II, 1B) is inoculated with a single colony from a plate of transformed BL21(DE3) cells with pT7CCP vector, and grown at 37°C with shaking (250 rpm) for 4-5 h or until some turbidity is evident. 500 μL of this culture is used to inoculate 50 mL of superbroth/amp. The inoculated media is grown at the same conditions as previously described for 2-3 h or until some turbidity is evident.

Step 2: 10 L of superbroth/amp in 2-L Erlenmeyer flasks is inoculated with 1 mL of the 50-mL culture grown from *step 1* and grown at 37°C, with shaking (250 rpm) for 10-11 h or until $OD_{600\ nm}$ ~ 2.0. The culture is induced with 0.5 mM IPTG and growth is continued for another 3 h.

Steps 3 to 6 are identical to procedure A, except that 1 mM PMSF is added when resuspending the cells in buffer to inhibit the action of cellular proteases.

Step 7: Supernatant is loaded onto a 2.5- X 4-cm DEAE Sepharose CL-6B column equillibrated with 50 mM KPi, pH 6.0 and CCP is eluted with a 50-500 mM KPi (pH 6.0) gradient.

Step 8: Fractions are checked for CCP on a 13% SDS-PAGE gel.

Step 9: The CCP-containing fractions are pooled and concentrated in an Amicon stirred concentrator with PM-10 membrane, in 100 mM KPi (pH 6.0), 1 mM Na_2EDTA to a final volume of ~10 mL.

Step 10: The solution from *Step 9* is loaded into a 2.5- X 100-cm column of G-75 (fine grade) equilibrated in the same buffer.

Step 11: The fractions collected are checked on a 13% SDS – PAGE gel and only those containing a reasonable amount of CCP are pooled.

Step 12: Pooled fractions are concentrated as in *Step 9* to 30-40 mL and the CCP concentration is estimated using $\varepsilon_{280\ nm} = 55\ mM^{-1}\ cm^{-1}$.

Step 13: Pooled fractions are dialyzed for 12 h vs 4 L of 0.1 M KPi, pH 7.5.

Step 14: Hemin solution (1.1 equivalents) is prepared in procedure A and added to the dialysis bag, and after mixing the solution, is let stand for 1 h for hemin incorporation.

Step 15: The solution from *step 14* is dialyzed vs 4 L of 0.1 M KPi, pH 6.2.

Steps 16-18: These involve crystallization and recrystallization of holo-CCP and are identical to *Steps 14 – 16* in procedure A.

~450 mg/15 L of culture is the typical yield of CCP obtained with this procedure as reported by Professor Mauk (UBC).

C. Protocol for purification of CCP from *E. Coli*

This procedure was provided by Professor Tom Poulos (UCI) and is a more detailed description of the procedure published in (90).

Step 1: Starter culture: 200 mL LB/Amp (Appendix II, 1C) is inoculated with a single colony from BL 21 cells transformed with pT7CCPZf1 vector. The cells are grown for 12 h at 37°C with shaking (250 rpm).

Step 2: The culture is diluted 100X in 6 L of TB media (Appendix II, 1A) with 100 μg/ml ampicillin and grown to $OD_{600\ nm}$ = 1.5. Following induction with 0.75 mM IPTG, the culture is grown for another 4-6 h.

Steps 3-16: These are identical to *Steps 3-16* of procedure A. The only differences are: *Step 4*, 1-5 mM PMSF is added, and *Step 13*, a shallower gradient elution is used for the anion exchange column (100-500 mM KPi, pH 6.0).

The typical CCP yield using this protocol as reported by Professor Poulos (UCI) is 500 mg of crystals/6 L of culture form the first crystallization step.

APPENDIX II (Protocols from Refs 97 and 111)

1. GROWTH MEDIA

A. Terrific Broth (TB) Medium (per liter of dH_2O)

Solution A: 100 mL 0.17 M KH_2PO_4 / 0.72 M K_2HPO_4

Solution B:

Bacto Tryptone	12 g	(DIFCO laboratories)
Yeast Extract	24 g	(DIFCO laboratories)
NaCl	10 g	(ICN)
Glycerol	4 mL	(ICN)

Add dH_2O to make up a final volume of 900 mL

Autoclave separately *solution A* and *solution B* for 45 min at 120°C, cool and mix. Add 2.5 mL filter-sterilized stock ampicillin solution.

B. Superbroth/Amp (per litre of dH_2O)

Bacto Tryptone	10 g	
Yeast Extract	8 g	
NaCl	5 g	
Glycerine	1 mL	(CALEDON laboratories)

Autoclave for 20 min at 120°C. When the solution cools to ~ 60°C, add 1 mL of the filter-sterilized ampicillin stock solution.

C. Luria-Bertini (LB) Medium (per litre of dH_2O)

Bacto Tryptone	10 g
Yeast Extract	5 g

NaCl 10 g

Autoclave for 20 min at 120°C. Add 1 mL of ampicillin stock solution (100mg/mL) to prepare LB/Amp.

D. 2X YT Medium (per litre of dH_2O)

Bacto Tryptone	16 g
Yeast Extract	10 g
NaCl	5 g

Autoclave for 20 min at 120°C. Add 1 mL of ampicillin stock solution (100 mg/mL) to prepare 2X YTA.

E. Culture Plates (per litre of dH_2O)

Bacto Tryptone	10 g	
Yeast Extract	5 g	
NaCl	10 g	
Agar	15 g	(ICN)

Autoclave for 20 min at 120°C, allowed to cool to 45-50°C, and add 1 mL stock ampicillin. Pour the medium into 100 mm^2 plates to a thickness of ~ 3 mm. Let plates stand on the bench until medium has solidified and store inverted at 4°C for up to 4 weeks.

F. X-GAL Plates

Spread 32 µl of 50 mg/mL X-Gal solution on LB/Amp plates and incubate the plates at 37°C for 30 min.

2. SOLUTIONS

A. Ampicillin

100 mg/mL ampicillin in dH_2O and filter sterilize using ValuePrep, 25 mm cellulose acetate, 0.2-μm, sterile syringe filters (VWR Scientific).

B. Dnase I solution

Dissolve 20 mg Dnase I in 1.8 mL in 50 mM KPi, pH 6.0.

C. Rnase A solution

12.5 mg/mL Rnase in dH_2O.

D. Lysozyme solution

Dissolve 0.13 g of lysozyme in 7 mL of 50 mM KPi, pH 6.0, to give a 18 mg/mL solution.

E. Hemin solution

For an estimated 400 mg yield of CCP, prepare a 5 mM hemin solution as follows: dissolve 38.4 mg hemin (MW 651.9 g/mol) in 2 mL of 0.1 N NaOH and add 9.8 mL of 50 mM KPi, pH 7.5 just before use.

F. 500 mM IPTG solution (per 20 ml dH_2O)

Dissolve 2.383 g IPTG (FW = 238.3) in 20 mL dH_2O. Filter-sterilized the solution and store at - 20°C in aliquots of 1 mL.

G. 30% Acrylamide/Bis Acrylamide Solution (per 100 mL dH_2O)

Acrylamide	29.2 g (ICN)
N'N'-bis-methylene-acrylamide	0.8 g (ICN)

Warm to dissolve, filter and store at 4°C in the dark for a maximum of 30 days.

H. SDS-PAGE Staining Solution

Coomassie Briliant Blue R250	250 g (Sigma)
Methanol	450 mL (ICN)
dH_2O	450 mL
Glacial Acetic Acid	100 mL (ICN)

I. SDS-PAGE Destaining Solution

Methanol	300 mL
Glacial Acetic Acid	100 mL
Glycerol	30 mL
dH_2O	460 mL

3. BUFFERS

A. 10X Lysis Buffer

1 M KPi, pH 7.5

150 g/L Na_2EDTA

Dilute 10X in dH_2O for lysis.

B. 6X Agarose Gel Loading Buffer

0.25 % Bromophenol blue (Sigma)

0.25 % Xylene Cyanol FF (Sigma)

30 % Glycerol in dH_2O

Mix and store at 4°C.

C. 5X TBE (Tris-Borate) Buffer (per litre of dH_2O)

Tris-base	54 g (ICN)
Boric acid	27.5 g (Fisher Chemical)
0.5 M EDTA (pH 8.0)	20 mL

D. 5X SDS-PAGE Gel Loading Buffer (Sample buffer)

dH_2O	4.0 mL
0.5 M Tris-HCl, pH 6.8	1.0 mL (ICN)
Glycerol	0.8 mL
10% (w/v) SDS	1.6 mL (ICN)
2-b-mercaptoethanol	0.4 mL (Sigma)
0.05% (w/v) bromophenol blue	0.2 mL (Sigma)

Dilute protein samples 4X with sample buffer, and heat at 95°C for 4 min before loading into the wells.

E. 5X SDS Running Buffer, pH 8.3 (per litre of dH_2O)

Tris Base 15 g

Glycine	72 g
SDS	3 g

Store at 4°C and dilute 5X with dH_2O for each electrophoretic run.

4. GELS

A. 1% Agarose Gel for DNA separation

Agarose	0.5 g
1X TBE buffer	50 mL

Heat the 1% agarose suspension in a microwave for ~ 2 min on high to melt. Cool to 60°C and add 2.5 µl of 10 mg/mL ethidium bromide stock. Pour the solution on a casting tray to solidify. Prior to polymerization, insert a comb to form loading wells. Use 1X TBE buffer as the running buffer. Load the samples in the wells and carry out electrophoresis at 75 – 85 V until bromophenol blue migrates about halfway through the gel.

B. 12% SDS-PAGE gel for protein separation

12% Resolving gel:

dH_2O	6.6 mL
30% acrylamide solution	8.0 mL
1.5 M Tris (pH8.8)	5.0 mL
10% (w/v) SDS	0.2 mL
10% (w/v) ammonium persulfate	0.2 mL (Anachemia chemicals)
TEMED	0.008 mL (ICN)

5% Stacking gel:

dH_2O	6.8 mL
30% acrylamide solution	1.7 mL
1.0 M Tris (pH 6.8)	1.25 mL
10% (w/v) SDS	0.1 mL
10% (w/v) ammonium persulfate	0.1 mL
TEMED	0.01 mL

Pour the resolving gel into the casting tray, and add a thin layer of n-butanol on top. When the gel solidifies, remove the n-butanol with filter paper and add the stacking gel. Insert a comb to form wells prior to polymerization of the stacking gel. Place the gel in an electrophoresis apparatus containing 1X SDS running buffer. Load the samples in the wells and run the gel at 105 volts. Remove the gel from the casting tray and place in staining solution for 1 h with smooth shaking on a rocking platform. Remove and place the gel destaining solution and continue the shaking for 4 h . Dry the gel at 80°C for 1 h.

APPENDIX III

Sequence of CCP(GS) gene:

#1

1 GGA TCC ACA CCG CTC GTT CAT GTC GCC TCT GTC GAA

37 AAA GGG AGG TCA TAC GAG GAC TTC CAA AAG GTG TAC

73 AAT GCG ATT GCA CTC AAG CTG AGG GAA GAT GAC GAA

109 TAT GAC AAC TAT ATA GGC TAT GGG CCC GTA TTA GTC

#2

145 CGT CTT GCT TGG CAC ATT TCA GGG ACC TGG GAC AAG

181 CAC GAC AAT ACA GGC GGG TCA TAC GGT GGT ACA TAC

217 AGA TTC AAA AAG GAG TTT AAC GAT CCA TCC AAT GCG

253 GGC TTG CAG AAT GGC TTT AAG TTC CTG GAG CCC ATT

289 CAC AAA GAG TTT CCC TGG ATC TCC TCG GGT GAT CTG

325 TTC AGT CTA GGG GGT GTC ACT GCT GTG CAG GAA ATG

361 CAG GGT CCC AAG ATT CCA TGG AGA TGT GGT AGA GTC

#3

397 GAC ACG CCA GAG GAT ACT ACC CCT GAC AAC GGG AGA

433 CTG CCT GAC GCT GAT AAG GAC GCT GGC TAT GTC AGA

469 ACG TTT TTT CAA AGA CTT AAT ATG AAT GAC AGA GAA

505 GTA GTT GCT CTT ATG GGG GCT CAC GCT CTG GGC AAG

541 ACC CAC TTG AAG AAC TCT GGA TAC GAA GGG CCA TGG

577 GGA GCC GCT AAC AAC GTC TTT ACC AAT GAG TTT TAC

613 TTG AAC TTG TTG AAT GAA GAC TGG AAA TTG GAA AAG

649 AAC GAC GCG AAC AAC GAA CAG TGG GAC TCT AAG AGC

#4

685 GGC TAC ATG ATG CTG CCC ACT GAT TAT TCT TTG ATT

721 CAG GAC CCC AAG TAC TTA AGC ATT GTG AAA GAA TAC

757 GCT AAT GAC CAG GAC AAG TTC TTC AAG GAT TTT TCC

793 AAA GCT TTT GAA AAA CTG TTG GAA AAC GGT ATC ACT

829 TTC CCT AAA GAC GCG CCC AGT CCA TTT ATT TTC AAG

#5

865 ACT TTA GAG GAA CAA GGT TTA TAG

1: primer SEQ 1A

2: primer CCP-H60Q-Mut-Anti/CCP-H60Q-Mut-Coding

3: primer SEQ 2A

4: primer Y236H-CCP(2)/CCP-Y236H-mut

5: primer CCP-GEX-3EX